

# *Synthesis, Structural Characterization and Spectroscopic Studies on Some Rhenium(I) Complexes*

*THESIS SUBMITTED FOR THE DEGREE OF DOCTOR OF  
PHILOSOPHY (SCIENCE)*

*OF JADAVPUR UNIVERSITY*

*May, 2022*



*By*

*Tapashi Das*

*[Index no. : 54/17/Chem./25]*

*Inorganic Chemistry Section*

*Department of Chemistry*

*Jadavpur University*

*Kolkata 700 032*

যাদবপুর বিশ্ববিদ্যালয়  
কলকাতা-৭০০০৩২, ভারত



\*JADAVPUR UNIVERSITY  
KOLKATA-700 032, INDIA

FACULTY OF SCIENCE: DEPARTMENT OF CHEMISTRY : INORGANIC CHEMISTRY SECTION

## CERTIFICATE FROM THE SUPERVISOR

This is to certify that the thesis entitled "Synthesis, Structural Characterization and Spectroscopic Studies on Some Rhenium (I) Complexes" submitted by **Tapashi Das** who got her name registered on 27.06.2017 for the award of Ph.D. (Science) degree of Jadavpur University, is absolutely based upon her own work under my supervision and neither this thesis nor any part of it has been submitted for any degree/diploma or any other academic award anywhere before.

Date: 19/05/2022

*Kajal Krishna Rajak*

(Prof. Kajal Krishna Rajak)

Signature of Supervisor date with office seal

*Dr Kajal Krishna Rajak*  
Professor of Chemistry  
Jadavpur University  
Kolkata-700032

\* Established on and from 24<sup>th</sup> December, 1955 vide Notification No.10986-Edn/IU-42/55 dated 6<sup>th</sup> December, 1955 under Jadavpur University Act, 1955 (West Bengal Act XXXIII of 1955) followed by Jadavpur University Act, 1981 (West Bengal Act XXIV of 1981)

দুরভাষ: ২৪১৪-৬৬৬৬/৬১৯৪/৬৬৪৩/৬৪৯৩/৬৪৯৩ প্রসারণ: ২৪৬৯

Website: www.jadavpur.edu

Phone: 2414-6666/6194/6643/6495/6443 Extn.2469

দুরবারী: (৯১)-০০০-২৪১৪-৬৪১৪/৬২১০/২৪১০-৭১২১

E-mail : hod@chemistry.jdvu.ac.in

Fax: (91)-033-2414-6414/6210/2413-7121

*To*

*To*

*My Family*

*My Family*

*Preface*  
*Preface*

## PREFACE

The work related to this thesis 'Synthesis, Structural Characterization and Spectroscopic Studies on Some Rhenium (I) Complexes' commenced on the month of July, 2017.

The thesis is subdivided into five chapters elaborating methods, strategy, experimental findings and analysis of the reaction behaviour of some rhenium (I) complexes.

**Chapter I** contains summary of the work presented in this thesis with short description of the physical methods and equipment employed.

**Chapter II** describes synthesis and characterization of two rhenium (I) complexes coordinated with a multifunctional ligand in different binding mode through NNO and NN binding sites. Experimental analysis of photophysical properties of these complexes along with a detailed DFT and TDDFT calculations are provided in this chapter.

**Chapter III** mainly deals with the reactivity of a rhenium (I) complex having multifunctional ligand towards zinc acetate and cyanide ion. This chapter elaborately discuss about the nature of interaction with zinc acetate and cyanide ion. The kinetics study was performed using UV-Vis spectroscopy. <sup>1</sup>H NMR titration was performed to elucidate the mechanism of the reaction between the complex and cyanide ion. The more important outcome of this study is that the complex is proved to be a good cyanide sensor having high detection limit.

**Chapter IV** contains synthesis and characterization of two mononuclear facial rhenium (I) complexes having two different Schiff base ligands. The ligands bind with the complex through NN binding sites. One of the complexes shows selective detection of cyanide ion. The mechanism of the reaction was interpreted by <sup>1</sup>H NMR titration.

**Chapter V** describes synthesis and characterization of a mononuclear facial rhenium (I) complex having dibenzofuran based imine linked ligand. This complex show molecular rearrangement in presence of zinc acetate in methanolic solution. The rearranged products were studied and structural characterization was done by single crystal X-ray diffraction. The photophysical properties of these complexes were measured through UV-Vis spectroscopy and fluorescence spectroscopy.

Tapashi Das  
19-5-2022

**(Tapashi Das)**

**Department of Chemistry  
Jadavpur University  
Kolkata -700032, India.**

*Acknowledgement*  
*Acknowledgement*

## **ACKNOWLEDGEMENT**

It is my pleasure to acknowledge the roles of several individuals who have profusely helped me during my years as a Ph.D. student.

First of all, I would like to express my deep regards and gratitude to my supervisor Prof. Kajal Krishna Rajak for his immense support, advice and guidance throughout my research work. His outstanding ability to keep calm in toughest situation inspired me to get through the difficult journey of Ph.D.

I would like to acknowledge with gratitude, the constant support and love of my family. Special thanks go to my parents and my sister-in-law. I am extremely grateful to my brother because of his enthusiastic fondness for chemistry which he seeded inside me. His inspiration always keeps me going forward. Inspiration awakens us to new possibilities by allowing us to transcend our ordinary experiences and limitations. This journey may not be possible without his encouragement.

I gratefully acknowledge my seniors: Dr. Debopam Sinha, Dr. Sohini Basuroy, Dr. Amit Maity and Dr. Sankar Prasad Parua for their help and support. I am also grateful to the other members of my research group: Mitali Majumder, Supriya Debnath, Roumi Patra, Niladri Sinha, Sneha Ray and Biswajit Khutia for their help and cooperation. I also thank to the research group of Dr. Kaushikisankar Pramanik. Thank you all my friends, the time we spent together will always be retained in my memory.

I want to thank Arpon, Ritashree, Tania and Renuka for their help in many ways throughout this journey. Thank you for being there for me.

I would also like to express my regards to Prof. Samaresh Bhattacharya, Dr. Kaushikisankar Pramanik and Dr. Sujoy Baitalik for their help in several ways.

I am grateful to all the faculty members of Department of Chemistry for their support.



I gratefully acknowledge Council of Scientific and Industrial Research, New Delhi, India and Science & Engineering Research Board, New Delhi, India, for financial support. I am thankful to West Bengal DST Board and RUSA 2.0.

Last but not the least I would gratefully acknowledge Jadavpur University for infrastructure facilities.

Tapashi Das

19-5-2022

(Tapashi Das)

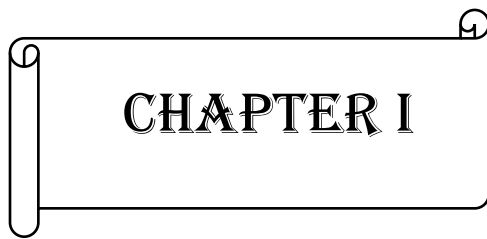
**Department of Chemistry  
Jadavpur University  
Kolkata -700032, India.**



# CONTENTS

	<b>Page</b>
<b>Preface</b>	<b>i-ii</b>
<b>Acknowledgement</b>	<b>iii-iv</b>
<b>Chapter I</b> Introduction	<b>1-22</b>
<b>Chapter II</b> Synthesis, Characterization and Theoretical Studies of a Multifunctional Ligand and Complexes of Rhenium (I)	<b>23-47</b>
<b>Chapter III</b> Reactivity of hydrazine based Rhenium (I) Complexes towards Certain Metal Ion and Toxic anion	<b>48-73</b>
<b>Chapter IV</b> Synthesis, Characterization and DFT studies of Complexes Bearing $[\text{Re}(\text{CO})_3]^+$ Core and Reactivity Towards Cyanide ion	<b>74-105</b>
<b>Chapter V</b> Metal assisted rearrangement in Rhenium (I) Complex Transforming Into Red Emitting Species	<b>106-123</b>
<b>List of Publications</b>	<b>v-vi</b>



A decorative scroll with a black outline, featuring a rolled-up edge on the left and a small loop on the right. The text "CHAPTER I" is centered within the scroll in a bold, serif font.

**CHAPTER I**



# *Introduction*

## **ABSTRACT**

This chapter consists of the brief introduction of all the chemical systems of this thesis followed by a preamble on chemistry of rhenium. The methods and equipments used in the work of this thesis are summarized comprehensively.





## I.1 PREAMBLE

### *I.1.1 Chemistry of Rhenium*

Rhenium<sup>1-4</sup> is one of the rarest metal on earth crust (with abundance of 1 parts per million) having atomic number 75 and has electronic configuration  $[\text{Xe}]4f^{14}5d^56s^2$ . It was 1925, when the element was discovered by German chemists Walter Noddack and Ida Tacke while working in Berlin. The isolation of rhenium was finally achieved by concentrating it from the ore gadolinite in which it was an impurity. This precious metal does not occur freely in nature but is found in the molybdenum ore with very low concentration which is about 0.2%<sup>5-9</sup>. Only tungsten and carbon has higher melting point than rhenium (3180°C). The literature study shows that it has one of the highest boiling points of all elements. Rhenium, in its metallic state, forms hexagonal close-packed crystal structure, with lattice parameters  $a = 276.1 \text{ pm}$  and  $c = 445.6 \text{ pm}$ <sup>10</sup>.

Rhenium shows a wide variety of oxidation states starting from -1 to +7. The most common oxidation state is +7. One of the striking feature of rhenium is the ability to form Re-Re quadrupole bond which was unknown before that. In 1964, F. Albert Cotton and C.B. Harris reported the crystal structure of potassium octachlorodirhenate or  $\text{K}_2[\text{Re}_2\text{Cl}_8] \cdot 2\text{H}_2\text{O}$  where Re-Re bond was found to be as short as 224 pm<sup>11</sup>. In the light of molecular orbital theory the bond was described as  $\sigma^2\pi^4\delta^2$  bond.

In search for more interesting properties of rhenium, extensive research was commenced in the field of catalysis<sup>12-13</sup>, nuclear medicine<sup>14-19</sup>, biology<sup>20-23</sup>, photophysical behaviour<sup>24-39</sup>, sensors<sup>40-45</sup> etc.

Rhenium complexes with varying oxidation states has been providing a rich source of homogeneous and heterogeneous catalysts. It is used as catalyst in numerous organic transformations<sup>46-54</sup> as deoxydehydration of vicinal OH groups, C-O

hydrogenolysis, hydrogenation of carboxylic acids, and so on. These catalysts have shown good activity in the hydrocarbon cracking and selective hydrogenation, hydrodesulfurization of heavy crude oil and also selective dehydroaromatization of methane and ethane to benzene<sup>55-62</sup>. Rhenium complexes, in particular, of the type fac-[Re(L)(CO)<sub>3</sub>Cl] (where L is a bidentate ligand such as 2,2'-bipyridyl or two monodentate ligands such as 4,4'-bipyridyl), was used as heterogeneous catalyst in the reduction of CO<sub>2</sub><sup>63-64</sup>. Molecular design principles for the creation of efficient heterogeneous catalysts for olefin metathesis with a specific focus on rhenium compounds have been reviewed by C. Coperet<sup>65</sup>.

Rhenium-188 (<sup>188</sup>Re) is a high energy beta-emitting radioisotope with a short 16.9 h physical half-life, which has been shown to be a very attractive candidate for use in therapeutic nuclear medicine. The high beta emission has an average energy of 784 keV and a maximum energy of 2.12 MeV, sufficient to penetrate and destroy targeted abnormal tissues. In addition, the low-abundant gamma emission of 155 keV (15%) is efficient for imaging and for dosimetric calculations. Clinical trials for the management of various primary tumors, bone metastasis, rheumatoid arthritis, and endocoronary interventions were the successful application of 188-Re labelled small molecules<sup>66-68</sup>.

Many rhenium complexes shows anticancer properties among which low valent complexes show promising results. Many of these compounds display promising cytotoxic and phototoxic properties against malignant cells but they are still at the stage of preclinical studies. In recent years researchers are aiming to generate anticancer drug from higher oxidation state of rhenium complexes.

Photophysics and photochemistry<sup>69-70</sup> of molecules with relatively long-lived highly excited electronic states are mainly the matter of concern due to the vast application in optoelectronics and by the development of molecular logic devices<sup>71</sup>. Those molecules which are photochemically stable and has relatively long-lived fluorescent states can act as electronic energy donors/acceptors when incorporated into larger

supramolecular or polymeric systems. Organometallic rhenium (I) complexes with diamine ligands are able to show rich photophysical phenomenon owing to its low lying excited state<sup>72-77</sup>. It is to be noted that these metal ions show strong spin-orbit coupling and as a result the triplet metal-to-ligand charge transfer excited state (<sup>3</sup>MLCT) can emit molecular phosphorescence by borrowing the intensity of the singlet MLCT excited state. They also have an important role in light induced electron transfer reaction, excited state proton transfer reaction etc.

Rhenium complexes are more explored in recent years as sensors. Most of the studies revealed the anion sensing ability of low valent rhenium complexes. For this interesting property, metal centre plays a vital role because mere organic moieties often fail to show similar phenomenon.

Rhenium in its +1 oxidation state is in particular more interesting due to its recent development in production of organic light-emitting diodes (OLEDs)<sup>78-82</sup>, photoinduced charge transfer in dye-sensitized solar cells, cell imaging<sup>83-86</sup> and reduction of CO<sub>2</sub> to CO. The stability and reactivity of such complexes is governed by the close environment<sup>87</sup> about the metal ion and the small change in the ligand architecture can strongly influence its chemistry. Thus, in this dissertation, our focus will remain on rhenium complexes in its +1 oxidation state. To correlate with the experimental observation, computational chemistry comes as important tool. Thus, in order to explain structure, geometry, ground and excited state behaviour of rhenium complexes in presence or absence of other metal ions and anions, density functional theorem (DFT/TDDFT) is applied<sup>88-90</sup>.

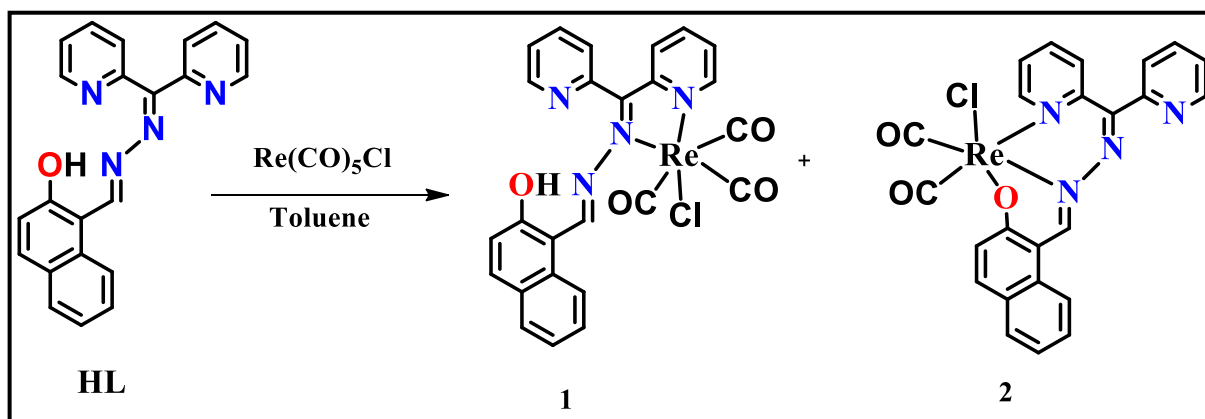
This laboratory has been active in this area and the present work forms a part of an endeavour.

## I.2 SUMMARY OF THE PRESENT WORK

The aim of the present work is to synthesize and characterization of some novel rhenium (I) complexes having polydentate Schiff base ligands. The work deals with the search for new photophysical properties of these complexes in solution phase in presence of some cations and anions. It is observed in most of the cases, that the interaction of rhenium (I) complex and cation like  $Zn^{2+}$  results in molecular rearrangements. On the other hand, anion like  $CN^-$  interact with rhenium (I) complexes by attacking the imine bond of the ligand moiety present in that complex. Some of the complexes are proved to be totally inactive in presence of cations and anions. Such behavioural pattern are well analysed by various spectroscopic techniques. Chapter-wise brief discussion about this work is given below.

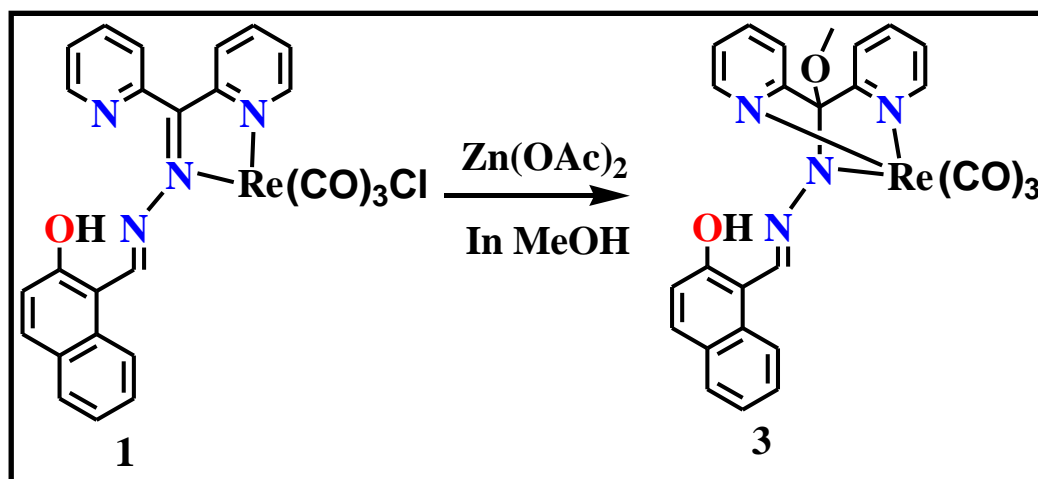
### I.2.1 Chapter II

This chapter describes the preparation of two mononuclear rhenium (I) complexes with a polydentate Schiff base ligand, HL. The complexes obtained from the reaction of HL and pentacarbonylchlororhenium(I)  $[Re(CO)_5Cl]$  was separated by column chromatography and was characterized by different spectroscopic methods. The experimental results are inter-related with the theoretical results by using Density Functional Theory (DFT) method.



### *1.2.2 Chapter III*

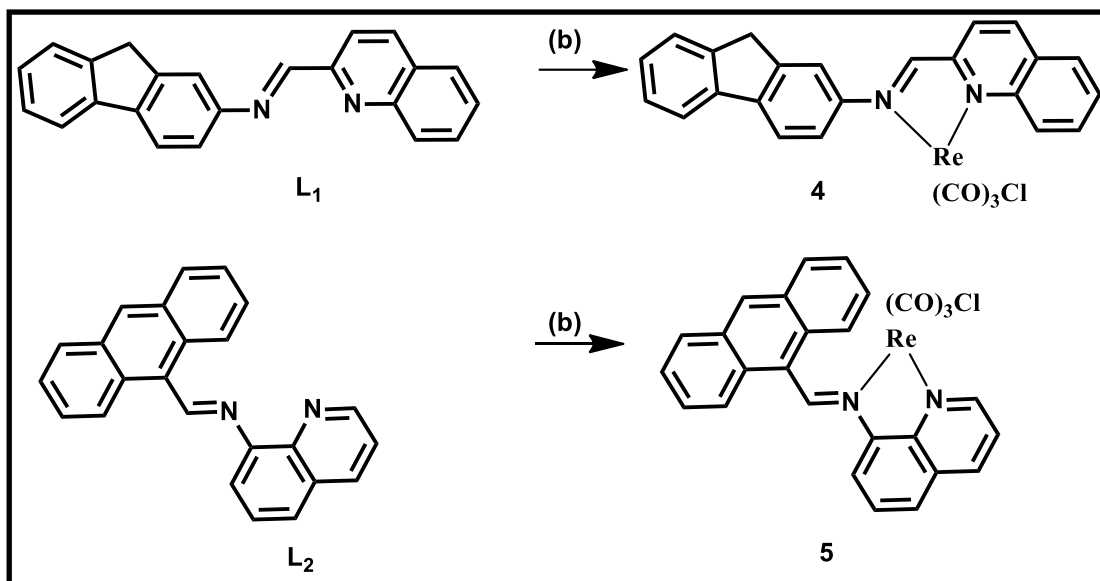
In this chapter a new kind of rhenium (I) complex was synthesized with the assistance of zinc acetate which is the extended work of chapter 1.



The structural elucidation was done by single crystal X-ray diffraction method which reveals the solvent incorporated new NNN binding rhenium (I) complex. Detailed study of the reaction is given here. Moreover, selective detection of cyanide ion by the complex was also studied and the mechanism was also established by various spectroscopic techniques.

### *1.2.3 Chapter IV*

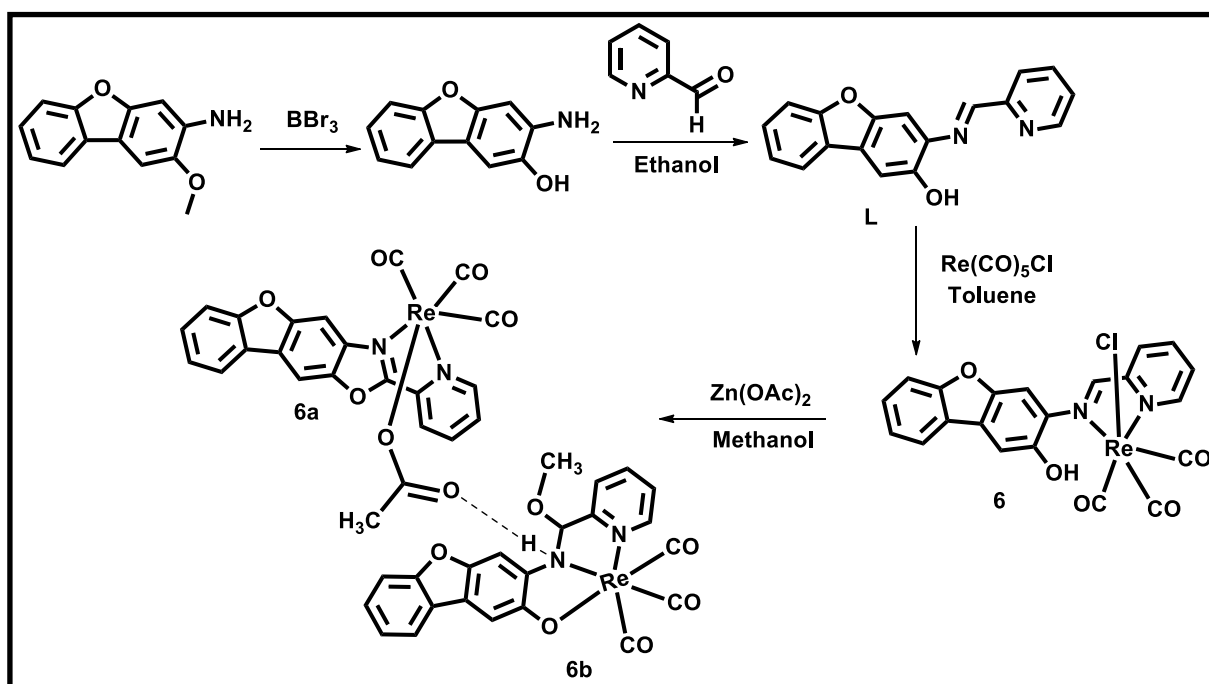
This chapter illustrate the synthesis and characterization of two mononuclear rhenium (I) complexes having anthracene and fluorene based Schiff base ligands. All the ligands and complexes were characterized by several spectroscopic techniques. The detailed study with DFT was performed for both ligands and complexes. Anthracene based complex was proved to be an efficient sensor of cyanide ion. The mechanistic study was done by  $^1\text{H}$  NMR titration.



\*\*'b' refers to  $[Re(CO)_5Cl]$  in toluene and reflux for 10 h.

### I.2.4 Chapter V

This chapter deals with the synthesis and characterization of rhenium (I) complex having dibenzofuran based Schiff base ligand. In presence of zinc acetate in methanol medium, that complex undergoes rearrangement reaction. The rearranged products are crystallized as co-crystal which is linked through hydrogen bonding with each other. The complex is able to show strong luminescence at 641 nm.



## **I.3 MEASUREMENTS**

Various physical methods have been employed for the characterization and elucidation of the properties of the synthesized compounds and these are described in the subsequent chapters. These are briefly described below.

### ***I.3.1 Elemental Analysis***

The C, H, N content of the samples were determined with the help of a Perkin-Elmer 2400 Series II elemental analyzer which utilizes thermal conductivity data for gas (CO<sub>2</sub>, H<sub>2</sub>O, N<sub>2</sub>) analysis. The sample (1.5-2.5 mg) was introduced into the combustion cell usually at a temperature in the range of 900–980° C. For combustion, pure oxygen was used and pure helium was used as the driving gas.

### ***I.3.2 Infrared Spectra***

IR spectra were recorded in KBr disk with the help of a Perkin-Elmer L-0100 spectrometer.

### ***I.3.3 Electronic Spectra***

Electronic spectra were recorded on Perkin-Elmer LAMBDA EZ-301 and a LAMBDA 25 UV/VIS spectrometer (190-1100 nm). A matched pair of quartz cells of path length 1 cm was used.

### ***I.3.4 Electrochemical Measurements***

A CHI-620A electrochemical analyzer was used for electrochemical measurements. All experiments were performed under pure nitrogen atmosphere at 295 and 298 K. The potentials are referenced to the standard calomel electrode (SCE) without junction correction.

A three-electrode system consisting of a planar Beckman model 39273 platinum inlay working electrode, platinum wire auxiliary electrode and a saturated calomel electrode (SCE) were used. In every case care was taken to obtain a flat current-voltage base line over the required voltage range in the absence of the relevant electroactive species.

### *1.3.5 Fluorescence Spectra*

The emission data were collected on Horiba Fluoromax-4 fluorescence spectrometer. For all luminescence measurements excitation and emission slit width of 5 nm were used. Cells are same as that of the electronic spectra.

### *1.3.6 Quantum yields Measurements*

Quantum yields of the complexes were determined in freeze-pump-thaw-degassed solutions of the complexes by a relative method using Quinine Sulfate in the same solvent as the standard.<sup>91</sup> The quantum yields were calculated using eq 1<sup>92</sup>,

$$\Phi_r = \Phi_{\text{std}} \frac{A_{\text{std}}}{A_r} \frac{I_r}{I_{\text{std}}} \frac{\eta_r^2}{\eta_{\text{std}}^2} \quad (1)$$

Where  $\Phi_r$  and  $\Phi_{\text{std}}$  were the quantum yields of unknown and standard samples ( $\Phi_{\text{std}} = 0.08951$  (at 298 K) in  $\text{CH}_3\text{CN}$  at  $\lambda_{\text{ex}} = 450$  nm),  $A_r$  and  $A_{\text{std}}$  ( $<0.1$ ) were the solution absorbances at the excitation wavelength ( $\lambda_{\text{ex}}$ ),  $I_r$  and  $I_{\text{std}}$  were the integrated emission intensities, and  $\eta_r$  and  $\eta_{\text{std}}$  were the refractive indices of the solvent. Experimental errors in the reported luminescence quantum yields were about 10%.

### *1.3.7 TCSPC Measurements*

Time-correlated single-photon-counting (TCSPC) measurements were carried out for the luminescence decay of complexes in a suitable solvent. For TCSPC measurement, the photoexcitation was made at 450 nm using a picosecond diode laser (IBH Nanoled-07) in an IBH Fluorocube apparatus. The fluorescence decay



data were collected on a Hamamatsu MCP photomultiplier (R3809) and were analyzed by using IBH DAS6 software.

### *1.3.8 Mass Spectra*

Electrospray ionization mass spectrometry (ESI-MS) spectra of the samples were recorded on a Micromass Qtof YA 263 mass spectrometer.

### *1.3.9 NMR Spectra*

<sup>1</sup>H and <sup>13</sup>C NMR spectra were recorded in mainly CDCl<sub>3</sub>, CD<sub>3</sub>CN and DMSO-d<sub>6</sub> with the help of Bruker FT 300 MHz spectrometer and Bruker FT 400 MHz spectrometer, respectively using tetramethylsilane (TMS) as an internal standard depending upon the solubility of the products. Signals are assigned to individual protons on the basis of chemical shifts, spin-spin structure and substituent effects. The atom-numbering scheme used for <sup>1</sup>H and <sup>13</sup>C was same as that used in the crystallography.

### *1.3.10 Crystallographic Studies*

The X-ray intensity data were collected on Bruker AXS SMART APEX CCD diffractometer (Mo K $\alpha$ ,  $\lambda = 0.71073 \text{ \AA}$ ) at 293 K. The detector was placed at a distance 6.03 cm from the crystal. Total 606 frames were collected with a scan width of 0.3 $^\circ$  in different settings of  $\varphi$ . The data were reduced in SAINTPLUS<sup>93</sup> and empirical absorption correction was applied using the SADABS package<sup>94</sup>. Metal atom was located by Patterson Method and the rest of the non-hydrogen atoms were emerged from successive Fourier synthesis. The structures were refined by full matrix least-square procedure on F<sup>2</sup>. All non-hydrogen atoms were refined anisotropically. All calculations were performed using the SHELXTL V 6.14 program package<sup>95</sup>. Molecular structure plots were drawn using the Oak Ridge thermal ellipsoid plot (ORTEP)<sup>96</sup>.

R1, wR2 and goodness-of-fit (GOF) are given by the following equations 1, 2 and 3 respectively.

$$R1 = \frac{\sum | |F_o| - |F_c| |}{\sum |F_o|} \dots\dots (1)$$

$$wR2 = [\Sigma[w(F_o^2 - F_c^2)^2] / \Sigma[w(F_o^2)^2]]^{1/2} \quad \text{..... (2)}$$

$$GOF = S = [\Sigma[w(F_o^2 - F_c^2)^2] / (n_o - n_p)]^{1/2} \quad \text{..... (3)}$$

**n<sub>o</sub>** = number of reflections

**n<sub>p</sub>** = total number of parameters refined

Specific details for each compound will be given in the concerned chapter.

### *1.3.11 DFT Study and Computational Details*

All the quantum mechanical calculations were performed with the Gaussian 09W software package<sup>97</sup>. GaussSum 2.1 program<sup>98</sup> was used to calculate the molecular orbital contributions from groups or atoms. Figures showing MOs, NTOs and the difference density plots were prepared by using the Gauss View 5.1 software. All the calculations were carried out in IBM Intellistation Z Pro 922892A machine and Super-micro Super-server work station. The geometrical structures of the singlet ground state (S<sub>0</sub>) and the lowest lying triplet excited state (T<sub>1</sub>) were optimized by the DFT<sup>99</sup> method with B3LYP exchange correlation functional<sup>100</sup> approach. The geometry of the complexes was fully optimized in solution phase without any symmetry constraints.

In the calculation, the quasirelativistic pseudopotentials of rhenium atoms proposed by Hay and Wadt<sup>101</sup> with 14 valence electrons (outer-core [(5s<sup>2</sup>5p<sup>6</sup>)] electrons and the (5d<sup>6</sup>) valence electrons) were employed, and a “double- $\xi$ ” quality basis set LANL2DZ was adopted as the basis set for Re atoms. For H we used 6-31(g) basis set and the 6-31+G(d)<sup>102</sup> basis set for C, N, O, and Cl atoms for the optimization of the ground state geometries.

The vibrational frequency calculation was also performed for all the complexes to ensure that the optimized geometries represent the local minima and there are only positive eigen values. There was a good agreement between the theoretical and experimental structures.

On the basis of the optimized ground and excited state geometry structures, the absorption and emission spectra properties in a particular solvent media were calculated by time-dependent density functional theory (TDDFT)<sup>103</sup> approach associated with the conductor-like polarizable continuum model (CPCM)<sup>104</sup>. We computed the lowest 40 singlet – singlet transition and results of the TD calculations were qualitatively very similar. The TDDFT approach had been demonstrated to be reliable for calculating spectra properties of many transition metal complexes<sup>105</sup>. Due to the presence of electronic correlation in the TDDFT (B3LYP) method it can yield more accurate electronic excitation energies. Hence TDDFT had been shown to provide a reasonable spectral feature for our complex of investigation.

Finally to understand the nature of excited states involved in absorption and emission processes natural transition orbital (NTO) analysis had been performed for all complexes. This approach provides the most compact representation of the electronic transitions in terms of an expansion into single particle orbitals by diagonalizing the transition density matrix associated with each excitation. The spin density difference map calculations were also performed to explain their optical properties.

## **I.4 CHEMICALS AND SOLVENTS**

All commercially available chemicals and solvents utilized in the present work were of analytical grade and were used without further purification. For the preparation of ligands, the solvents were dried in their usual method. Purification steps, where required, will be elaborated in appropriate chapters. The chemicals required for the synthesis of ligands were purchased from MERCK (India) and Sigma Aldrich chemicals limited.

All references in this thesis are given in the following format: Name of the author(s), *Journal*, **year**, *volume*, page.

## I.5 REFERENCES

- (1) F. A. Cotton, Wilkinson, G. *Advanced Inorganic Chemistry*, 5<sup>th</sup> Ed.; *John Wiley & Sons*, **1988**, p 850.
- (2) K. A. Conner, R. A. Walton, In *Comprehensive Coordinated Chemistry, The Synthesis, Reactions, Properties and Application of Coordination Compounds*. G. Wilkinson, R. D. Gillard, J. A. McCleverty, Eds.; *Permagon Press, Oxford*, **1987**, vol. 4, p125
- (3) N. V. Sidgewick, *The chemical Elements and Their Compounds*, *Oxford*, **1952**, vol. II, p 1292
- (4) J. D. Lee, *Concise Inorganic Chemistry*, 5<sup>th</sup> Ed.; *ELBS*, **1996**, p 734
- (5) W. Noddack, I. Tacke, O. Berg, *Naturwissenschaften*, **1925**, 3, 567
- (6) "Rhenium: Statistics and Information". Minerals Information. United States Geographical Survey, 2011, Retrieved 2011-05-25
- (7) K. K. Turekian in "Handbook of Geochemistry". Vol. I, K. H. Wedepohl, Ed., Springer-Verlag, Heidelberg, **1969**, Chapter 10.
- (8) Greenwood, N. Norman, Alan. Earnshaw, *Chemistry of the Elements*, 2<sup>nd</sup> Ed., Butterworth-Heinemann, **1997**.
- (9) George, R. "Recent Advances in the Chemistry of Rhenium". *Chem. Rev.* **1974**, 74 (5), 531-566
- (10) L. G.Liu, T. Takahashi, W.A. Bassett, "Effect of Pressure and Temperature on Lattice Parameters of Rhenium". *Journal of Physics and Chemistry of solids*, **1970**, 31 (6), 1345-1351.
- (11) F.A. Cotton, R. A., Walton *Multiple Bonds between Metal Atoms*; *Oxford Univ. Press.* **1993**.
- (12) H. S. Broadbent, G. C. Campbell, W. J. Bartley and J. H. Johnson, *J. Org. Chem.* **1959**, 24, 12, 1847-1854
- (13) H. Chen, J. F. Hartwig, *Angew. Chem. Int. Ed.*, **1999**, 13 (12), 3391-3393
- (14) N. Lepareur, F. Laccœuille, C. Bouvry, F. Hindré, E. Garcion, M. Chérel, N. Noiret, E. Garin and F. F. Russ Knapp Jr., *Frontiers in medicine*, **2019**, 6, 132. doi.org/10.3389/fmed.2019.00132

- (15) A. Guertin, C. Duchemin, F. Haddad, N. Michel, V. Métivier, *Nucl Med Biol.* **2014**, *41* 16–8. doi: 10.1016/j.nucmedbio.2013.11.003
- (16) M. E. Moustapha, G. J. Ehrhardt, C. J. Smith, L. P. Szajek, Eckelman WC, S. S. Jurisson, *Nucl Med Biol.* **2006**, *33*, 81–9. doi: 10.1016/j.nucmedbio.2005.09.006
- (17) J. R. Dilworth, S. J. Parrott, *Chem Soc Rev.* **1998** *27*, 43–55.  
doi: 10.1039/a827043z
- (18) F. Mévellec, N. Lepareur, A. Roucoux, N. Noiret, H. Patin, G. Bandoli, *Inorg Chem.* **2002**, *41*, 1591–7. doi: 10.1021/ic0110979
- (19) J. H. Wang, R. Eychenne, M. Wolff, S. Mallet-Ladeira, N. Lepareur, E. Benoist, *Eur J Inorg Chem.* **2017**, 3908–18. doi: 10.1002/ejic.201700632
- (20) J. L. Wedding, H. H. Harris, C. A. Bader, S. E. Plush, R. Mak, M. Massi, D. A. Brooks, B. Lai, S. Vogt, M. V. Werrett, P. V. Simpson, B. W. Skelton, S. Stagni, *Metallomics*, **2017**, *9*, 382.
- (21) V. Sathish, E. Babu, A. Ramdass, Z-Z. Lu, M. Velayudham, P. Thanasekaran, K-L. Lu, S. Rajagopal, *Talanta*, **2014**, *130*, 274.
- (22) J. Shelly, P. M. Kevin, W. B. John, F. V. John, D. Laurie, Z. Jon, *Bioconjugate chemistry*, **2006**, *17*, 590.
- (23) H. Y. V. Ching, X. Wang, M. He, N. P. Holland, R. Guillot, C. Slim, S. Griveau, H. C. Bertrand, C. Policar, F. Bedioui, M. Fontecave, *Inorg. Chem.*, **2017**, *56*, 2966.
- (24) J. Rohacova, O. Ishitani *Dalton Trans.*, **2017**, *46*, 8899-8919.
- (25) R. Sun, T. Wang, S. Zhang, X. Chu, B. Zhu, *RSC Adv.*, **2017**, *7*, 17063.
- (26) M. Felber, M. Bauwens, S. Imstepf, T. Fox,; F. M. Mottaghy, R. Alberto, *Eur. J. Inorg. Chem.*, **2017**, 1772.
- (27) A. Frei, D. Sidler, P.Mokolokolo, H. Braband, T. Fox, B. Spingler, A. Roodt, R. Alberto, *Inorg. Chem.*, **2016**, *55*, 9352.
- (28) C. Y. Chan, P. A. Pellegrini, I.Greguric, P. J. Barnard, *Inorg. Chem.*, **2014**, *53*, 10862.
- (29) T. Mukuta, P. V. Simpson, J. G. Vaughan, B. W. Skelton, S. Stagni, M. Massi, K. Koike, O. Ishitani, K. Onda, *Inorg. Chem.*, **2017**, *56*, 3404.
- (30) S. Satoa, O. Ishitani; *Coordination Chemistry Reviews*, **2015**, *282*, 50–59.

- (31) J. Rohacova, A. Sekine, T. Kawano,; S. Tamari, O. Ishitani, *Inorg. Chem.*, **2015**, *54*, 8769.
- (32) C. Liu, Y. Si, S. Shi, G. Yang, and X. Pan, *Dalton Trans.*, **2016**, *45*, 7285.
- (33) C. Y. Chan, P. A. Pellegrini, I. Greguric, P. J. Barnard, *Inorg. Chem.*, **2014**, *53*, 10862.
- (34) M. P. Coogan, J. A. Platts, *Chem. Commun.* **2016**, *52*, 12498
- (35) C. M. Ivarez, R. Carrillo, R. G. Rodriguez, D. Miguel, *Chem. Eur. J.*, **2013**, *19*, 8285
- (36) (a) P. Gómez Iglesias, F. Guyon, A. Khatyr, G. Ulrich, M. Knorr, J. M. MartínAlvarez, D. Miguel, F. Villafaña, *Dalton Trans.*, **2015**, *44*, 17516.  
(b) P. Gómez-Iglesias, J. M. Martín-Alvarez, D. Miguel, F. Villafaña, *Dalton Trans.*, **2015**, *44*, 17478.
- (37) (a) T. Kaur, W-Z. Lee, M. Ravikanth *Inorg. Chem.*, **2016**, *55*, 5305.  
(b) T. Kaur, A. Ghosh, P. Rajakannu, M. Ravikanth, *Inorg. Chem.*, **2014**, *53*, 2355.  
(c) A. Ghosh, M. Ravikanth, *Inorg. Chem.* **2012**, *51*, 6700.
- (38) (a) P. Mondal, R. Sarkar, A. Hens, K. K. Rajak, *RSC Adv.* **2014**, *4*, 38769.  
(b) R. Sarkar, P. Mondal; K. K. Rajak, *Dalton Trans.* **2014**, *43*, 2859.
- (39) P. Piehl, M. Peña-López, A. Frey, H. Neumann, M. Beller, *Chem. Commun.* **2017**, *53*, 3265.
- (40) N. J. Lundin, P. J. Walsh, S. L. Howell, A. G. Blackman and K. C. Gordon, *Chem.-Eur. J.* **2008**, *14*, 11573
- (41) S. T. Lam, N. Zhu, V. W. W. Yam, *Inorg. Chem.* **2009**, *48*, 9664
- (42) X. Li, D. Zhang, G. Lu, G. Xiao, H. Chi, Y. Dong, Z. Zhang and Z. Hu, *J. Photochem. Photobiol.* **2012**, *241*, 1
- (43) W. K. Chu, C. C. Ko, K. C. Chan, S. M. Yiu, F. L. Wong, C. S. Lee and V. A. L. Roy, *Chem. Mater.* **2014**, *26*, 2544
- (44) G. W. Zhao, Y. X. Hu, H. J. Chi, Y. Dong, G. Y. Xiao, X. Li and D. Y. Zhang, *Opt. Mater.* **2015**, *47*, 173

- (45) X. Li, D. Zhang, W. Li, B. Chu, L. Han, J. Zhu, Z. Su, D. Bi, D. Wang, D. Yang and Y. Chen, *Appl. Phys. Lett.* **2008**, *92*, 083302
- (46) M. Naruto, S. Agrawal, K. Toda, & S. Saito, *Scientific Reports*, **2017**, *7*, 3425.
- (47) (a) R. G. Harms, W. A. Herrmann, F. E. Kühn, *Coord. Chem. Rev.* **2015**, *296*, 1.  
(b) M. Cokoja, I. I. Markovits, E. M. H. Anthofer, S. A. Poplata, D. S. Pöthig, P. A. T. Morris, W. A. Herrmann, F. E. Kühn, J. B. Love, *Chem. Commun.* **2015**, *51*, 3399.  
(c) F. E. Kuhn, A. Scherbaum, W. A. Herrmann, *J. Organomet. Chem.* **2004**, *689*, 4149.  
(d) C. C. Romão, F.E. Kühn, W. A. Herrmann, *Chem. Rev.* **1997**, *97*, 3197.
- (48) (a) N. Kishino, J. H. Espenson, *Inorg. Chem.* **2003**, *42*, 5735.  
(b) X. Shan, A. Ellern, I. A. Guzei, and J. H. Espenson, *Inorg. Chem.* **2003**, *42*, 5735.  
(c) J. Dixon, J. H. Espenson, *Inorg. Chem.*, **2002**, *41*, 4727.
- (49) (a) M. G. Mazzotta, M. Xiong, M. M. Abu-Omar, *Organometallics* **2017**, *36*, 1688.  
(b) J. Arias, C. R. Newlands, M. M. Abu-Omar, *Inorg. Chem.* **2001**, *40*, 2185.  
(c) G. S. Owens, J. Arias, M. M. Abu-Omar, *Catal. Today* **2000**, *55*, 317.
- (50) (a) N. Zwettler, J. A. Schachner, F. Belaj, N. C. Mo sch-Zanetti, *Inorg. Chem.* **2016**, *55*, 5973.  
(b) N. Zwettler, J. A. Schachner, F. Belaj, N. C. Mo sch-Zanetti, *Inorg. Chem.* **2014**, *53*, 12832.  
(c) K. R. Grünwald, G. Saischek, M. Volpe, N. C. Mösch-Zanetti, *Inorg. Chem.* **2011**, *50*, 7162.
- (51) (a) M. G. Mazzotta, M. Xiong, M. M. Abu-Omar, *Organometallics*, **2017**, *36*, 1688.  
(b) J. Arias, C. R. Newlands, M. M. Abu-Omar, *Inorg. Chem.*, **2001**, *40*, 2185.  
(c) G. S. Owens, J. Arias, M. M. Abu-Omar, *Catal. Today* **2000**, *55*, 317.
- (52) (a) N. S. Lambic, C. A. Brown, R. D. Sommer, E. A. Ison, *Organometallics* **2017**, *36*, 2042.

- (b) D. E. Pérez, J. L. Smeltz, R. D. Sommer, P. D. Boyle, E. A. Ison, *Dalton Trans.* **2017**, 46, 4609.
- (c) N. S. Lambic, R. D. Sommer, E. A. Ison, *ACS Catal.* **2017**, 7, 1170.
- (d) L. K. Robbins, C. P. Lilly, R. D. Sommer, E. A. Ison, *Organometallics* **2016**, 35, 3530.
- (53) (a) S. Das, A. Chakravorty, *Eur. J. Inorg. Chem.* **2006**, 2285.
- (b) I. Chakraborty, S. Bhattacharya, S. Banerjee, B. K. Dirghangi, A. Chakravorty, *J. Chem. Soc. Dalton Trans.* **1999**, 3747.
- (54) (a) J. R. Bernardo, A. C. Fernandes, *Green Chem.* **2016**, 18, 2675.
- (b) I. Gryca, B. Machura, J. G. Małeck, J. Kusz, L. S. Shul'pina, N. S. Ikonnikov, G. B. Shul'pin, *Dalton Trans.* **2016**, 45, 334.
- (c) S. Dinda, A. Genest, N. Rosch, *ACS Catal.* **2015**, 5, 4869.
- (d) Sousa, S. C.; Cabrita, I.; Fernandes, A. C. *Chem. Soc. Rev.*, 2012, 41, 5641.
- (55) Laurenti, D.; NinhThi, K.T.; Escalona, N.; Massin, L.; Vrinat, M.; Llambias, F.J.G. *Catal. Today* **2008**, 130, 50–55.
- (56) Okal, J.; Kubicka, H. *Appl. Catal. A* **1998**, 171, 351–359. Escalona, N.; Vrinat, M.; Laurenti, D.; Llambias, F.J.G. , *Appl. Catal. A* **2007**, 322, 113–120.
- (57) Rätty, J.; Pakkanen, T.A. *Catal. Lett.* **2000**, 65, 175–180.
- (58) Escalona, N.; Llambias, F.J.G.; Vrinat, M.; Nguyen, T.S.; Laurenti, D.; Agudo, A.L. *Catal. Comm.* **2007**, 8, 285–288.
- (59) Escalona, N.; Ojeda, J.; Cid, R.; Alves, G.; Agudo, A.L.; Fierro, J.L.; Llambias, F.J.G. *Appl. Catal. A* **2002**, 234, 45–54.
- (60) Wang, L.; Ohnishi, R.; Ichikawa, M. *J. Catal.* **2000**, 190, 276–283.
- (61) Shu, Y.; Ohnishi, R.; Ichikawa, M. *Appl. Catal. A* **2003**, 252, 315–329.
- (62) Wang, L.S.; Murata, K.; Inaba, M. *Catal. Today* **2003**, 82, 99–104
- (63) K. Talukdar, S. Sinha Roy, E. Amatya, E. A. Sleeper, P. Le Magueres, and J. W. Jurss, *Inorg. Chem.* **2020**, 59, 9, 6087–6099
- (64) M. R. Crawley, K. J. Kadassery, A. N. Oldacre, A. E. Friedman, D. C. Lacy, and T. R. Cook, *Organometallics* **2019**, 38, 7, 1664–1676
- (65) C. Coperet, *New. J. Chem.* **2004**, 28, 1–10
- (66) W. A. Volkert, T. J. Hoffman *Chem Rev.* **1999**, 99, 2269–92



- (67) J. F. Chatal, C. A. Hoefnagel, *Lancet*. **1999**, 354, 931-5. 10.1016/S0140-6736(99)06002-X
- (68) S. Srivastava, E. Dadachova *Recent Nucl Med*. **2001**, 31, 330-41. 10.1053/snuc.2001.27043
- (69) (a) N. Akabar, V. Chaturvedi, G. E. Shillito, B. J. Schwehr, K. C. Gordon, G. S. Huff, J. J. Sutton, B. W. Skelton, A. N. Sobolev, S. Stagni, D. J. Nelsonb and M. Massi, DOI: 10.1039/C9DT02198A, *Dalton Trans*. **2019** Advance Article  
(b) D. Sinha, S. P. Parua, K. K. Rajak, *Journal of Organometallic Chemistry* **2019** 889, 62-69  
(c) L. D. Ramos, R. N. Sampaio, F. F. de Assis, K. T. de Oliveira, P. Homem-de-Mello, A. O. T. Patrocinio and K. P. M. Frin, *Dalton Trans*. **2016**, 45, 11688-11698
- (70) (a) G. Balakrishnana, T. Rajendrana, K. S. Murugana, M. Ganesana, V. K. Sivasubramaniana, S. Rajagopal, *Journal of Luminescence* **2019**, 205, 51-60
- (71) P. Gómez-Iglesias, F. Guyon, A. Khatyr, G. Ulrich, M. Knorr, J. M. Martín-Alvarez, D. Miguela, F. Villafaña *Dalton Trans*. **2015**, 44, 17516-17528
- (72) L. Veronese, E. Q. Procopio, F. De Rossi, T. M. Brown, P. Mercandelli, P. Mussini, G. D'Alfonso, M. Panigati, *New J. Chem.*, **2016**, 40, 2910 and references therein.
- (73) C.-C. Chou, F. -C. Hu, H. -H. Yeh, H. -P. Wu, Y. Chi, J. N. Clifford, E. Palomares, S. -H. Liu, P. -T. Chou, G. -H. Lee, *Angew. Chem. Int. Ed*. **2014**, 53, 178
- (74) C. A. Bignozzi, R. Argazzi, R. Boaretto, E. Busatto, S. Carli, F. Ronconi, S. Caramori, *Coord. Chem. Rev*. **2013**, 257, 1472
- (75) A. Hagfeldt, G. Boschloo, L. -C. Sun, L. Kloo, H. Pettersson, *Chem. Rev*. **2010**, 110, 6595
- (76) M. K. Nazeeruddin, M. Graätzel, In *Comprehensive Coordination Chemistry II, Vol. 9*; J. A. McCleverty, T. J. Meyer, Eds. Elsevier Pergamon: Oxford, U.K., **2004**, 719-758.
- (77) L. J. Raszeja, D. Siegmund, A. L. Cordes, J. Gu'ldenhaupt, K. Gerwert, S. Hahnc, N. Metzler-Nolte, *Chem. Commun*. **2017**, 53, 905

- (78) B. J. Coe, S. P. Foxon, R. A. Pilkington, S. Sa'nchez, D. Whittaker, K. Clays, N. V. Steerteghem, B. S. Brunshwig, *Organometallics* **2016**, *35*, 3014-3024 and references therein
- (79) X.-L. Yang, X. -B. Xu, G.- J. Zhou, *J. Mater. Chem. C.* **2015**, *3*, 913-944.
- (80) C. -L. Ho, H. Li, W. -Y. Wong, *J. Organomet. Chem.* **2014**, *751*, 261-285.
- (81) Y. Chi, P. -T. Chou, *Chem. Soc. Rev.* **2010**, *39*, 638-655.
- (82) Yersin, H. Ed.; Wiley-VCH: Weinheim, Germany, Highly Efficient OLEDs with Phosphorescent Materials; **2008**.
- (83) J. L.; Wedding, H. H. Harris, C. A. Bader, S. E. Plush, R. Mak, M. Massi, D. A. Brooks, B. Lai, S. Vogt, M. V. Werrett, P. V. Simpson, B. W. Skelton, S. Stagni, *Metallomics*, **2017**, *9*, 382.
- (84) Sathish, V.; Babu, E.; Ramdass, A.; Lu, Z-Z.; Velayudham, M.; Thanasekaran, P.; Lu, K-L.; Rajagopal, S. *Talanta*, **2014**, *130*, 274.
- (85) Shelly, James.; Kevin, P. M.; John, W. B.; John, F. V.; Laurie, D.; Jon, Z. *Bioconjugate chemistry*, **2006**, *17*, 590.
- (86) Ching, H. Y. V.; Wang, X.; He, M.; Holland, N. P.; Guillot, R.; Slim, C.; Griveau, S.; Bertrand, H. C.; Policar, C.; Bedioui, F.; Fontecave, M. *Inorg. Chem.*, **2017**, *56*, 2966.
- (87) (a) P. Mondal, A. Hens, S. Basak, K. K. Rajak *Dalton Trans.* 2013, **42**, 153 (b) R. Sarkar, P. Mondal, K. K. Rajak *Dalton Trans.* 2014, **43**, 2859
- (88) J. Eng, C. Daniel, *J. Phys. Chem. A* **2015**, *119*, 10645
- (89) D. H. Valdés, R. U. J. Alberto, *RSC Adv.*, **2016**, *6*, 107127.
- (90) E. Gindensperger, H. Koppel, C. Daniel, *Chem. Commun.* **2010**, *46*, 8225
- (91) (a) B. P. Sullivan, D. J. Salmon, T. J. Meyer, J. Peedrin, *Inorg. Chem.*, **1979**, *18*, 3369-3374
- (b) A. Juris, V. Balzani, F. Barigelletti, S. Campagna, P. Besler, von Zelewsky, A. *Coord. Chem. Rev.* **1988**, *84*, 85-277.
- (92) J. Van Houten, R. J. Watts, *J. Am. Chem. Soc.* **1976**, *98*, 4853-4858.
- (93) SMART; SAINT; SADABS; XPREP; SHELXTL, Bruker AXS Inc., Madison, WI, **1998**.
- (94) Sheldrick, G. M. SHELXTL, v. 6.14, Bruker AXS Inc., Madison, WI, **2003**.

- (95) Johnson, C. K. ORTEP Report ORNL-5138, Oak Ridge National Laboratory, Oak Ridge, TN, **1976**.
- (96) J. Wagler, D. Gerlach and G. Roewer, *Inorg. Chim. Acta*, **2007**, *360*, 1935–1942.
- (97) M. J. Frisch, G. W. Trucks, H. B. Schlegel, G. E. Scuseria, M. A. Robb, J. R. Cheeseman, G. Scalmani, V. Barone, B. Mennucci, G. A. Petersson, H. Nakatsuji, M. Caricato, X. Li, H. P. Hratchian, A. F. Izmaylov, J. Bloino, G. Zheng, J. L. Sonnenberg, M. Hada, M. Ehara, K. Toyota, R. Fukuda, J. Hasegawa, M. Ishida, T. Nakajima, Y. Honda, O. Kitao, H. Nakai, T. Vreven, J. A. Montgomery Jr., J. E. Peralta, F. Ogliaro, M. Bearpark, J. J. Heyd, E. Brothers, K. N. Kudin, V. N. Staroverov, R. Kobayashi, J. Normand, K. Raghavachari, A. Rendell, J. C. Burant, S. S. Iyengar, J. Tomasi, M. Cossi, N. Rega, J. M. Millam, M. Klene, J. E. Knox, J. B. Cross, V. Bakken, C. Adamo, J. Jaramillo, R. Gomperts, R. E. Stratmann, O. Yazyev, A. J. Austin, R. Cammi, C. Pomelli, J. W. Ochterski, R. L. Martin, K. Morokuma, V.G. Zakrzewski, G.A. Voth, P. Salvador, J. J. Dannenberg, S. Dapprich, A. D. Daniels, O. Farkas, J. B. Foresman, J. V. Ortiz, J. Cioslowski, D. J. Fox, Gaussian 09, (Revision A.1), Gaussian, Inc., Wallingford, CT, 2009
- (98) N. M. O'Boyle, A. L. Tenderholt, K. M. Langner, *J. Comput. Chem.* **2008**, *29*, 839-845
- (99) E. Runge, E. K. U. Gross, *Phys. Rev. Lett.* **1984**, *52*, 997-1000
- (100) (a) A. D. Becke, *J. Chem. Phys.*, **1993**, *98*, 5648-5652.  
(b) C. Lee, W. Yang, R. G. Parr, *Phys. Rev. B.*, **1988**, *37*, 785-789.
- (101) (a) P. J. Hay, W. R. Wadt, *J. Chem. Phys.*, **1985**, *82*, 270-283.  
(b) P. J. Hay, W. R. Wadt, *J. Chem. Phys.*, **1985**, *82*, 299-310.
- (102) X. Gao, Y. Wang, Y. Wang, J. Jia, X. Su, *Sci. Sin. Chim.* **2011**, *41*, 1145-1155.
- (103) (a) M. E. Casida, C. Jamoroski, K. C. Casida, D. R. Salahub, *J. Chem. Phys.* **1998**, *108*, 4439-4449.  
(b) R. E. Stratmann, G. E. Scuseria, M. J. Frisch, *J. Chem. Phys.* **1998**, *109*, 8218-8224  
(c) R. Bauernschmitt, R. Ahlrichs, *Chem. Phys. Lett.*, **1996**, *256*, 454-464
- (104) (a) V. Barone, M. J. Cossi, *Phys. Chem. A.*, **1998**, *102*, 1995-2001

- (b) M. Cossi, V. J. Barone, *Chem. Phys.*, **2001**, *115*, 4708-4717
- (c) M. Cossi, N. Rega, G. Scalmani, V. J. Barone, *Comp. Chem.*, **2003**, *24*, 669-681.
- (105) (a) T. Liu, H. -X. Zhang, B. -H. Xia, *J. Phys. Chem. A.*, **2007**, *111*, 8724-8730.
- (b) X. Zhou, H. -X. Zhang, Q.-J. Pan, B. -H. Xia, Tang, A.-C. *J. Phys. Chem. A.*, **2005**, *109*, 8809-8818.
- (c) X. Zhou, A. -M. Ren, J. -K. Feng, *J. Organomet. Chem.*, **2005**, *690*, 338-347.
- (d) A. Albertino, C. Garino, S. Ghiani, R. Gobetto, C. Nervi, L. Salassa, E. Rosenverg, A. Sharmin, G. Viscardi, R. Buscaino, G. Cross, M. J. Milanesio, *Organomet. Chem.*, **2007**, *692*, 1377-1391.

A decorative scroll with a black outline, featuring a rolled-up edge on the left and a small loop at the top right. The text "CHAPTER II" is centered within the scroll in a bold, black, serif font.

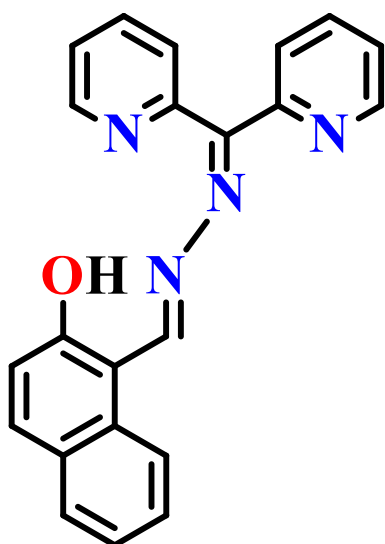
**CHAPTER II**



# Synthesis, Characterization and Theoretical Studies of a Multifunctional Ligand and Complexes of Rhenium (I)

## ABSTRACT

HL [(E)-1-(((di(pyridin-2-yl)methylene)hydrazono)methyl)naphthalen-2-ol], which is a multifunctional ligand was synthesized using two distinct carbonyl compounds and hydrazine. Two different mononuclear rhenium (I) complexes were synthesized by performing only one reaction using HL and rhenium (I) precursor  $\text{Re}(\text{CO})_5\text{Cl}$  [pentacarbonylchlororhenium (I)]. The complex **1**,  $[\text{Re}(\text{HL})(\text{CO})_3\text{Cl}]$ , was obtained



**HL**

in excellent yield by reacting with  $\text{Re}(\text{CO})_5\text{Cl}$  with HL in a 1:1 ratio in dry toluene under argon atmosphere. The complex **2**,  $[\text{Re}(\text{L})(\text{CO})_3]$ , was found as a co-product of the above mentioned reaction. Experiments proved that the complex **2** can also be prepared in high yield from the similar reaction using triethylamine as an additional ingredient. X-ray crystallographic study reveals that in complex **1**, the ligand binds as NN coordinating bidentate ligand while that of in **2** it behaves as monoanionic NNO coordinating tridentate ligand. The complexes **1** and **2** were characterised by different physicochemical

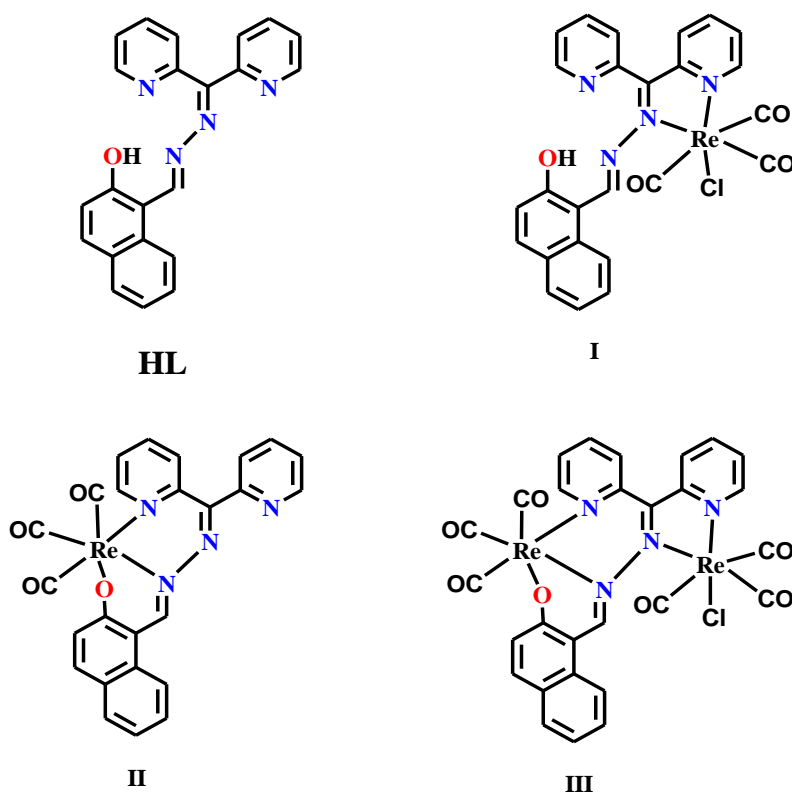
techniques (NMR, IR, ESI-Mass spectroscopy, UV-Vis Spectroscopy) and the observed properties have been interpreted with the help of DFT (density functional theory) and TDDFT (time dependent density functional theory) calculations. The complexes were found to be weakly emissive in nature.





## II.1. INTRODUCTION

Studies on rhenium (I)  $\alpha$ -diimine complexes<sup>1</sup> have received a great deal of attention in recent years. The interest mainly arises because these classes of compounds exhibit interesting light harvesting properties,<sup>2</sup> as well as activate the energy or electron transfer processes in protein molecules.<sup>3</sup> Emission properties of rhenium (I) complexes with NN coordinating pyridine-imine based ligands are associated with the low lying metal-to-ligand charge-transfer (MLCT) states.<sup>1(a), (b), 4</sup> The close environment around the metal center regulates the excited state properties of the molecule and the small change in the ligand architecture can strongly influence its properties.<sup>5</sup> This work concerns about the design of unsymmetrical bi-functional ligand and the coordination pattern of the same with  $[\text{Re}(\text{CO})_3]^+$  core. In this paper, we have used a mixed Schiff base ligand, HL, derived from di-pyridylketone and 2-hydroxynaphthaldehyde linked via hydrazine. Having multiple donor sites the ligand is expected to coordinate with rhenium (I) centre through different mode of binding as shown below.



In practical, only two mononuclear facial rhenium (I) complexes II and III are obtained and isolated. The complexes were characterized by single crystal X-ray structure determination along with the help of various spectroscopic methods. The electrochemical behaviour in acetonitrile solution is also examined.

The properties of both ground and excited states the complexes can be calculated at the first-principle level using Density functional theory (DFT) and especially the improvement of time-dependent density functional theory (TDDFT), with good accuracy. Here we also report a detailed theoretical calculation aiming to get better insight into its geometry, electronic structure and complete assignment of experimentally observed spectral properties of the complexes using density functional theory (DFT), time-dependent density functional theory (TDDFT) as well as natural transition orbital (NTO) analysis.

## **II.2. EXPERIMENTAL SECTION**

### *A. Materials*

Re(CO)<sub>5</sub>Cl, 2,2'-Dipyridyl ketone, 2-hydroxynaphthaldehyde were purchased from Sigma Aldrich. All solvents and chemicals are analytically pure. All the reactions with Re(CO)<sub>5</sub>Cl are carried out under argon atmosphere.

### *B. Preparation of Compounds*

#### *LIGAND*

2,2'-Dipyridyl ketone (1 gm, 5.428 mmol), 2 ml hydrazine hydrate and 1 drop of HCl was dissolved in 20 ml ethanol and refluxed for 2 h. The resulting yellow coloured solution was refluxed for 8 h. Then the solvent was evaporated under reduced pressure. The remaining oily product was washed with water and separated into ethyl acetate to eliminate unreacted reactants. Then the organic part was collected over dry Na<sub>2</sub>SO<sub>4</sub> and evaporated to obtain an oily product SB.NH<sub>2</sub> (given in scheme 1). Yield: 75%, <sup>1</sup>H NMR (CDCl<sub>3</sub>, 400 MHz): δ 8.58 (d, 1H, J=16 Hz); 8.41 (s, 1H); 7.71 (d, 1H, J=8), 7.60 (q, 1H), 7.28 (d, 1H, J=8), 7.16-7.06 (m, 3H), 4.24 (s, 1H). The product

obtained from above procedure (500 mg, 2.52 mmol) was dissolved in 20 ml ethanol followed by addition of 2-hydroxy naphthaldehyde (433mg, 2.52 mmol). The solution was then refluxed for another 6 h. It was cooled to room temperature and yellow colour precipitate was obtained. It was collected under suction filtration and washed with ethanol. Yield: 80%,  $^1\text{H NMR}$  ( $\text{CDCl}_3$ , 400 MHz):  $\delta$  12.71 (s, 1H); 9.79 (s, 1H); 8.84 (d, 1H,  $J=4$ ), 8.7 (s, 1H), 8.16 (t, 2H,  $J=4$ ), 7.91 (d, 1H,  $J=4$ ), 7.78-7.82 (m, 3H), 7.53 (t, 2H,  $J=8$ ), 7.45 (s, 1H), 7.26 (d, 1H,  $J=8$ ), 7.07 (s, 1H). Anal. Calcd for  $\text{C}_{22}\text{H}_{16}\text{N}_4\text{O}$ : C, 48.00; H, 2.15; N, 5.60. Found: C, 48.10; H, 2.30; N, 5.73. IR ( $\text{cm}^{-1}$ ):  $\nu$  (O-H): 3043;  $\nu$  (imine C=N): 1622, 1603

### *COMPLEX 1, fac-[Re(HL)(CO)<sub>3</sub>Cl]*

HL (97 mg, 0.276 mmol) and  $\text{Re}(\text{CO})_5\text{Cl}$  (100mg, 0.276 mmol) were refluxed in 30 ml of toluene in oil bath for 8 h. After cooling to room temperature, the solvent was removed under reduced pressure. The crude mass was dissolved in a minimum volume of benzene and subjected to column chromatography on a silica gel column (60–120 mesh). A faint red band was observed and eluted by 20% ethyl acetate: hexane solution. A red product was obtained with a very low yield. After that, an orange band was eluted by 45% ethyl acetate: hexane solution. An orange coloured solid was obtained after removal of solvent under reduced pressure. The product was recrystallized in dichloromethane-hexane. Slow diffusion of dichloromethane into hexane afforded beautiful red coloured crystal. Yield: 60%,  $^1\text{H NMR}$  ( $\text{CDCl}_3$ , 400 MHz):  $\delta$  11.206 (s, 1H); 10.28 (s, 1H), 9.16 (d, 1H,  $J=8$ ), 8.88 (d, 1H), 8.27 (d, 1H,  $J=12$ ), 7.42 (t, 1H,  $J=12$ ), 7.76 (d, 1H,  $J=8$ ), 7.89 (d, 1,  $J=12$ ), 7.97 (s, 1H). ESI-MS ( $\text{CH}_2\text{Cl}_2$ ):  $m/z$  657  $[\text{M}]^+$ . Anal. Calcd for  $\text{C}_{25}\text{H}_{16}\text{N}_4\text{O}_4\text{Re}$ : C, 45.42; H, 2.90; N, 8.47. Found: C, 45.50; H, 2.93; N, 8.60. IR ( $\text{cm}^{-1}$ ):  $\nu$  (CO): 2017, 1886.25, 1917.02;  $\nu$  (imine C=N): 1621.96;  $\text{IR}_{\text{theo}}$  ( $\text{cm}^{-1}$ ):  $\nu$  (CO): 2009, 1898, 1935;  $E_{\text{pa}}$  ( $\text{Re}^{\text{I}}/\text{Re}^{\text{II}}$  couple): 1.30 V (irr).

### *COMPLEX 2, fac-[Re(L)(CO)<sub>3</sub>]*

Re(CO)<sub>5</sub>Cl (100 mg, 0.276 mmol), HL (70 mg, 0.276 mmol) and triethylamine (0.039 ml, 0.28 mmol) were taken in 30 ml toluene and then the resulting mixture was refluxed for 10 h. After cooling to room temperature, the solvent was removed under reduced pressure. The crude mass was dissolved in a minimum volume of benzene and subjected to column chromatography on a silica gel column (60–120 mesh). A red band was eluted using 45% ethyl acetate: hexane solution. A red coloured solid was obtained after removal of the solvent under reduced pressure. The product on recrystallization from dichloromethane–hexane afforded red coloured crystals. Now the red product was obtained with high yield. Yield: 60%, <sup>1</sup>H NMR (CDCl<sub>3</sub>, 300 MHz): δ 9.18 (t, 1H, J=3), 8.70 (t, 1H, J=3), 8.61 (s, 1H), 8.26 (d, 1H, J=6), 7.9–7.45 (m, 9H), 6.95 (d, 1H, J=9). ESI-MS (CH<sub>2</sub>Cl<sub>2</sub>): m/z 623.007 [M+H]<sup>+</sup>. Anal. Calcd. for C<sub>25</sub>H<sub>15</sub>N<sub>4</sub>O<sub>4</sub>Re: C, 48.00; H, 2.15; N, 5.60. Found: C, 48.10; H, 2.30; N, 5.73. IR (cm<sup>-1</sup>): ν (CO): 2011, 1906, 1882; ν (C=N): 1620, IR<sub>theo</sub> (cm<sup>-1</sup>): ν (CO): 2030, 1917, 1892; E<sub>pa</sub> (Re<sup>I</sup>/Re<sup>II</sup> couple): 1.48 V (irr).

### *C. X-Ray Structure Determination*

The single crystal suitable for X-ray crystallographic analysis of complexes *fac*-[Re(HL)(CO)<sub>3</sub>Cl] and *fac*-[Re(L)(CO)<sub>3</sub>] were grown by slow diffusion of dichloromethane into hexane at room temperature. Details of the X-ray work are given in tabular form in **Table II.1** and **Table II.2** (See also Chapter I).

### *D. Physical Measurements*

All physical measurements that included elemental analyses, IR, absorption spectra, <sup>1</sup>H NMR and spectra, ESI mass spectra, emission spectra measurement were performed as described in **Chapter I**.

**Table II.1** Atomic coordinates and isotropic thermal parameters complexes 1 and 2

<b>Data collection</b>		
	<b>Complex 1</b>	<b>Complex 2</b>
Total refl. Collected	38281	75022
Unique refl.(R <sub>int</sub> )	5474	5043
Used refl.	3937	4116
h k l range	-40<h<40 -12<k<12 -21<l<22	-27<h<29 -29<k<29 -22<l<22

<b>Structure solution and refinement</b>		
	<b>Complex 1</b>	<b>Complex 2</b>
Solution	Patterson	Patterson
Refinement	Full-matrix least-squares on F <sup>2</sup>	Full-matrix least-squares on F <sup>2</sup>
GOF on F <sup>2</sup>	1.301	0.789
R1, <sup>a</sup> [I>2σ(I)]	0.0343	0.0255
wR2 <sup>b</sup> [I>2σ(I)]	0.0834	0.1011
R1[alldata]	0.0421	0.0374
wR2[alldata]	0.1619	0.1011

**Table II.2** Crystal data and structure refinement parameters for complexes **1** and **2**

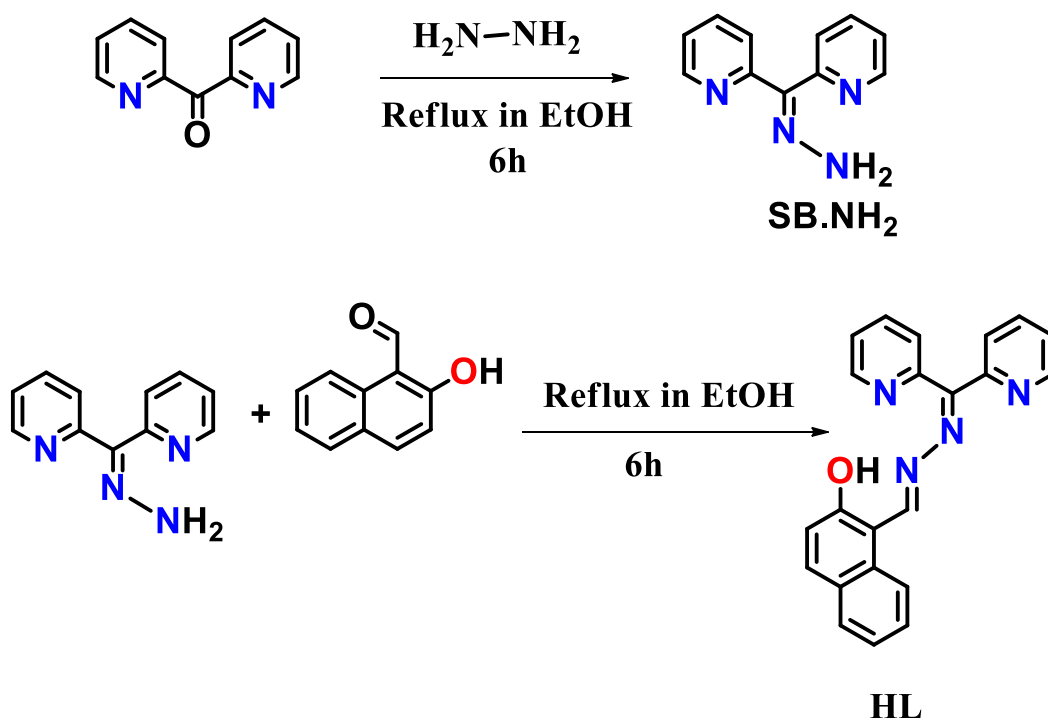
	<b>1</b>	<b>2</b>
Formula	C <sub>25</sub> H <sub>16</sub> N <sub>4</sub> O <sub>4</sub> ClRe	C <sub>25</sub> H <sub>15</sub> N <sub>4</sub> O <sub>4</sub> Re
M <sub>r</sub>	658.08	621.06
Crystal system	Monoclinic	Tetragonal
Space group	C 2/c	I 41/a
a / Å	31.198 (8)	22.5847(5)
b / Å	9.814(2)	22.5847(5)
c / Å	17.652(4)	17.1723(5)
α /°	90	90
β /°	117.801(12)	90
γ /°	90	90
V / Å <sup>3</sup>	4781(2)	8759.1(5)
Z	8	16
D <sub>calcd</sub> / g cm <sup>-3</sup>	1.829	1.886
μ / mm <sup>-1</sup>	5.235	5.591
θ /°	1.476-27.498	1.490-27.498
T /K	296	296

$${}^a R1 = \frac{\sum ||F_o| - |F_c||}{\sum |F_o|}, {}^b wR2 = \left[ \frac{\sum [w(F_o^2 - F_c^2)^2]}{\sum [w(F_o^2)^2]} \right]^{1/2}$$

## II.3. RESULT AND DISCUSSION

### A. Synthesis

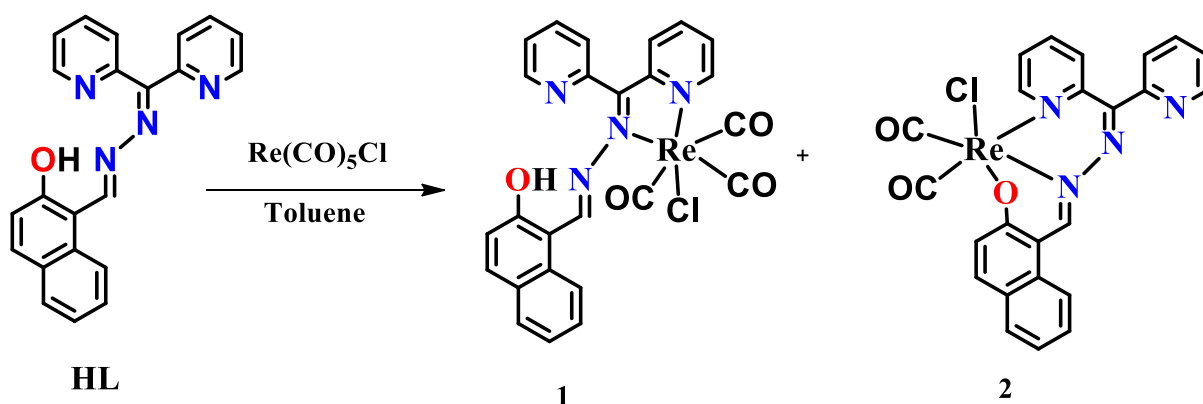
*Ligand (HL)*: The synthesis of the multifunctional ligand (**HL**) was accomplished by two steps. The stoichiometric reaction of hydrazine hydrate and 2,2'-dipyridylketone fabricates the yellow coloured oily compound **SB.NH<sub>2</sub>**. The compound **SB.NH<sub>2</sub>** was further allowed to react with 2-hydroxynaphthaldehyde, which effectively produce **HL** as yellow solid (**Scheme II.1**).



*Scheme II.1* Schematic representation for the synthesis of the ligand

*Complexes 1, [Re(HL)(CO)<sub>3</sub>Cl] and 2, [Re(L)(CO)<sub>3</sub>]*: The stoichiometric reaction of  $[\text{Re}(\text{CO})_5\text{Cl}]$  with **HL** in boiling toluene for 8 hours under argon atmosphere afforded complexes **1** and **2** (**Scheme II.2**). These complexes were separated by column chromatography. Complex **1** was obtained as orange coloured product after eluting with 45% ethyl acetate: hexane mixture in good yield. Complex **2** was

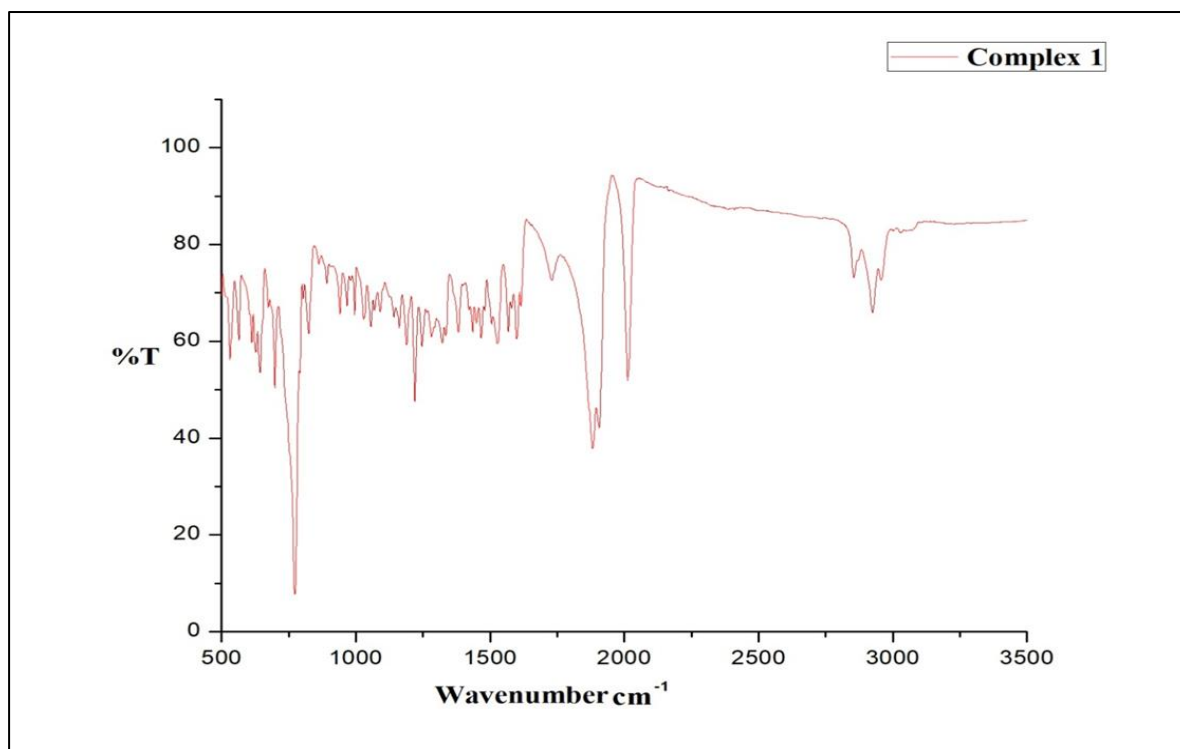
obtained as co product in low yield eluting with 20% ethyl acetate: hexane mixture. A similar reaction using triethylamine afforded complex 2 in high yield.



*Scheme II.2 Schematic representation for the synthesis of the Complexes*

### ***B. Characterization***

*IR Spectra:* The IR spectra of all the complexes were measured in a KBr disk. The presence of a fac-[Re(CO)<sub>3</sub>]<sup>+</sup> core having pseudo-C<sub>3v</sub> symmetry can be attributed to the three metal carbonyl stretching frequencies observed in the range 1900–2014 cm<sup>-1</sup>.



*Figure II.1 IR spectrum of Complex 1*



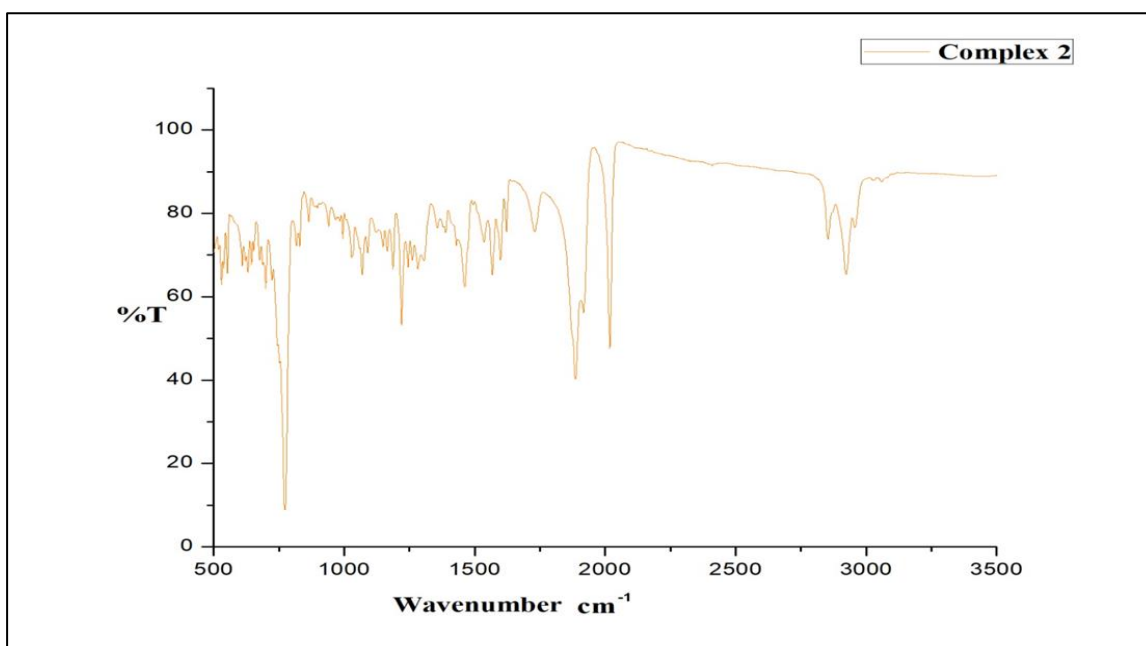


Figure II.2 IR spectrum of Complex 2

*NMR Spectra:* Complexes 1 and 2 are diamagnetic and display well resolved NMR spectra in  $\text{CDCl}_3$  solution. The assignment of NMR peaks is based on the intensity and spin-spin splitting pattern. These complexes show a doublet near 9 ppm, the proton adjacent to the pyridyl nitrogen atom appears as doublet at  $\sim 8.9$  ppm. A singlet due to azomethine hydrogen atom observed at  $\sim 10$  ppm in all cases. In phenolic OH of 1 is observed at 11.20 ppm which disappears upon addition of  $\text{D}_2\text{O}$ .

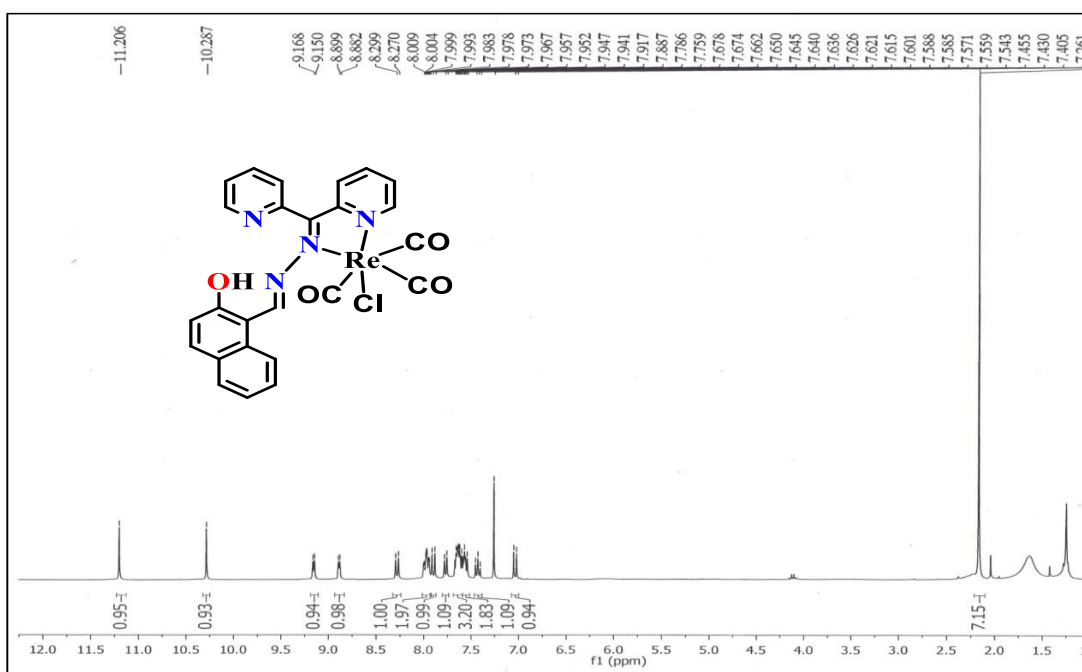


Figure II.3  $^1\text{H}$  NMR spectrum of Complex 1

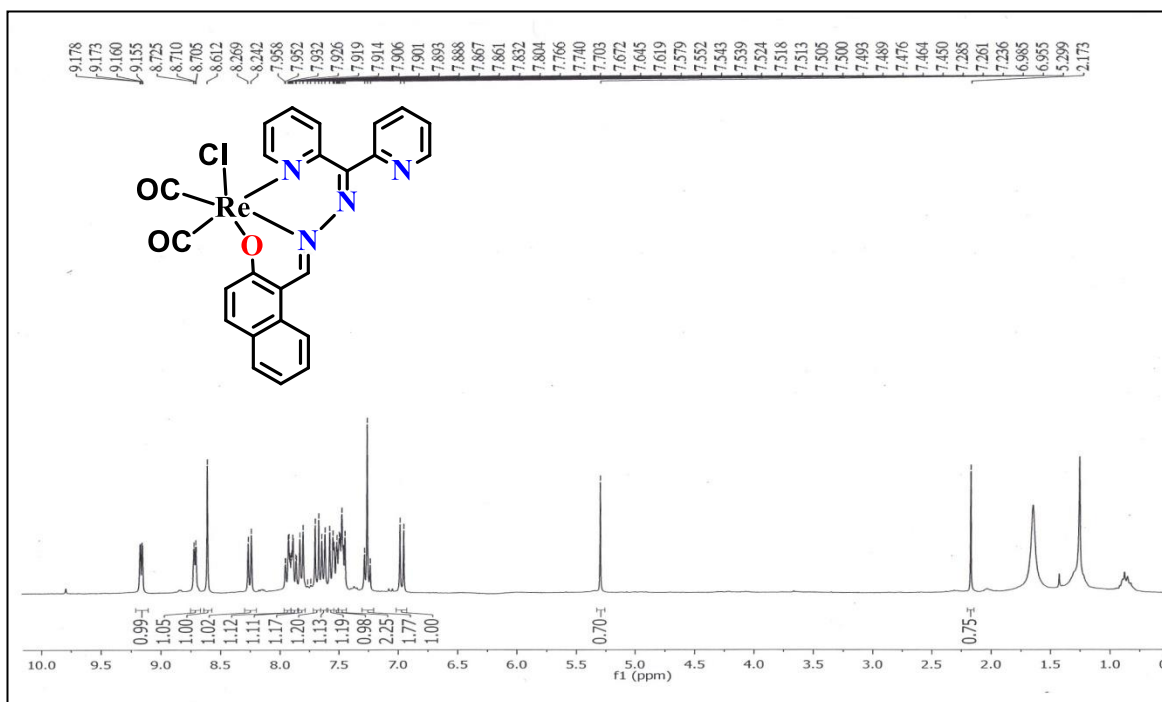


Figure II.4 <sup>1</sup>H NMR spectrum of Complex 2

*Mass Spectra:* Electrospray ionization mass spectrometry (ESI-MS) of the complex was done. Complex 1 displayed the highest  $m/z$  peak at 657  $[M]^+$  and complex 2 at 623.007  $[M+2]^+$ .

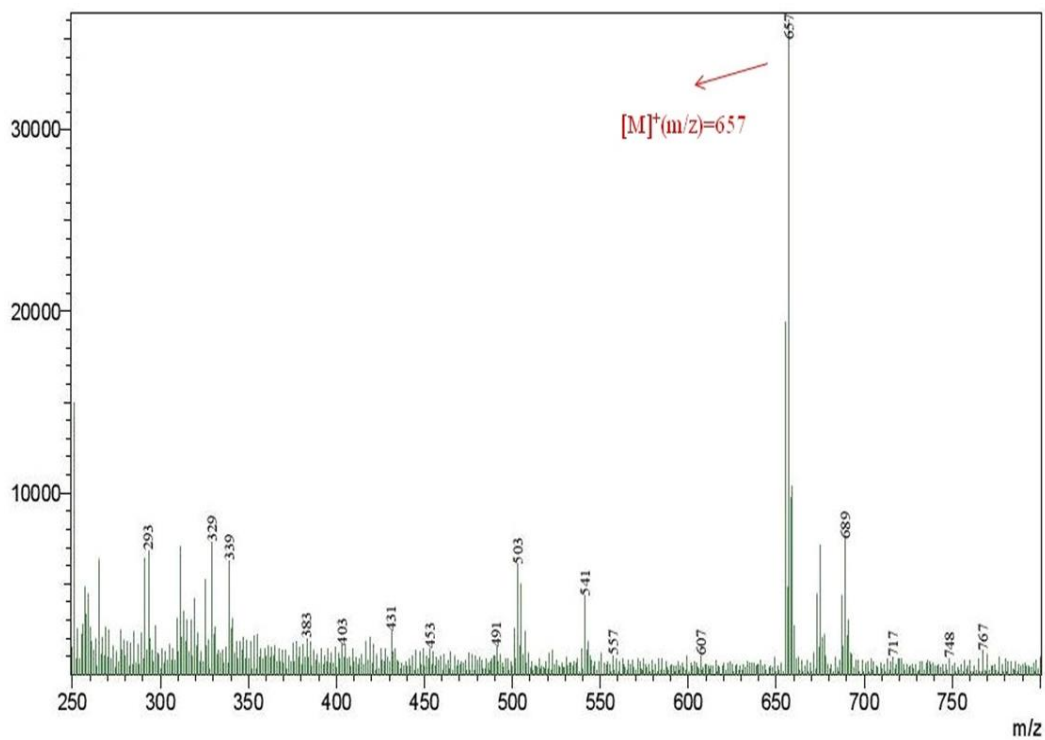
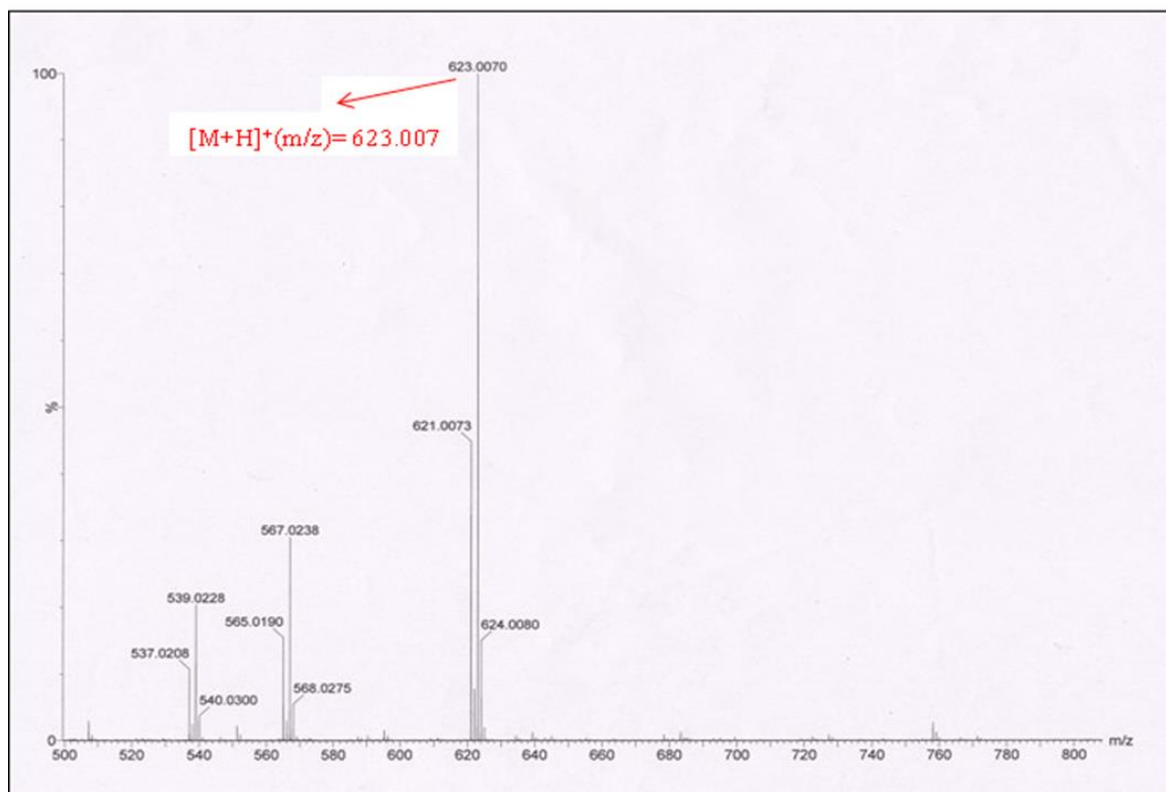


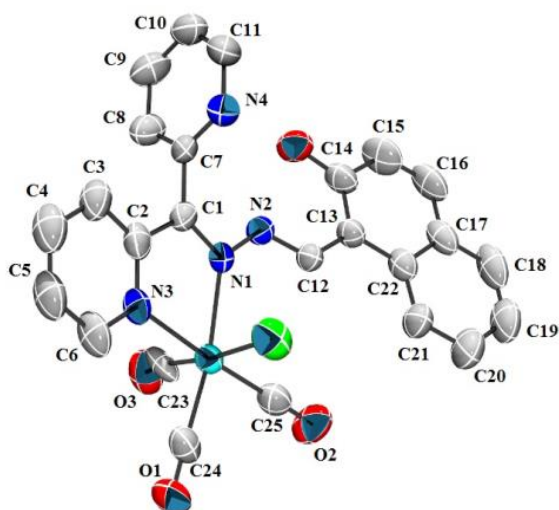
Figure II.5 Mass spectrum of Complex 1



**Figure II.6** Mass spectrum of Complex 2

**Crystal Structure:** Single crystals of complexes **1** and **2** were grown by diffusion of

dichloromethane into hexane. The crystallographic data collection and refinement parameters are given in **Table II.1** and **Table II.2**, selected bond lengths and angles are given in **Table II.3**. The perspective view of complex **1** is shown in **Figure II.7**. In complex **1**, the geometry around rhenium (I) is distorted octahedral. It crystallizes in monoclinic

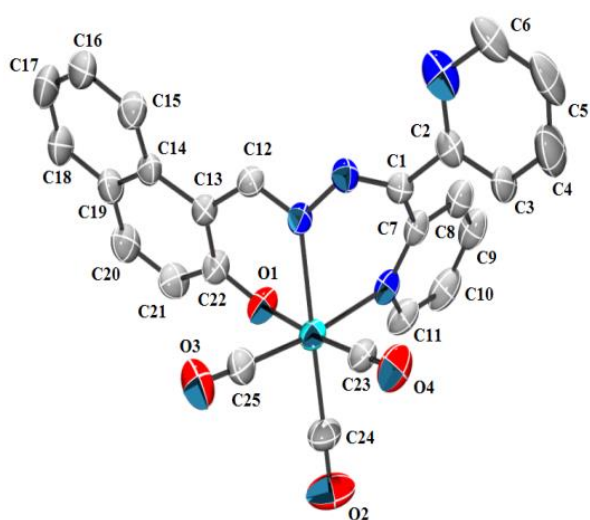


**Figure II.7** Perspective view of complex **1**  $[Re(HL)(CO)_3Cl]$  and hydrogens are omitted for clarity.

system with space group  $C2/c$ . In **1**, the ligand (HL) binds with the metal ion as NN coordinating neutral bidentate ligand, leaving the pyridyl nitrogen (N4) and phenolic -OH group uncoordinated. The

coordinated pyridyl moiety and uncoordinated hydroxy-naphthyl moiety lies on the same plane (dihedral angle  $2.97^\circ$ ) whereas, the coordinated and uncoordinated pyridyl groups are out of plane (dihedral angle  $85.44^\circ$ ). The distance between imine nitrogen and phenolic oxygen ( $O \cdots N = 2.565 \text{ \AA}$ ) recommends the existence of strong hydrogen bond.

In contrast, complex **2** binds with **HL** in NNO coordinating fashion. Slow Diffusion of dichloromethane into hexane afforded single crystals which diffracted



in tetragonal crystal system with space group  $I41/a$ . The perspective view of complex **2** is shown in **Figure II.8**. Unlike **1**, complex **2** forms two adjacent six membered rings binding with  $N_2$  and one of the pyridyl nitrogen. Here also one uncoordinated pyridine ring left behind. In both complexes carbonyl groups are arranged in facial mode. The  $Re-(CO)$

**Figure II.8** Perspective view of complex **2**  $[Re(L)(CO)_3]$  and hydrogens are omitted For clarity.

bond distances trans to nitrogen atoms of the quinoline and azo ( $N=N$ ) moiety is found to be slightly longer than  $Re-(CO)$  bond distance trans to the phenoxo group and this can be attributed to the better  $\pi$ -accepting ability of nitrogen atoms than oxygen.

**Table II.3** Selected Bond Distances (Å) and Angles (°) for complexes **1** and **2**

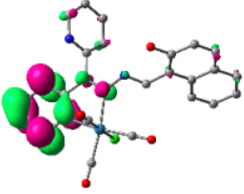
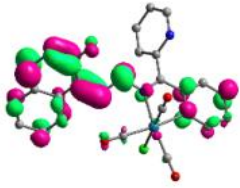
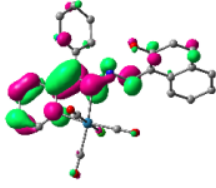
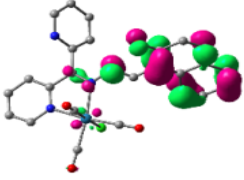
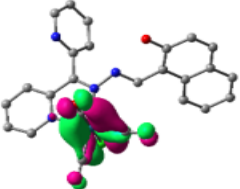
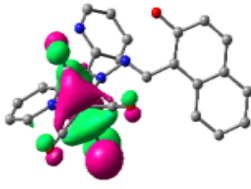
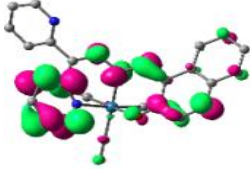
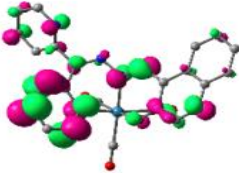

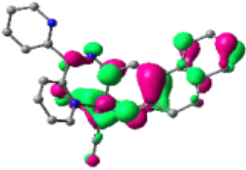
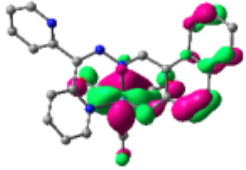
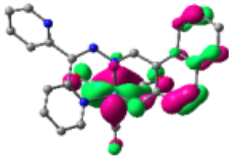
<b>1</b>			<b>2</b>		
<b>Bond Length (Å)</b>					
	<i>Exp.</i>	<i>Theo.</i>		<i>Exp.</i>	<i>Theo.</i>
C1-N1	1.299(7)	1.304	C1-N1	1.403(4)	1.29
Re1-C24	1.918(7)	1.926	Re1-O1	2.121(3)	2.15
Re1-C25	1.925(8)	1.929	Re1-C23	1.892(4)	1.91
Re1-C23	2.028(9)	1.913	Re1-C25	1.913(5)	1.92
Re1-N3	2.181(5)	2.208	Re1-C24	1.916(5)	1.93
Re1-N1	2.198(5)	2.221	Re1-N2	2.126(3)	2.16
Re1-Cl1	2.459(2)	2.551	Re1-N4	2.194(4)	2.23
<b>Bond Angles(°)</b>					
C24-Re1-C25	86.0(3)	88.77	C23-Re1-C25	89.47(19)	89.66
C24-Re1-C23	92.2(3)	90.77	C23-Re1-C24	89.3(2)	89.19
C25-Re1-C23	90.6(3)	90.44	C25-Re1-C24	89.6(2)	89.71
C24-Re1-N3	96.3(3)	97.69	C23-Re1-O1	176.14(16)	176.06
C25-Re1-N3	175.3(2)	172.67	C25-Re1-O1	92.34(16)	92.11
C23-Re1-N3	93.4(3)	92.88	C23-Re1-N2	96.93(15)	96.95
C24-Re1-N1	169.8(3)	170.86	C24-Re1-O1	94.13(17)	94.33
C25-Re1-N1	104.2(2)	99.76	C25-Re1-N2	95.06(17)	96.25
C23-Re1-N1	87.5(3)	92.38	C24-Re1-N2	172.24(18)	171.43
N3-Re1-N1	73.59(18)	73.59	O1-Re1-N2	79.52(12)	79.36
C24-Re1-Cl1	93.6(2)	91.50	C23-Re1-N4	92.38(16)	92.70
C25-Re1-Cl1	91.0(2)	91.77	C25-Re1-N4	173.39(17)	173.35
C23-Re1-Cl1	174.0(2)	176.84	C24-Re1-N4	96.75(18)	96.52
N3-Re1-Cl1	84.77(14)	84.65	O1-Re1-N4	85.45(12)	85.15
N1-Re1-Cl1	86.54(14)	85.027	N2-Re1-N4	78.41(13)	77.29
C2-C1-C7	121.0(5)	120.61	C2-C1-C7	117.9(4)	118.04

### *C. Geometry Optimisation*

Rhenium (I) complexes (**1** and **2**) are diamagnetic at room temperature possessing  $t_{2g}^6$  configuration. Optimizations for these complexes are accomplished in presence of solvent. Main geometrical optimized parameters (bond length and bond angle) of complexes **1** and **2** are given in **Table II.3**. The modelled geometries possess a distorted octahedral arrangement around rhenium (I) metal centre. Optimized structures of these complexes are very close to experimentally observed structures. A slight variation in structural parameters may arise due to the crystal lattice distortion in the real molecules. The Re-N, Re-O bond lengths are in the range of 2.13-2.29 Å in both the theoretical calculation and experimental observation. The good agreement between calculated and experimental data highlights the importance of relativistic effects for a proper description of the geometrical structures of the present rhenium (I) complexes. The isodensity plot of some selected frontier molecular orbitals in their singlet ground state ( $S_0$ ) is listed in **Table II.4**.

Partial molecular orbital diagram with HOMO and LUMO for these two complexes is shown in **Figure II.9**. In the ground state ( $S_0$ ), the HOMO of **2** is of much lower energy than **1**, which is same in case of LUMO. The HOMO-LUMO energy gap in all mononuclear complexes is close to each other and the corresponding values are 3.06 eV for **1** and 2.88 eV for **2**. The corresponding orbital contribution for the three complexes is given in the **Table II.5**. The electron density in the HOMO of all the complexes mainly resides on the naphthalene moiety (in the range of 40-78%) and the imine bonds (in the range of 25-40%). In case of **2**, the electron density also resides on rhenium (I) centre (11%) which is not observed in other two complexes. In the case of LUMO, the electron density mainly resides on the pyridyl moiety (in the range 40-95%) and imine bond (in the range of 35-47%) whereas **1** bears very low density around imine bond.

**Table II.4** Isodensity plot of some frontier molecular orbital of complexes **1** and **2**

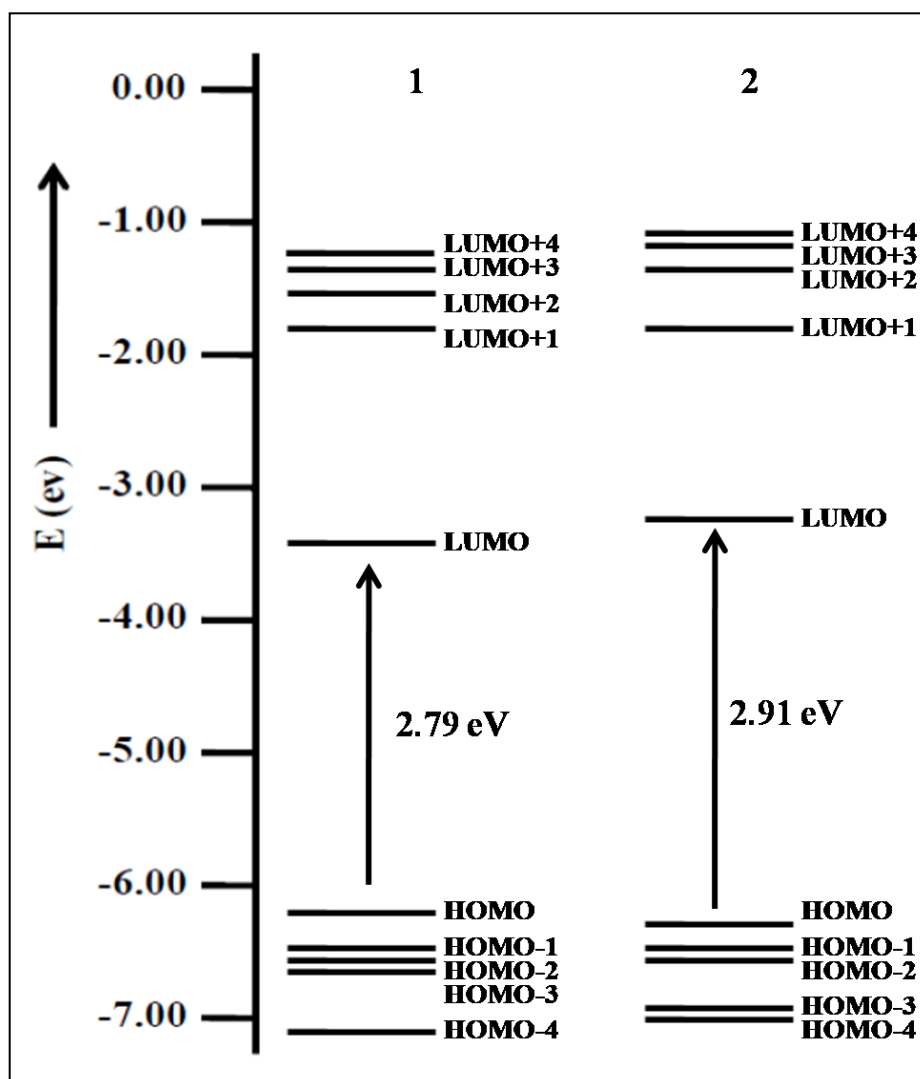
<b>Complex 1</b>				
	LUMO+2	LUMO+1	LUMO	
				
	HOMO	HOMO-1	HOMO-2	
	<b>Complex 2</b>			
		LUMO+2	LUMO+1	LUMO
				
HOMO		HOMO-1	HOMO-2	

**Table II.5** Energies (eV) and composition (%) of frontier molecular orbitals of complexes **1** and **2**

<b>Complex-1</b>		<b>% contribution</b>						
<b>MO</b>		<b>CO</b>	<b>Naph</b>	<b>Re</b>	<b>SB</b>	<b>PyA</b>	<b>PyF</b>	<b>Main Bond type</b>
124	L+3	0	6	0	4	42	47	$\pi^*(\text{PyA})+\pi^*(\text{PyF})$
123	L+2	3	0	1	14	50	32	$\pi^*(\text{PyA})+\pi^*(\text{PyF})+\pi(\text{SB})$
122	L+1	3	46	1	27	23	0	$\pi^*(\text{Naph})+\pi^*(\text{PyA})+\pi(\text{SB})$
121	LUMO	1	18	1	37	36	7	$\pi^*(\text{PyA})+\pi^*(\text{Naph})+\pi(\text{SB})$
120	HOMO	9	56	11	25	-4	4	$\pi(\text{Naph})+d(\text{Re})+\pi(\text{SB})$
119	H-1	13	56	26	4	1	0	$\pi(\text{CO})+\pi(\text{Naph})+d(\text{Re})$
118	H-2	27	14	56	1	1	0	$\pi(\text{CO})+\pi(\text{Naph})+d(\text{Re})$
117	H-3	22	22	47	8	1	0	$\pi(\text{CO})+\pi(\text{Naph})+d(\text{Re})$

<b>Complex 2</b>		<b>% Contribution</b>						
<b>MO</b>		<b>CO</b>	<b>Naph</b>	<b>OMe</b>	<b>Re</b>	<b>C=N</b>	<b>Py</b>	<b>Main Bond type</b>
133	L+3	0	16	0	1	4	79	$\pi^*(\text{Naph})+\pi^*(\text{Py})$
132	L+2	2	38	-1	0	15	47	$\pi^*(\text{Naph})+\pi^*(\text{SB})+\pi^*(\text{Py})$
131	L+1	7	16	0	4	7	66	$\pi^*(\text{Naph})+\pi^*(\text{Py})$
130	LUMO	6	1	-1	2	-1	95	$\pi^*(\text{Naph})+\pi^*(\text{Py})$
129	HOMO	5	41	0	4	46	4	$\pi(\text{Naph})+\pi(\text{SB})$
128	H-1	9	55	0	17	17	1	$\pi(\text{Naph})+d(\text{Re})+\pi(\text{SB})$
127	H-2	2	91	0	6	2	0	$\pi(\text{Naph})$
126	H-3	28	0	0	62	1	9	$\pi(\text{CO})+d(\text{Re})$





*Figure II.9 Partial molecular orbital diagram of the complexes 1 and 2*

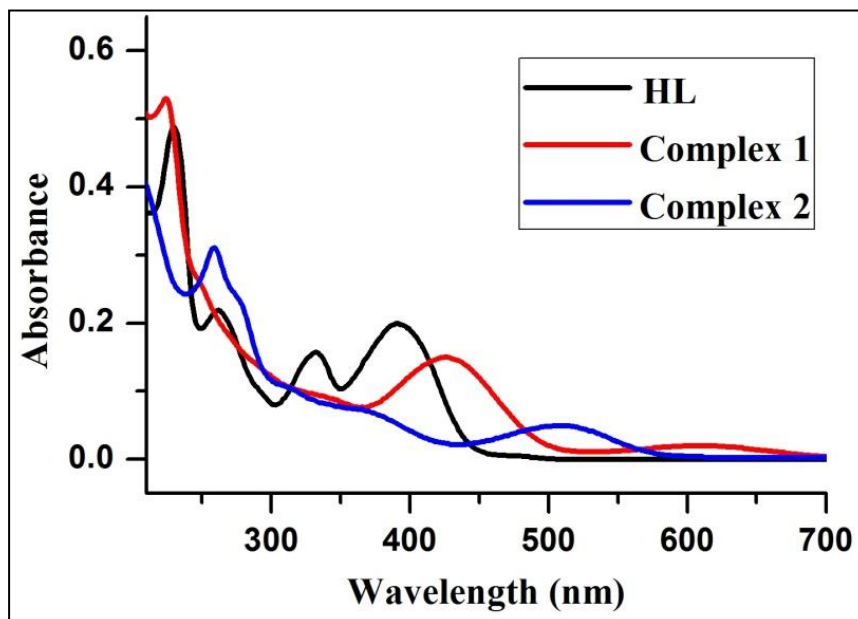
#### *D. Electronic Spectra and TDDFT Calculations*

The absorption spectral behaviour of the ligand and complexes **1** and **2** are recorded in acetonitrile at room temperature. The UV-Vis spectral parameters with experimental molar extinction coefficient ( $\epsilon$ ) of HL, **1** and **2** are listed in **Table II.6**. The relevant electronic spectra are given in **Figure II.10**. HL shows four characteristic peaks in the range of 229-392 nm which can be assigned as  $n\text{-}\pi^*$  and  $\pi\text{-}\pi^*$  intramolecular charge transfer transitions. The absence of peak above 400 nm ensures the predominance of enol over keto tautomer in HL.

**Table II.6** Main calculated optical transition for complexes **1** and **2** with vertical excitation energies and oscillator strength in acetonitrile.

<b>Complex 1</b>						
Electronic transition	Composition	Excitation energy (eV) (nm)	Oscillator Strength (f)	CI	Assign	$\lambda_{exp}$ in nm ( $\epsilon$ in $M^{-1}cm^{-1}$ )
$S_0 \rightarrow S_3$	H-2→L	2.7780 (446 nm)	0.0585	0.6965	$^1MLCT$	426 (14,970)
$S_0 \rightarrow S_8$	H-1→L+1	3.7070 (334 nm)	0.0085	0.6240	$^1MLCT$	336 (9,200)
$S_0 \rightarrow S_{68}$	H-3→L+5	5.4515 (227 nm)	0.0652	0.4371	$^1MLCT/^1IL$ CT	225 (53,000)
<b>Complex 2</b>						
$S_0 \rightarrow S_1$	H→L	2.2722 (545 nm)	0.1470	0.6981	$^1MLCT/^1I$ LCT	507 (5,000)
$S_0 \rightarrow S_4$ $S_0 \rightarrow S_5$	H→L+1 H-3→L	3.1538 (393 nm) 3.2471 (381 nm)	0.0264 0.0969	0.6787 0.6806	$^1MLCT/^1I$ LCT $^1ILCT$	372 (7,100)
$S_0 \rightarrow S_{35}$	H-3→L+5	4.7941 (258 nm)	0.0132	0.4522	$^1MLCT/^1I$ LCT	258 (31,000)

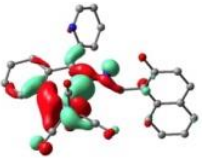
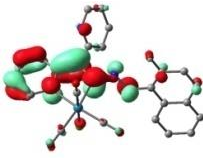
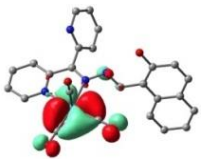
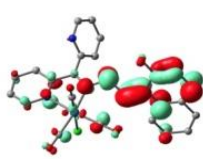
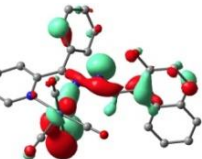
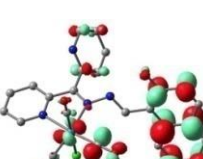
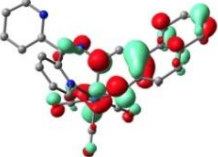
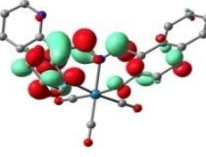

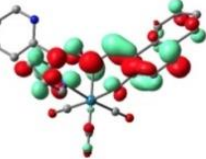
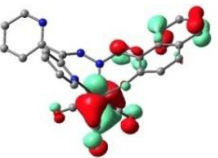
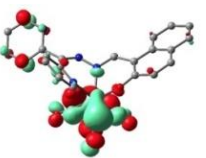
The complexes display a strong peak varying between 336-500 nm having extinction coefficient in the range of 6,000-10,200  $M^{-1} cm^{-1}$ . The bands at longer wavelength region of these complexes can be assigned as metal to ligand charge transfer [Re (d $\pi$ ) → HL] transition. The intense absorption bands ( $\epsilon = 31,000 - 53000 M^{-1} cm^{-1}$ ) of the complexes at 220-260 nm are assigned as ligand  $\pi-\pi^*$  transition.



*Figure II.10* Absorption spectra of HL, complex 1 and 2 in acetonitrile

In order to get a clear insight on the vertical excitation and the nature of absorption, NTO analysis is performed based on the calculated transition density matrices. This method describes the most compact representation of the transition density between the ground and excited states in terms of an expansion into single-particle transitions (hole and electron states for each given excitation). The unoccupied and occupied NTOs are referred as “electron” and “hole” transition orbitals, respectively. *Table II.7* illustrates the natural transition orbitals (NTOs) for complexes 1 and 2. Based on our TDDFT NTOs analysis the band at 260 nm of 1 can be characterized as an admixture of  $^1\text{MLCT}$  and  $^1\text{ILCT}$  states. Bands in region 300-400 nm originate from mixed  $^1\text{MLCT}$  and  $^1\text{ILCT}$  state where as that of in the region 400-500 nm mainly arises from  $^1\text{ILCT}$  along with very little amount of  $^1\text{MLCT}$  characters.

**Table II.7** Natural transition orbitals (NTOs) for the complexes **1-2** illustrating the nature of singlet excited states in the absorption bands. For each state, the respective number of the state, transition energy (eV), and the oscillator strength (in parentheses) are listed. Shown are only occupied (holes) and unoccupied (electrons) NTO pairs that contribute most towards each excited state.

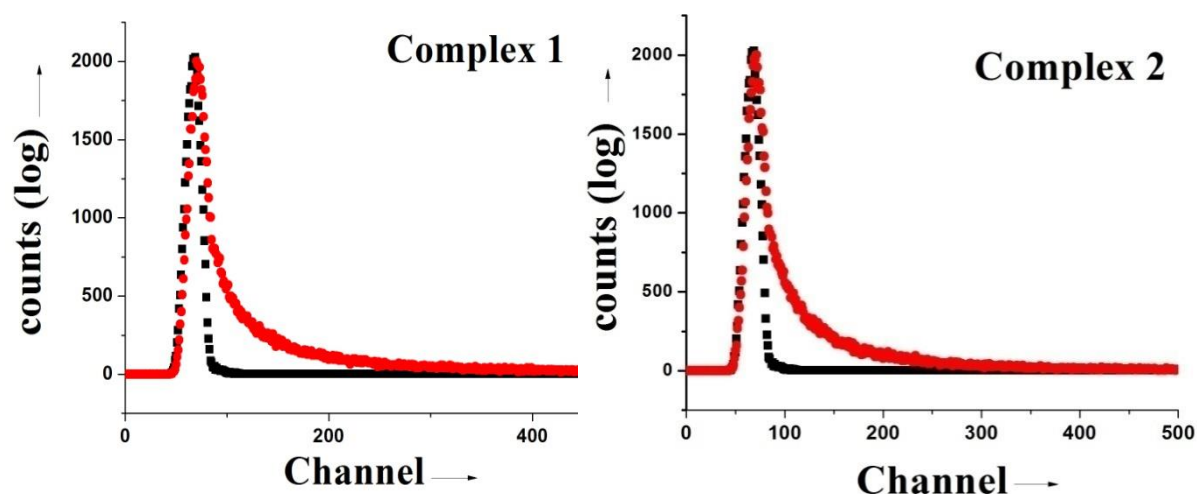
Complex	Transition	Hole	Electron	Assignment
1	S <sub>3</sub> W=0.97 2.78eV(0.06)			<sup>1</sup> MLCT/ <sup>1</sup> ILCT
	S <sub>9</sub> W=0.87 3.81eV(0.02)			<sup>1</sup> MLCT/ <sup>1</sup> ILCT
	S <sub>68</sub> W= 0.38 5.42eV(0.06)			<sup>1</sup> MLCT/ <sup>1</sup> ILCT
2	S <sub>1</sub> W=0.97 2.27eV(0.14)			<sup>1</sup> ILCT/ <sup>1</sup> MLCT
	S <sub>4</sub> W=0.92 3.15eV(0.02)			<sup>1</sup> MLCT/ <sup>1</sup> ILCT
	S <sub>35</sub> W=0.40 4.79eV(0.01)			<sup>1</sup> MLCT/ <sup>1</sup> ILCT

## E. Emission Spectroscopy

The emission spectral behaviour of the ligand and complexes were studied at room temperature. The ligand shows strong emission at 510 nm when excited at 400 nm with well intensity. But the complexes are very weak emitters when they are excited at the 380 nm and 372 nm giving rise to the emission at 471 and 405 nm respectively. It is worth mentioning that those complexes are non emissive when they are excited at MLCT wavelength. This suggests that the weak emission of the complexes is responsible for the ligand centred emission, i.e.  $^3\text{IL}$  (intraligand). **Table II.8** depicts the experimental data of emission spectra of two complexes. The quantum yield of complexes **1** and **2** was found to be 0.006, 0.005 respectively. The excited state lifetime measurement in acetonitrile solution displays bi-exponential decay (see **Figure II.11**) having very low life times ranging in between 1 to 7 ns.

**Table II.8** Main calculated optical transition for complexes **1** and **2** with vertical excitation energies and oscillator strength in acetonitrile.

Sample	$\lambda_{\text{ex}}$	$\lambda_{\text{em}}$	$\tau_1$ ns	$\tau_2$ ns	Quantum yield( $\Phi$ )	$k_r$ , ns $^{-1}$	$k_{nr}$ , ns $^{-1}$
<b>1</b>	380	471	1.86	7.45	0.015	0.0099	0.636
<b>2</b>	372	405	1.52	5.57	0.093	0.059	0.58



**Figure II.11** Emission spectra of HL, complex **1** and **2** in acetonitrile

## II.4. CONCLUSION

In summary, we have successfully developed a new multifunctional ligand to generate rhenium (I) complexes of our choice. We have synthesized NN and NNO binding mononuclear rhenium (I) complexes **1** and **2** respectively. The compounds are characterized by single crystal X-ray crystallography and other analytical techniques. The complexes give intense absorption bands in the range of 426-510 nm. The present work investigated the ground and excited state geometries, optical properties of two mononuclear rhenium (I) complexes by DFT and TDDFT methods.

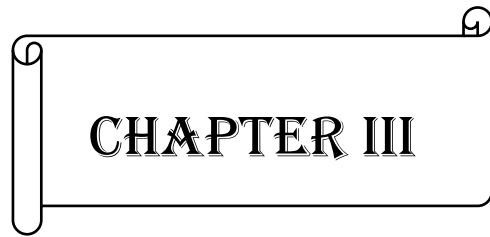
## II.5. REFERENCES

- (1) (a) G. E. Shillito, T. B. J. Hall, D. Preston, P. Traber, L. Wu, K. E. A. Reynolds, R. Horvath, X. Z. Sun, N. T. Lucas, J. D. Crowley M. W. George, S. Kupfer, K. C. Gordon, *J. Am. Chem. Soc.* **2018**, *140*, 4534–4542
- (b) L. A. Faustino, A. E. H. Machado, A. O. T. Patrocínio *Inorg. Chem.* **2018**, *57*, 2933–2941
- (c) J. Ishitani, O. Rohacova *Dalton Trans.* **2017**, *46*, 8899
- (d) S. Mai, H. Gattuso, M. Fumanal, A. Muñoz-Losa, A. Monari, C. Daniel L. González *Phys. Chem. Chem. Phys.* **2017**, *19*, 27240-27250
- (e) D. Sieh, C. P. Kubiak *Chem. Eur. J.* **2016**, *22*, 10638 – 10650
- (f) M. V. Vollmer, C.W. Machan, M. L. Clark, W. E. Antholine, J. Agarwal, H. F. Schaefer III, C. P. Kubiak, J. R. Walensky *Organometallics* **2015**, *34*, 3–12
- (g) S. Sengupta, I. Chakraborty, A. Chakravorty *Eur. J. Inorg. Chem.* **2003**, 1157-1160
- (h) A. Vogler, H. Kunkely, *Coord. Chem. Rev.* **2000**, *200–202*, 991–1008
- (i) D. J. Stufkens; A. Vlček, *Coord. Chem. Rev.* **1998**, *177*, 127–179
- (2) (a) Yersin, H. Ed.; Wiley-VCH: Weinheim, Germany, *Highly Efficient OLEDs with Phosphorescent Materials*; **2008**

- (b) L. Veronese, E. Q. Procopio, F. De Rossi, T. M. Brown, P. Mercandelli, P. Mussini, G. D'Alfonso, M. Panigati, *New J. Chem.* **2016**, *40*, 2910
- (c) C. C. Chou, F.-C. Hu, H.-H. Yeh, H. -P Wu, Y. Chi, J. N. Clifford, Palomares P.-T. Chou, G.-H. Lee, *Angew. Chem., Int. Ed.* **2014**, *53*, 178
- (d) C. A. Bignozzi, R. Argazzi, R. Boaretto, E. Busatto, S. Carli, F. Ronconi, S. Caramori, *Coord. Chem. Rev.* **2013**, *257*, 1472
- (e) A. Hagfeldt, G. Boschloo, L.-C. Sun, L. Kloo, H. Pettersson, *Chem. Rev.* **2010**, *110*, 6595
- (f) M. K. Nazeeruddin, M. Graätzel, In *Comprehensive Coordination Chemistry II*, Vol. 9; J. A. McCleverty, T. J. Meyer, Eds.; Elsevier Pergamon: Oxford, U.K. **2004**, 719-758
- (g) I. N. Booyesen, M. B. Ismail, O.Q. Munro *Inorganic Chemistry Communications*, **2013**, *30*, 168-172
- (3) (a) L. Sacksteder, M. Lee, J. N. Demas, B. A. De Graff, *J. Am. Chem. Soc.* **1993**, *115*, 8230
- (b) Zipp A. P. *Coord. Chem. Rev.* **1988**, *84*, 47-83
- (c) J. V. Caspar, B. P. Sullivan, T. J. Meyer *Organometallics* **1986**, *5*, 1500-1502
- (d) C. R. Carbera, H. D. J. Abruna *J. Electroanal. Chem.* **1986**, *209*, 101-107
- (e) H. Takeda, K. Koike, T. Morimoto, H. Inumaru, O. Ishitani *Adv. Inorg. Chem.* **2011**, *63*, 137-186
- (4) (a) A. Wilting, T. Stolper, R. A. Mata, I. Siewert, *Inorg. Chem.* **2017**, *56*, 4176-4185
- (5) (a) P. Mondal, A. Hens, S. Basak, K. K. Rajak *Dalton Trans.* **2013**, *42*, 1536
- (b) R. Sarkar, P. Mondal, K. K. Rajak *Dalton Trans.* **2014**, *43*, 2859





A decorative scroll with a black outline and a white fill. The scroll is oriented horizontally and has a rolled-up appearance at both ends. The text "CHAPTER III" is centered within the scroll in a bold, black, serif font.

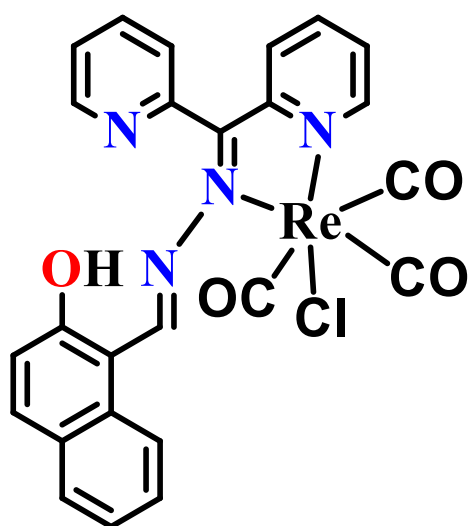
**CHAPTER III**



## *Reactivity of hydrazine based Rhenium (I) Complexes towards Certain Metal Ion and Toxic anion*

### **ABSTRACT**

A Rhenium (I) complex (complex 1) having multifunctional ligand attached with it displayed magnificent chemistry with a metal ion in particular i.e. Zn (II) and a certain toxic anion  $\text{CN}^-$ . A solvent assisted molecular rearrangement had been observed when the complex was made contact with zinc acetate  $[\text{Zn}(\text{OAc})_2]$ . The rearranged product was characterised by X-ray diffractometer and other spectroscopic analysis. The course of reaction was analysed through kinetic study by UV-Vis spectroscopy which unveiled the pseudo 1<sup>st</sup> order type nature of the reaction



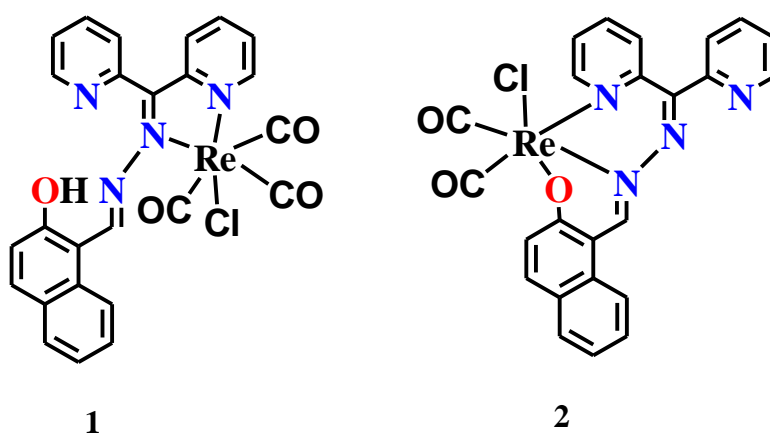
having rate constant  $1.1 \times 10^{-3} \text{ s}^{-1}$ . The complex was also proved to be sensitive towards  $\text{CN}^-$  which is a very toxic anion and transmits harmful effect in environment. The reaction of the complex 1 and  $\text{CN}^-$  was studied extensively by UV-Vis spectroscopy and emission spectroscopy. In presence of  $\text{CN}^-$  the complex 1 exhibited highly intense phosphorescence at 471 nm with lifetime  $\sim 7$  ns when excited at 380 nm.  $^1\text{H}$  NMR titration elucidated the key factor

of reaction mechanism. Complex 1 was also able to detect  $\text{CN}^-$  selectively over other toxic anions. The detection limit was found to be  $5.0 \times 10^{-8} \text{ M}$ .



### III.1. INTRODUCTION

The complexes **1** and **2** mentioned in previous chapter have been extensively studied and expressed in this chapter in search for its application in solution in presence of alien cations and anions. Several results show that complex **1** is more responsive than complex **2**. Ligand HL plays vital role in determining the character of reaction of such complexes. If we closely observe the structure of these **2** complexes it appears differently in the form of binding sites to the rhenium (I) centre. Complex **2** forms NNO complex whereas complex **1** forms NN complex with the ligand (HL). It is very interesting that such binding nature of rhenium (I) allows the multifunctionality of HL by creating a vacant pocket of uncoordinated -OH group and pyridyl group in complex **1**. Due to the lack of availability of free binding sites in complex **2**, it is not reactive relative to complex **1**. **Figure III.1** shows the structural variation of complexes **1** and **2**.



*Figure III.1 Structural representation of the Complexes 1 and 2*

We have used  $d^{10}$  metal ion particularly Zn(II) aiming to isolate a new series of luminescent mixed-metal rhenium(I) complexes.<sup>1</sup> Unfortunately, we were unable to isolate any mixed-metal rhenium(I) complexes bearing Zn(II) when complex **1** is allowed to react Zn(II) ion in methanol. Instead of that we have isolated rhenium (I) complex having *fac*-[Re(CO)<sub>3</sub>]<sup>+</sup> core containing reactive  $\alpha$ -amino ether group. Only a limited numbers of examples are reported in the literature<sup>2</sup> where the  $\alpha$ -amino ether is stabilized via metal ion coordination. However, to the best of our knowledge the

authentic isolation of rhenium(I) complexes containing reactive  $\alpha$ -amino ether group are not known. In addition to the feasibility of cationic binding, the presence of acidic OH proton in the suitably oriented vacant pocket of the coordinated rhenium (I) species, **1**, gives an open access to interact with the anionic species. It is believed that the incoming anion interact with the receptor via hydrogen bonding interaction or proton transfer reactions<sup>3</sup>. This has motivated us to check the change in properties of **1** with various anions such as F<sup>-</sup>, Cl<sup>-</sup>, Br<sup>-</sup>, I<sup>-</sup>, NO<sub>3</sub><sup>-</sup> and CN<sup>-</sup> ions. In practice only cyanide ion responds.

The use of cyanide as important raw materials in pharmaceutical industries, insecticides and fertilizers as well as an important reagent in plastic manufacturing, extraction of metals, electroplating industries are mainly responsible for the cyanide ion toxicity in the environment<sup>4</sup>. Thus the detection of cyanide ion is an important task to the scientific community as cyanide ion is highly toxic to living body and it has also detrimental effect to the environment and human health<sup>5</sup>. The fluorometric determination of cyanide in various samples is an emerging field of research due its low cost and easy operation<sup>6</sup>. It has been listed in the literature that CN<sup>-</sup> ion is able to adjust the ICT state which also triggers the emission properties by interacting with the fluorescent dyes<sup>6</sup>. In this context, detection of cyanide ion by the metal ion coordinated receptor has become an influential subject<sup>7</sup> to the researchers to overcome the difficulties such as slow reaction rate<sup>8</sup> and poor selectivity in presence of other anions. Although a limited number of metaloreceptors<sup>9</sup> bearing [Re(CO)<sub>3</sub>]<sup>+</sup> core have been used as an optical sensor to detect different anions based on the abstraction of dissociable proton present at the ligand frame<sup>10</sup>. However the paucity of well-characterized rhenium(I) complexes which can detect exclusively the cyanide ion, has prompted us to search for new systems. Herein we also describe the spectroscopic detection (UV-Vis and PL method) of cyanide using the synthesized complex. The most probable pathways for the observed spectral behaviour upon addition of cyanide ion are reported. The uncoordinated vacant sites of **1** have given an opportunity of increase in functionality by allowing the interaction with other cations and anions. In the present study we have checked the reacting ability of complex **1** with Zn(OAc)<sub>2</sub>.

## III.2. EXPERIMENTAL SECTION

### *A. Materials*

Re(CO)<sub>5</sub>Cl, Zn(OAc)<sub>2</sub>, tetrabutylammonium salts of Cl<sup>-</sup>, Br<sup>-</sup>, I<sup>-</sup>, NO<sub>3</sub><sup>-</sup>, F<sup>-</sup>, OAc<sup>-</sup>, OH<sup>-</sup> under study were purchased from Sigma Aldrich. All solvents and chemicals are analytically pure.

*Caution! Cyanide salts are highly toxic and should be handled with care and in very small amounts.*

### *B. Synthesis of complex*

*Complexes 3, fac-[Re(HL-OMe)(CO)<sub>3</sub>Cl]*: Here the reaction is carried out in dichloromethane – methanol (1:1) solvent due to the low solubility of **1** in methanol. Addition of Zn(OAc)<sub>2</sub> into the solution mixture of **1** changes the reddish yellow solution to dark red rapidly. Again, it decolorizes to yellow within two hours. A pure complex **3**, *fac*-[Re(HL)(CO)<sub>3</sub>], crystallizes out from the reaction mixture. ESI-MS (CH<sub>2</sub>Cl<sub>2</sub>): m/z 655.259 [M+H]<sup>+</sup>; Anal. Calcd for C<sub>26</sub>H<sub>19</sub>N<sub>4</sub>O<sub>5</sub>Re: C, 47.55; H, 3.38; N, 8.53. Found: C, 47.58; H, 3.40; N, 8.59; IR (cm<sup>-1</sup>): ν (O-H): 3375.69; ν (CO): 2005.46 (2 py), 1878.99; ν (methoxy): 1190; IR<sub>theo</sub> (cm<sup>-1</sup>): ν (CO): 2015, 1906.

### *C. X-Ray Structure Determination*

The single crystal suitable for X-ray crystallographic analysis of complex *fac*-[Re(HL-OMe)(CO)<sub>3</sub>Cl] was obtained through direct evaporation of solvent at room temperature. Details of the X-ray work are given in tabular form in **Table III.1** and **Table III.2** (See also Chapter I).

### *D. Physical Measurements*

All physical measurements that included elemental analyses, IR, absorption spectra, <sup>1</sup>H NMR and spectra, ESI mass spectra, emission spectra measurement were performed as described in **Chapter I**.

**Table III.1** Atomic coordinates and isotropic thermal parameters complex 3

	<b>Complex 3</b>
Total refl. Collected	34815
Unique refl.( $R_{int}$ )	4418
Used refl.	4054
h k l range	-10<h<10 -13<k<13 -29<l<29

	<b>Complex 3</b>
Solution	Patterson
Refinement	Full-matrix least-squares on $F^2$
<i>GOF on <math>F^2</math></i>	1.042
$R1,^a[I > 2\sigma(I)]$	0.0343
$wR2^b[I > 2\sigma(I)]$	0.0834
$R1[alldata]$	0.0464
$wR2[alldata]$	0.1619



**Table III.2** Crystal data and structure refinement parameters for complex 3

---

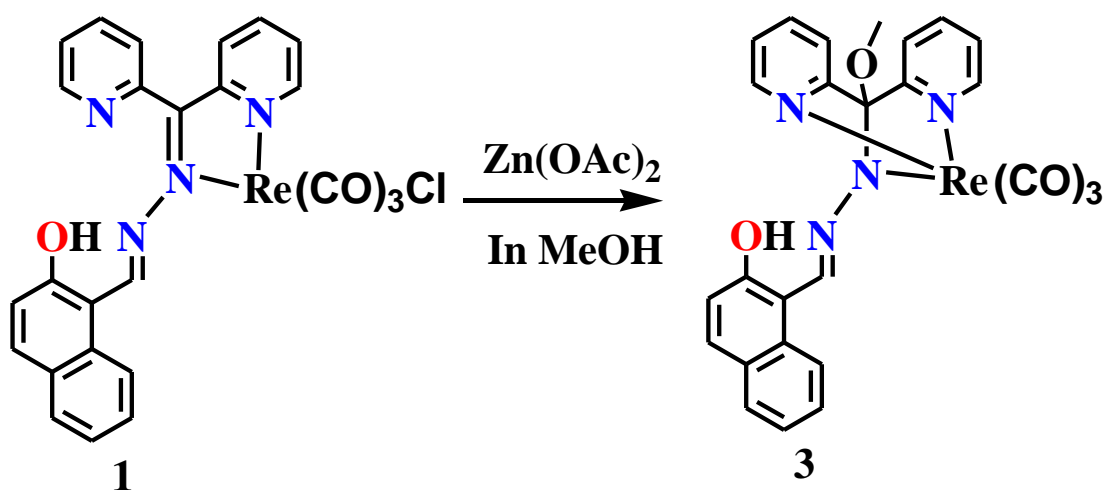
	<b>Complex 3</b>
Formula	C <sub>26</sub> H <sub>20</sub> N <sub>4</sub> O <sub>5</sub> Re
Mr	654.67
Crystal system	Monoclinic
Space group	<i>P</i> 21/ <i>n</i>
<i>a</i> / Å	8.7123(2)
<i>b</i> / Å	11.2312(3)
<i>c</i> / Å	24.3530(6)
$\alpha$ /°	90
$\beta$ /°	90.308(2)
$\gamma$ /°	90
<i>V</i> / Å <sup>3</sup>	2382.90(10)
<i>Z</i>	4
D <sub>calcd</sub> /g cm <sup>-3</sup>	1.825
$\mu$ /mm <sup>-1</sup>	5.145
$\theta$ /°	1.672-25.527
T /K	296

$${}^a R1 = \Sigma ||F_o| - |F_c| | / \Sigma |F_o|. \quad {}^b wR2 = [\Sigma[w(F_o^2 - F_c^2)^2] / \Sigma[w(F_o^2)^2]]^{1/2}$$

### III.3. RESULT AND DISCUSSION

#### A. Synthesis

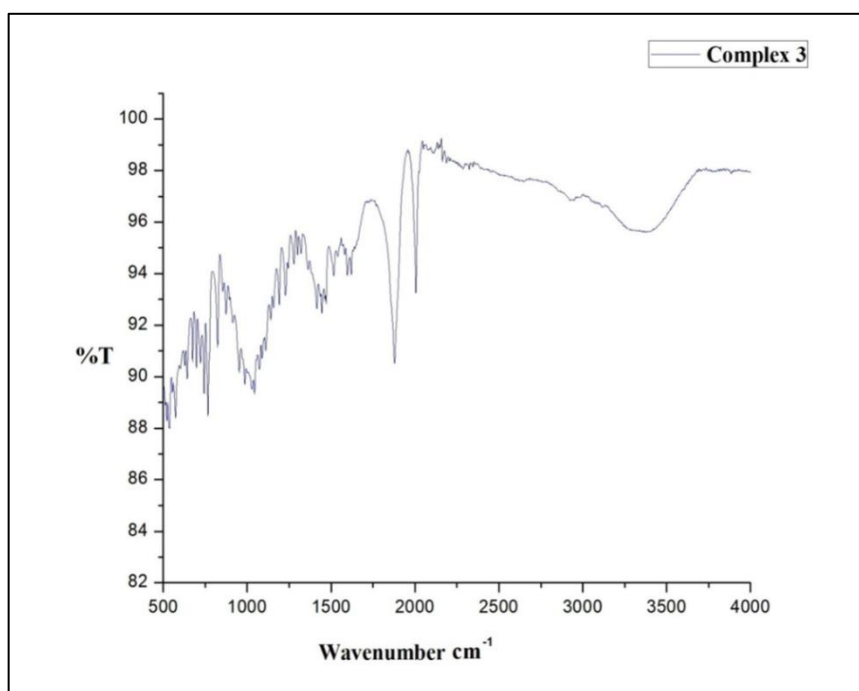
Complex **3** was synthesized by the reaction of complex **1** with  $\text{Zn}(\text{OAc})_2$  in methanol at room temperature. It is very interesting that in the complex **1**, the azomethine nitrogen and phenolic  $-\text{OH}$  of the naphthol moiety was suitably oriented to create a vacant pocket to interact with incoming cationic species. Thus, it was expected that a metal ion could be fit into it. To our surprise, no metal ion incorporation was there. Instead a molecular rearrangement was observed via solvent incorporation in the ligand moiety of complex **1** generating a new NNN coordinated facial rhenium (I) complex, **3**. **Figure III.2** represents the synthesis of complex **3**.



*Figure III.2 Synthetic procedure of the complex 3.*

#### B. Characterization

*IR Spectra:* The IR spectra of all the complexes were measured in a KBr disk. The presence of a fac-[Re(CO)<sub>3</sub>]<sup>+</sup> core having pseudo-C<sub>3v</sub> symmetry can be attributed to the three metal carbonyl stretching frequencies observed in the range 1900–2014 cm<sup>-1</sup>. A broad peak around 3500 cm<sup>-1</sup> depicts the presence of free  $-\text{OH}$  group in the complex **3**. **Figure III. 2** show the experimental curve of IR spectra of complex **3**.

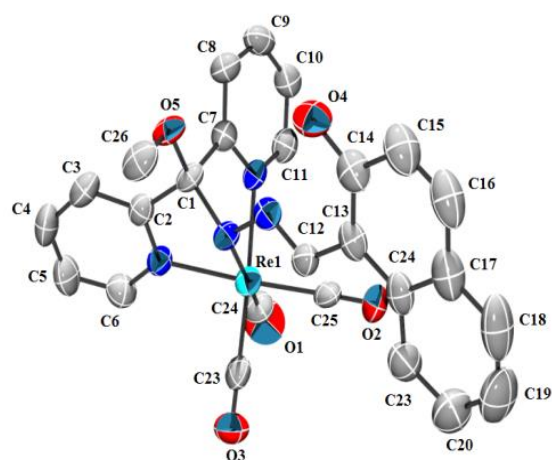


**Figure III.3** IR spectrum of Complex 3

**Mass Spectra:** Electrospray ionization mass spectrometry (ESI-MS) of complex 3 was done. The experimental value displayed the highest  $m/z$  peak at 655.2401  $[M]^+$ .

**Crystal Structure:**

Single crystal of complexes 3 was collected and was diffracted by Single crystal X-ray diffractometer. The crystallographic data collection and refinement parameters



are given in **Table III.1** and **Table III.2**, selected bond lengths and angles are given in **Table III.3**. The perspective view of complex 3 is shown in **Figure III.4**. In complex 3 the geometry around rhenium (I) is distorted octahedral. It crystallizes in monoclinic system with space group  $P21/n$ . In this complex, the ligand is attached

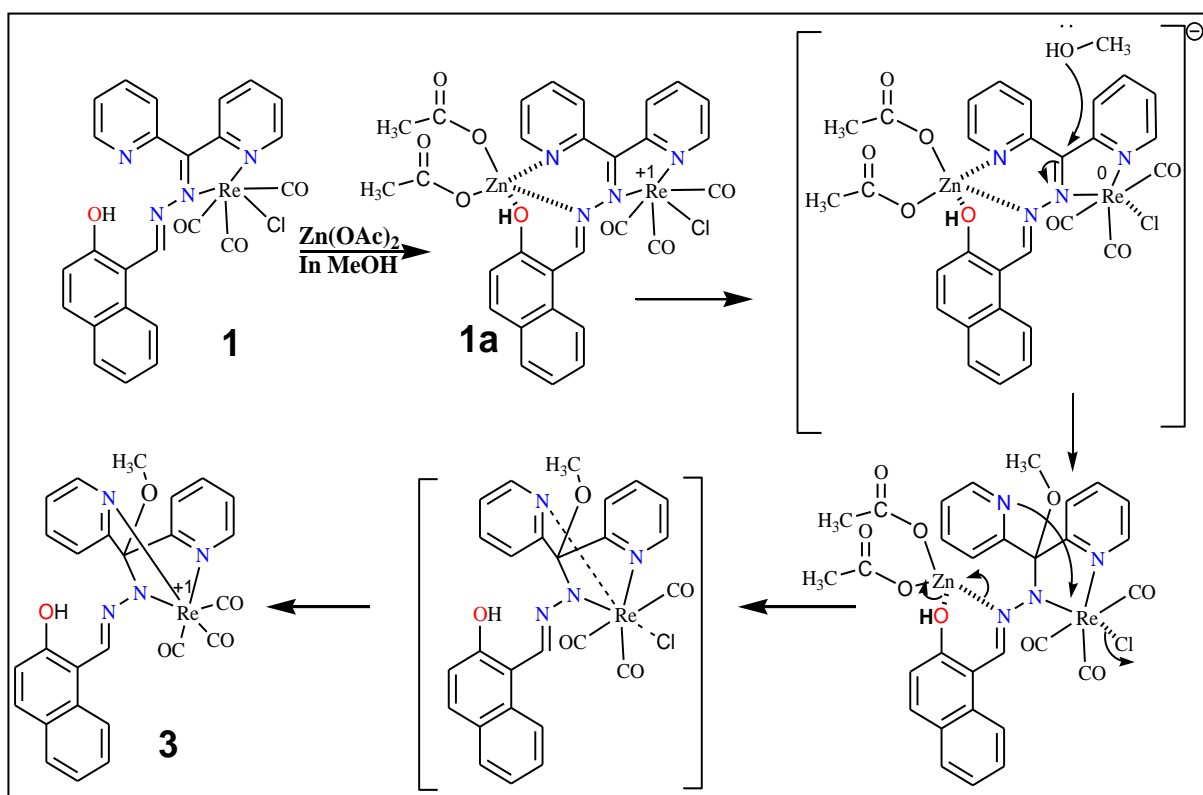
**Figure III.4** Perspective view of complex 3  $[Re(HL-OMe)(CO)_3Cl]$  and hydrogens are omitted For clarity.

**Table III.3.** Selected Bond Distances (Å) and Angles (°) for complex 3

<b>Complex3</b>		
<b>Bond Length (Å)</b>		
	Exp.	Theo.
C1-N1	1.479(7)	1.47
Re1-C24	1.915(7)	1.93
Re1-C23	1.909(7)	1.91
Re1-C25	1.918(7)	1.92
Re1-N1	2.140(4)	2.18
Re1-N3	2.153(5)	2.20
Re1-N4	2.207(5)	2.25
<b>Bond Angles(°)</b>		
C24-Re1-C23	89.2(3)	90.71
C24-Re1-C25	89.3(3)	89.5
C23-Re1-C25	86.8(3)	91.44
C24-Re1-N1	170.0(3)	166.8
C23-Re1-N1	98.2(2)	98.4
C25-Re1-N1	97.8(2)	99.6
C24-Re1-N3	98.1(3)	96.05
C23-Re1-N3	94.4(2)	94.68
C25-Re1-N3	172.5(2)	171.63
N1-Re1-N3	74.70(18)	73.87
C24-Re1-N4	97.1(3)	96.25
C23-Re1-N4	173.3(2)	172.24
C25-Re1-N4	95.4(2)	92.05
N1-Re1-N4	75.34(17)	74.07
N3-Re1-N4	82.61(18)	81.22
C2-C1-C7	107.1(5)	105.81

as a mono anionic NNN-coordinating tridentate ligand where -OH group remains free. In distorted  $\text{ReC}_3\text{N}_3$  environment, the equatorial plane is made by two nitrogen atoms N(3) and N(4) of the ligand and two carbonyl group C(23)-O(3) and C(25)-O(2). The axial position is occupied by pyridyl nitrogen atom N(1) and remaining carbonyl group C(24)-O(1). The C(2)-C(1)-C(7) ( $107.11^\circ$ ), C(2)-C(1)-N(1) ( $105.16^\circ$ ), O(5)-C(1)-C(7) ( $106.11^\circ$ ) bond angles and the C(1)-N(1) ( $1.479\text{\AA}$ ) distance of the ligand frame in the complex **3** reveals the approximate  $\text{sp}^3$  hybridisation of C(1) carbon atom. The short Re-N(1) bond distance ( $2.140\text{\AA}$ ) and  $\text{sp}^3$  hybridisation of C(1) atom confirm the presence of Re(I)-amido bond in the complex. The other Re-N bond lengths are usual.

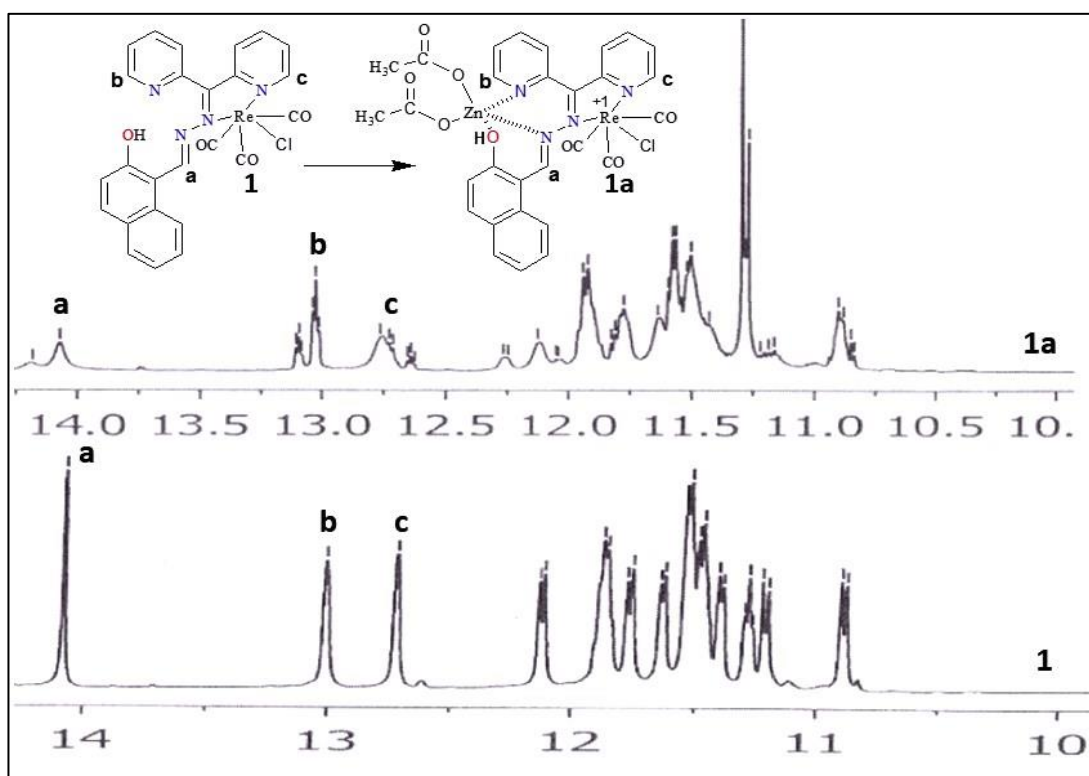
The mechanism behind the formation of **3** is not very much clear to us but it is believed that a weak interaction of **1** with  $\text{Zn}(\text{OAc})_2$  is responsible for the above mentioned transformation.



**Figure III.5** Most probable mechanism of generation of complex **3** from complex **1**.

At first, the interaction of  $\text{Zn}(\text{OAc})_2$  with uncoordinated pyridine nitrogen (N4), imine nitrogen (N2) and phenolic oxygen of **1** enhance the electrophilicity of ketimine carbon (C1). In the next step, solvent methanol attacks C1 and simultaneously ketimine bond gets reduced and N4 binds with rhenium (I) center followed by removal of chloride ion and  $\text{Zn}(\text{OAc})_2$ . The proposed mechanism of the reaction and the NMR spectra of interaction of **1** with  $\text{Zn}(\text{OAc})_2$  is given in **Figure III.5** and **Figure III.6**.

In support of the mechanism proposed above,  $^1\text{H}$  NMR of **1** is performed in mixed solvent ( $\text{CDCl}_3 + \text{CD}_3\text{OD}$ ) due to low solubility of **1** in  $\text{CD}_3\text{OD}$ . As a result, all the proton signals of **1** are shifted towards downfield region. In **Figure III.6**, the lower most spectra represent proton signals for **1**, where a peak at  $\delta 14.195$  shows aldimine proton signal (a). The protons adjacent to pyridyl nitrogen (b and c in **Figure III.6**) show doublet at  $\delta 13.023$  and  $\delta 12.735$  respectively.

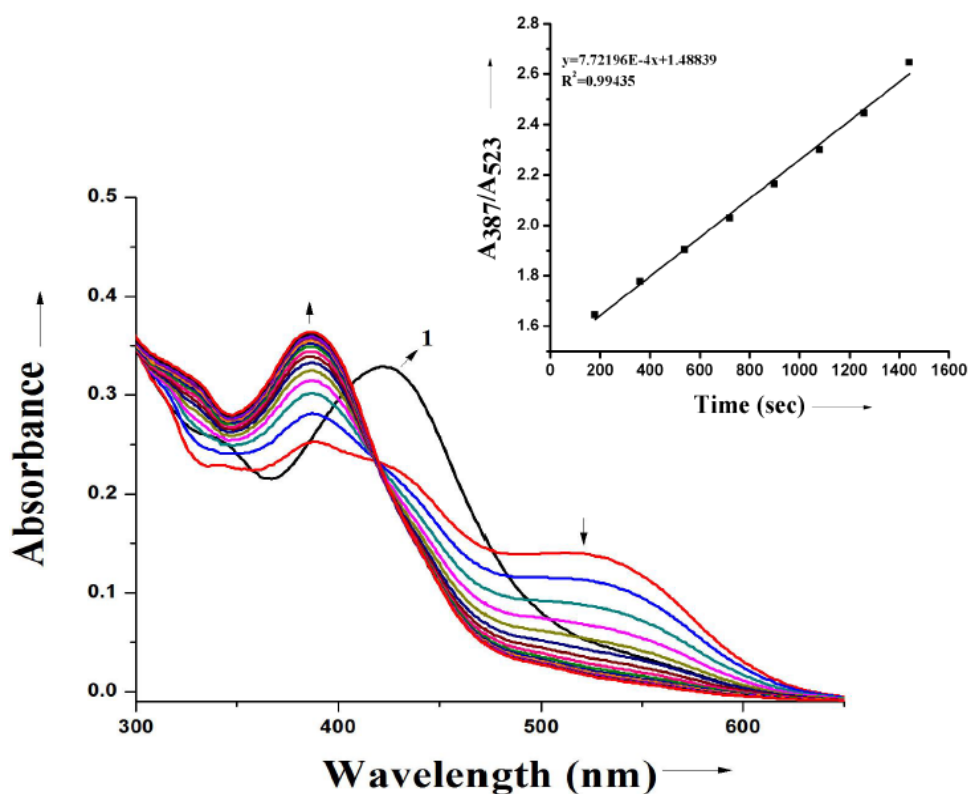


**Figure III.6**  $^1\text{H}$  NMR spectra of **1** (below) and **1a** (above) followed by addition of  $\text{Zn}(\text{OAc})_2$ . Aldimine proton and protons adjacent to pyridyl moiety are represented by a, b and c respectively.

After addition of stoichiometric amount of  $\text{Zn}(\text{OAc})_2$  into the solution of **1**, an immediate spectra is recorded. It reveals that, addition of  $\text{Zn}(\text{OAc})_2$  causes the proton signals of 'a', 'b' and 'c' to shift more towards downfield region by  $\sim 0.097$  ppm,  $\sim 0.1$  ppm and  $\sim 0.05$  ppm respectively. This observation clearly indicates the interaction of  $\text{Zn}(\text{OAc})_2$  with **1**. Here,  $\text{Zn}(\text{OAc})_2$  weakly binds with NNO donor sites of **1**, resulting in the relatively low electron density around aldimine proton and pyridyl protons as  $\text{Zn}(\text{II})$  pulls electrons towards itself. This interaction is mainly responsible for the downfield shift of protons.

### C. Electronic Spectroscopy

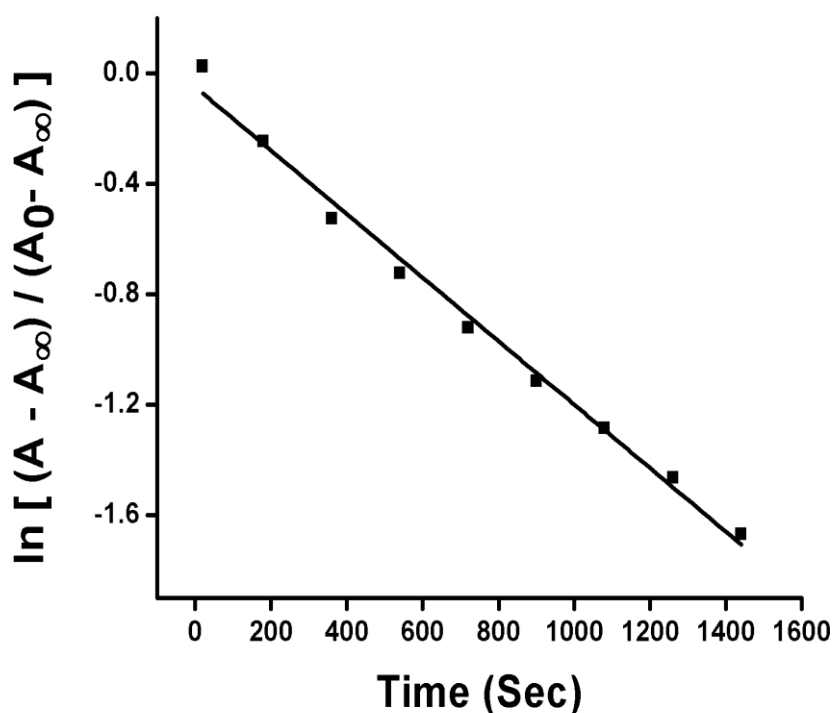
Time dependent UV-spectral studies were performed in methanol - dichloromethane (1:1) to get better insight into the rate of the reaction in the presence of  $\text{Zn}(\text{OAc})_2$ .



**Figure III.7** Time evolution of UV-Vis spectra of **1** with  $\text{Zn}(\text{OAc})_2$  at room temperature. Inset: a ratio-metric plot of  $A_{387}/A_{523}$

The absorption band at 426 nm of **1** diminishes instantly and two new peaks appeared at 387 and 523 nm respectively after stoichiometric addition of  $\text{Zn}(\text{OAc})_2$  to the solution of **1**. This spectral change can be attributed to the generation of new species formed by interacting  $\text{Zn}(\text{OAc})_2$  with **1**. The time dependent spectral plot of decolourization of dark red solution to yellow is given in **Figure III.7**.

It is clear from the plot that the newly generated peak at 523 nm decreases and that of 387 nm increases with time and this spectral changes passes through an isobestic point at 413 nm which is associated with the transformation of this species into complex **3**, with advancement to time. The plot of  $A_{387}/A_{523}$  vs. time (sec) gives a straight line having  $R^2$  value 0.99 (see **Figure III.7**) corroborates with the gradual decay of the intermediate with respect to the time. The reaction is found to be found to be a pseudo first order reaction (**Figure III.8**). Hence, the calculated rate constant of the formation of complex **3** is  $1.1 \times 10^{-3} \text{ s}^{-1}$ .

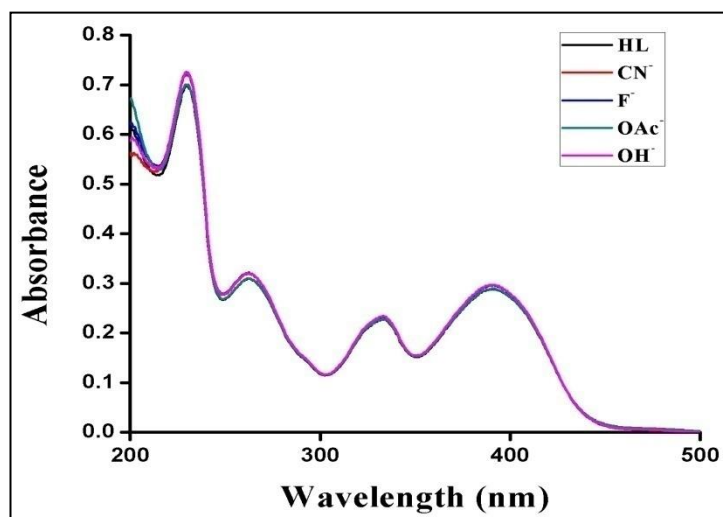


*Figure. III.8 Plot of  $\ln [(A - A_{\infty}) / (A_0 - A_{\infty})]$  vs. time (monitored at 387 nm).*



### *Selective response towards cyanide*

The selective sensing of anions is highly significant because anions are widely used and play important roles in both environmental and life sciences. In this connection, the anion sensing properties of the ligand as well as the complexes were studied with various anions. In the present study we have found that complex **1** exhibit sensing activity for the cyanide ion only while that of complexes **2**, **3** and the ligand, HL exhibit no sensing activity (**Figure III.9**). The sensing activity was monitored with the help of UV-Vis and luminescence spectral method.

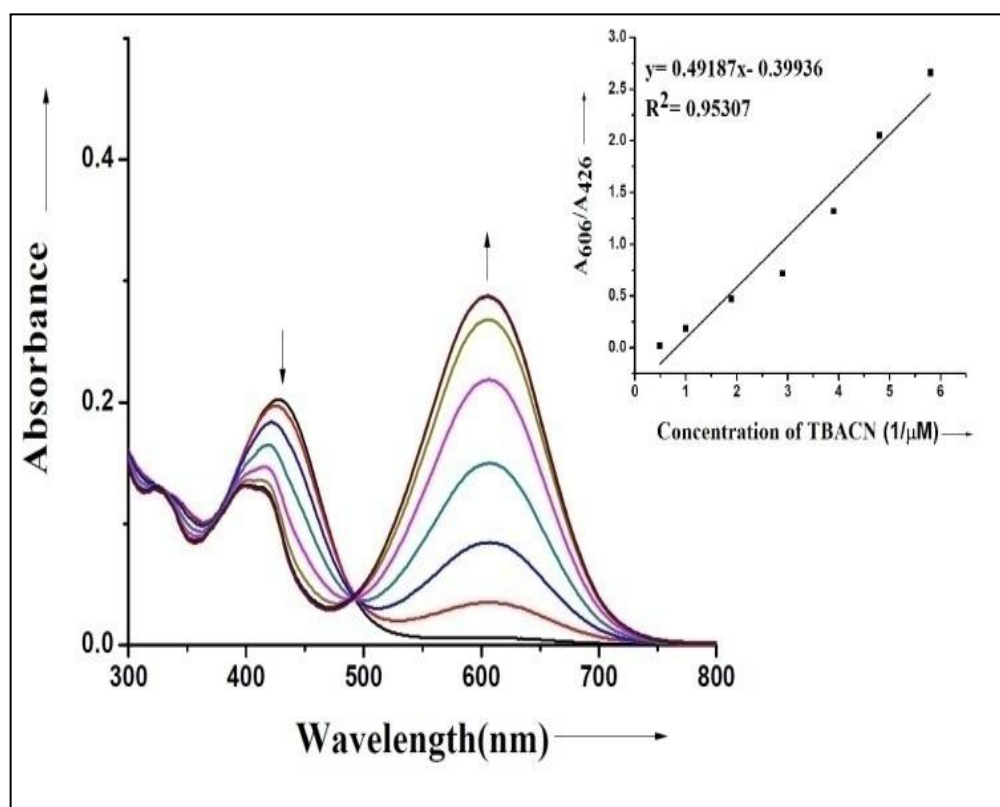


**Figure III.9** UV-Vis spectra of HL in acetonitrile in presence of various anions. No change in spectra is observed.

### *UV-Vis spectroscopic method*

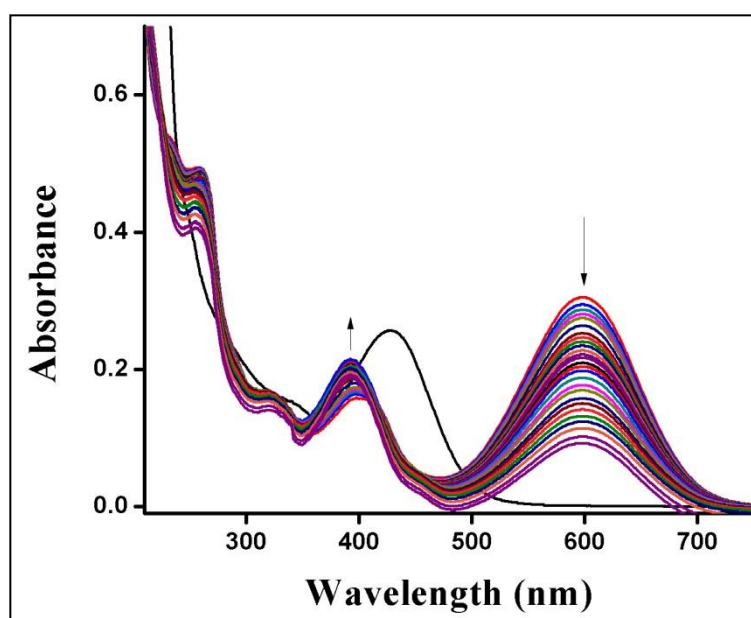
UV-Vis spectra of **1** in CH<sub>3</sub>CN show two absorption peaks at wavelength of 426 nm and 336 nm at room temperature (See Chapter 2, **Table II.6**). Investigation of spectral behaviour of **1** (20 μM) is carried out in CH<sub>3</sub>CN solution in presence of various anions such as Cl<sup>-</sup>, Br<sup>-</sup>, I<sup>-</sup>, NO<sub>3</sub><sup>-</sup>, F<sup>-</sup>, OAc<sup>-</sup>, OH<sup>-</sup>. The orange colour solution of **1** change into blue upon addition of F<sup>-</sup>, OAc<sup>-</sup>, OH<sup>-</sup> and CN<sup>-</sup> in which a new band

appears at 606 nm and a blue shift of 426 nm band observed at 408 nm. However, no such changes are observed in case of  $\text{Cl}^-$ ,  $\text{Br}^-$ ,  $\text{I}^-$ ,  $\text{NO}_3^-$  ions. Upon gradual addition of 1.5 equivalents of  $\text{X}^-$  ( $\text{F}^-$ ,  $\text{OAc}^-$ ,  $\text{OH}^-$  or  $\text{CN}^-$ ) ions in the acetonitrile solution of the complex **1** ( $c = 20 \mu\text{M}$ ), the intensity of the band at 606 nm increases while that of at 408 nm decreases with a generation of an isobestic point at 492 nm (**Figure III.10**). The new band at 606 nm can be attributed to the intramolecular charge transfer (ICT) band. A plot of the absorbance ratio at 606 and 426 nm ( $A_{606}/A_{426}$ ) vs concentration of cyanide clearly indicates that  $A_{606}/A_{426}$  increases linearly  $R^2 = 0.95$ . The blue colour is stable in case of  $\text{F}^-$ ,  $\text{OAc}^-$  and  $\text{OH}^-$ .



**Figure III.10** Absorption titration of **1** ( $c = 2 \times 10^{-5} \text{ M}$ ) with  $\text{CN}^-$  upto 1.5 equivalents ( $c = 2 \times 10^{-3} \text{ M}$ ) in acetonitrile and inset shows plot of  $A_{606}/A_{426}$  vs. concentration of  $\text{CN}^-$

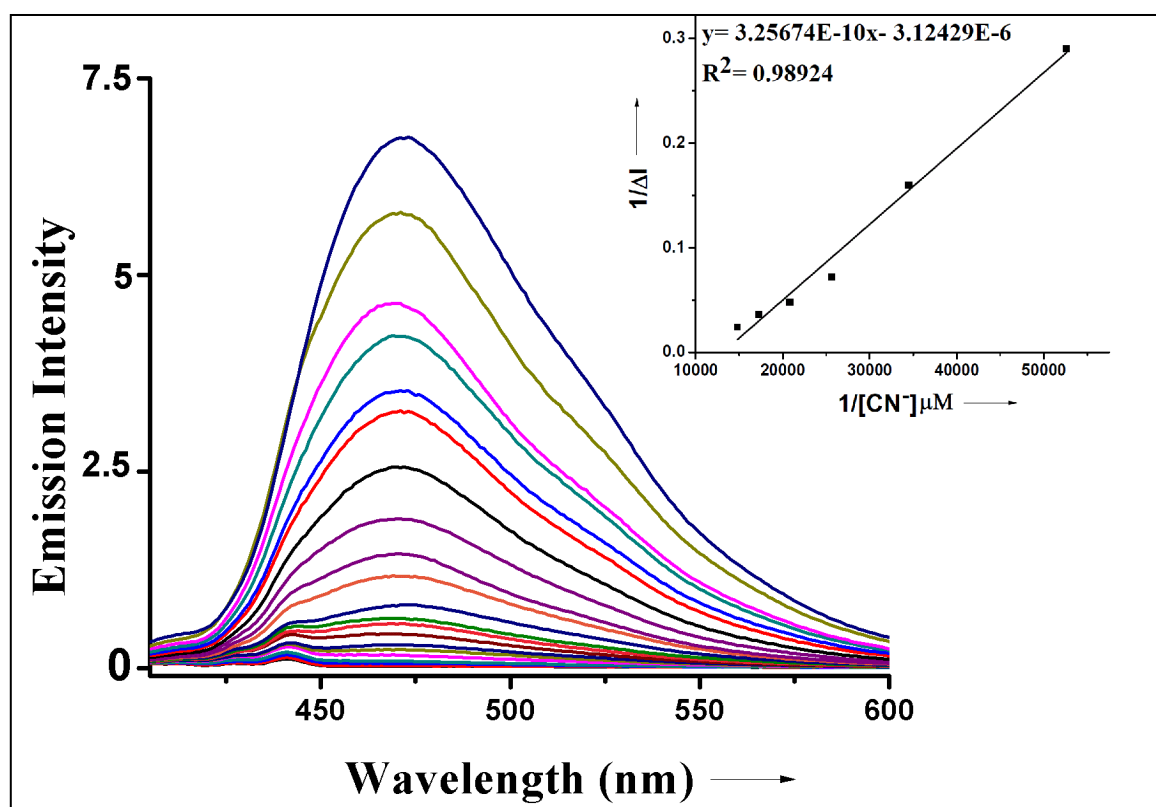
But in case of  $\text{CN}^-$  ion, the blue solution gradually changes to greenish yellow with time. With advancement of time the absorption maxima at 606 nm was decreased gradually, on the other hand enhancement of intensity at 390 nm (**Figure III.11**) was observed. The absorption band at 390 nm presumably assigned as MLCT character. This unique feature can be attributed to the involvement of classical “Strecker” reaction, where aldimine ( $\text{HC}=\text{N}$ ) carbon of **1** is attacked by cyanide ion. It is assumed that 1.5 equivalent cyanide ion first abstract  $-\text{OH}$  proton and form  $\text{HCN}$  in the reaction medium which on increase in time, undergoes Strecker reaction to produce  $[\text{1-CN}]$  adduct. To check the selectivity of the anions we have performed the reaction with 1.5 equivalent of  $\text{CN}^-$  ion and 1.5 equivalent of  $\text{F}^-$ ,  $\text{OAc}^-$  or  $\text{OH}^-$  ions. It is to be noted that here we observed the same spectral changes i.e. the blue solution gradually changes to yellow with time. Thus, we can say that the bi-functional ligand possesses superior selectivity to detect the cyanide ion over the reported system bearing  $[\text{Re}(\text{CO})_3]^+$ . So, the choice of such ligands help us to achieve our goal to generate metalloreceptor containing rhenium (I) which can detect exclusively the cyanide ion.



**Figure III.11** Time evolution absorption spectra of the solution containing complex **1** and 1.5 equivalents of  $\text{CN}^-$  in acetonitrile at room temperature.

#### D. Emission spectroscopy

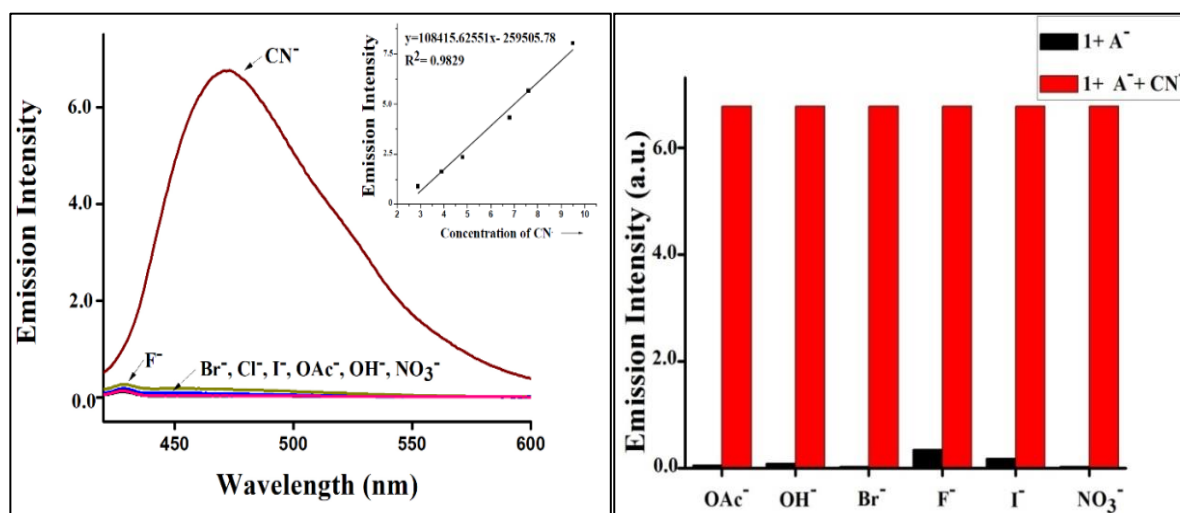
Upon gradual addition of  $\text{CN}^-$  ion to the acetonitrile solution of sensor ( $c = 2 \times 10^{-5}$  M), the emission intensity increases by 272 fold at 470 nm. The Stokes shift of emission maxima is 90 nm. Initially, **1** shows very low phosphorescence upon exciting at 380 nm. With increasing the concentration of  $\text{CN}^-$  (0-200  $\mu\text{M}$ ) to a solution of **1** (20  $\mu\text{M}$ ), the intensity of emission increases periodically at 470 nm (**Figure III.12**). Further addition of  $\text{CN}^-$  does not influence the emission intensity.



**Figure III.12** Spectrofluorometric titrations of **1** ( $c = 2 \times 10^{-5}$  M) with 10 equivalents of TBACN in acetonitrile solution. Inset: the plot of  $1/\Delta I$  vs.  $1/[\text{CN}^-]$ , where  $\Delta I = I - I_0$  ( $I$  = intensity after cyanide addition,  $I_0$  = intensity before cyanide addition).

A competitive experiment were also carried out in a acetonitrile solution of **1** in the presence of 10 equivalents of  $\text{CN}^-$  and 10 equivalents of various other anions  $\text{Cl}^-$ ,  $\text{Br}^-$ ,

I<sup>-</sup>, NO<sub>3</sub><sup>-</sup>, F<sup>-</sup>, OAc<sup>-</sup>, OH<sup>-</sup> to further explore the utility of complex **1** as an ion-selective chemosensor for CN<sup>-</sup> (**Figure III.13**). The emission spectrum of **1** with CN<sup>-</sup> was not influenced by the subsequent addition of competing anions. This result indicates that **1** can selectively detect the cyanide ion.



**Figure III.13** Anion sensitivity of complex **1** by spectrofluorometric method. Inset: the plot of emission intensity vs. concentration of CN<sup>-</sup> (left); Black bars represent the emission sensitivity of **1** ( $c = 2 \times 10^{-5}$ ) towards various anions. Red bars represent the emission response measured after the addition of CN<sup>-</sup> (10 equivalents) in **1** in presence of anions (A<sup>-</sup>) (right).

The detection limit was estimated from the luminescence titration. The plot of emission intensity vs. the CN<sup>-</sup> concentration monitored at 471 nm shows a good linear relationship (**Figure III.13**). We have calculated the detection limit on the basis of  $3\sigma/k$ , where  $\sigma$  is the standard deviation of blank measurement. The calculated detection limit<sup>12</sup> is found to be 0.050  $\mu$ L i.e.  $5.0 \times 10^{-8}$  M, which is higher than the reported complexes bearing [Re(CO)<sub>3</sub>]<sup>+</sup> core.

The weak luminescence of rhenium (I) complexes is connected with the internal charge transfer (ICT) processes in the excited state. In **1**, the  $\pi$ - electron clouds of the ligand moiety are linked through the ketimine and aldimine bonds (vide supra). This conjugation facilitates the internal charge transfer (ICT) process in the pure complex as well as in its deprotonated form of free -OH group. The ICT process in the excited state favours the non-radiative decay process in the system which corroborates with the weak luminescence properties of rhenium (I) complex in presence or absence of  $\text{Cl}^-$ ,  $\text{Br}^-$ ,  $\text{I}^-$ ,  $\text{NO}_3^-$ ,  $\text{F}^-$ ,  $\text{OAc}^-$ ,  $\text{OH}^-$  ions. However, the addition of cyanide ion into the acetonitrile solution of **1** probably stops the ICT process through the breaking of aldimine bond by the cyanide ion and hence enhances the emission intensity.

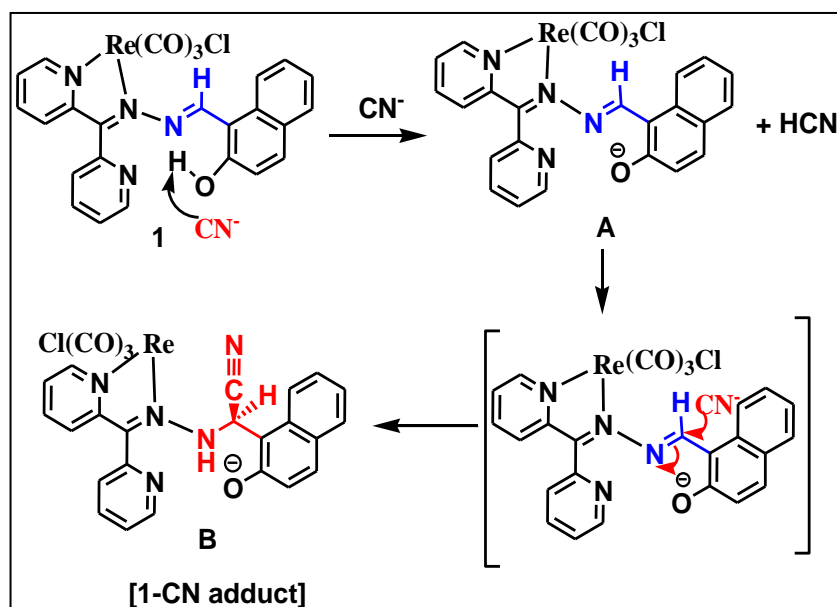
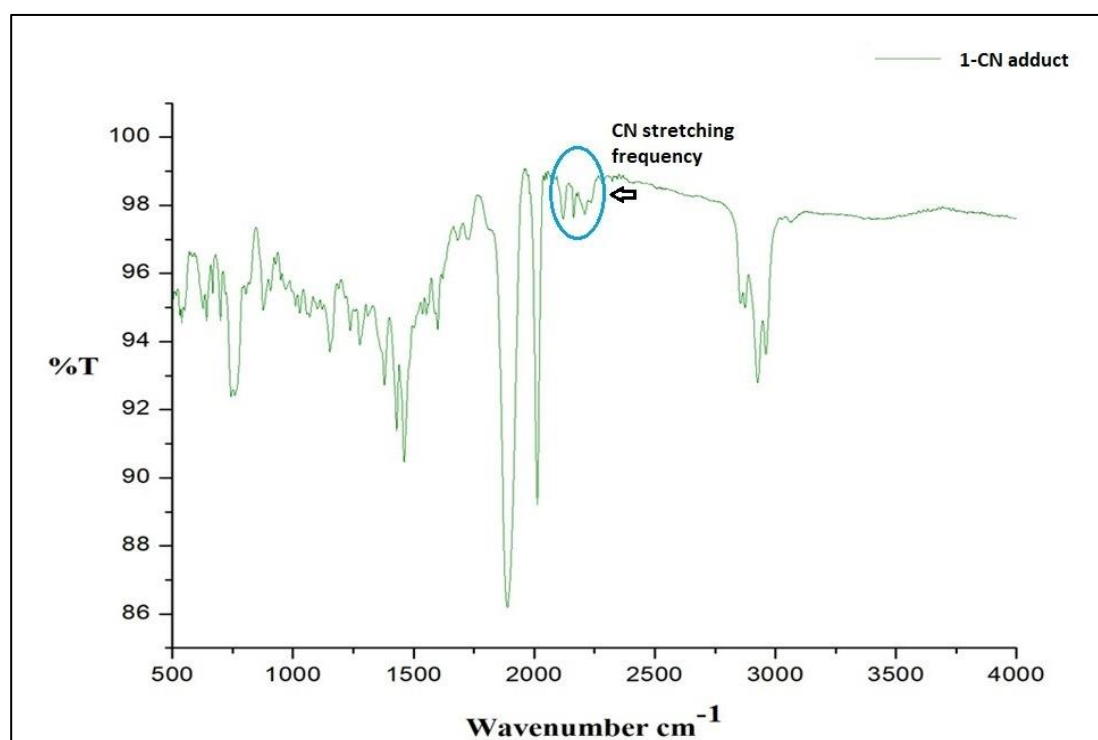


Figure III.14 Plausible mechanism for the formation of [1-CN] adduct

### E. Confirmation of the Interaction of complex **1** with $\text{CN}^-$ by $^1\text{H}$ NMR, IR spectroscopy and ESI-MS Studies

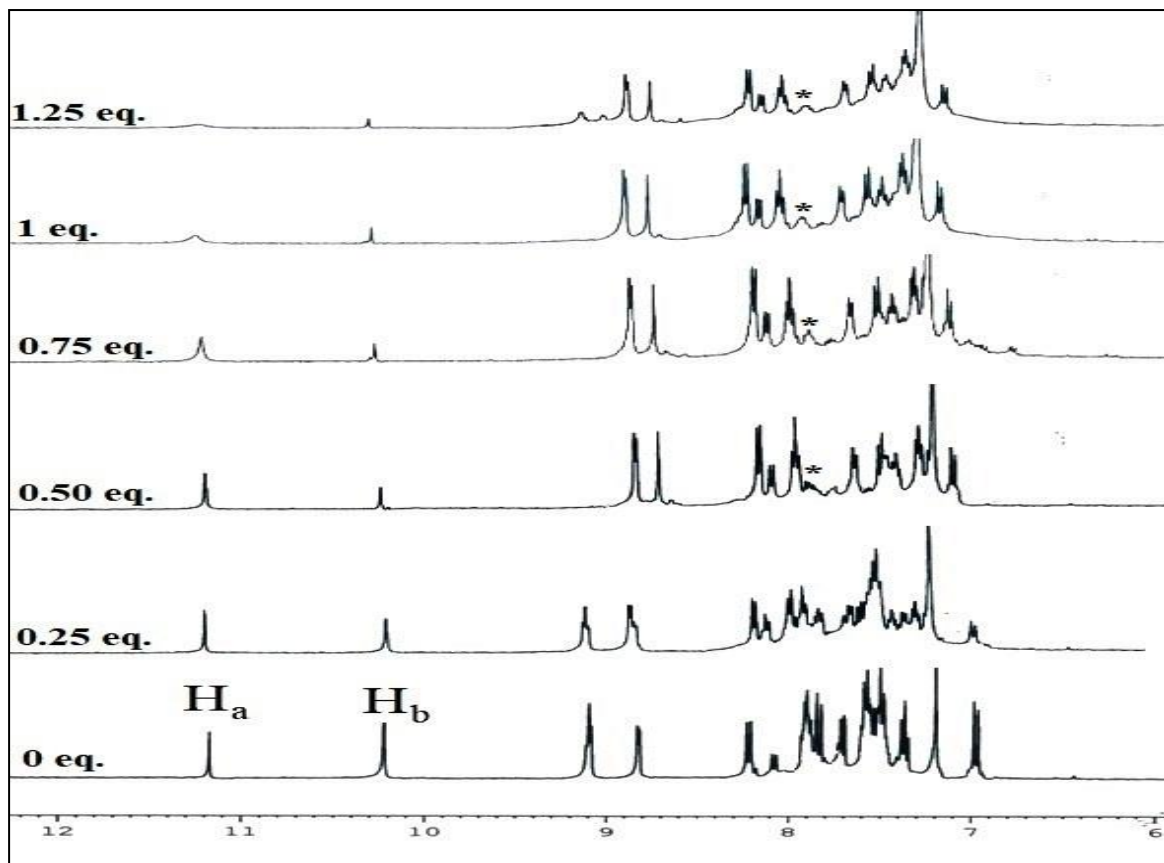
To evaluate the nature of the interaction of  $\text{CN}^-$  with **1**, ESI mass, IR and  $^1\text{H}$  NMR spectroscopy were performed. The mass spectrum of the isolated compound (**1-CN** adduct) shows molecular mass of 687.0701 ( $[\text{M}^+]$ ) which corresponds to the formula of [1-CN] adduct (calculated  $m/z$  687.120). The formation of [1-CN] adduct is further confirmed by IR spectroscopy.

An appearance of a new peak at  $2206\text{ cm}^{-1}$  in IR spectroscopy (**Figure III.15**) clearly indicates the addition of cyanide on aldimine bond, which is absent in the mother compound.  $^1\text{H}$  NMR titration of **1** upon gradual addition of  $\text{CN}^-$  was carried out in  $\text{CDCl}_3$  solution to get better insight into the interaction between **1** and cyanide ions. It is clear from the  $^1\text{H}$  NMR (see **Figure III.16**) titration plot that there is a periodical disappearance of  $-\text{OH}$  at  $\delta$  11.2 ppm and aldimine proton ( $\text{H}^*$ ) at  $\delta$  10.28 ppm with increasing concentration of cyanide ions. On the other hand there is an appearance of a new proton at  $\delta$  7.8 ppm. The disappearance of NMR signal at 11.2 ppm is due to the abstraction of phenolic proton. Whereas the signal at  $\delta$  10.28 ppm diminishes and appearance of new peak at  $\delta$  7.8 ppm can be assigned to the attack at aldimine carbon atom resulting the transformation of aldimine proton to cyanomethanamine,  $[-\text{CH}(\text{CN})\text{N}]$  proton ( $\text{H}_a$ ).



*Figure III.15 IR spectra of cyanide adduct 1-CN*

The chemical shifts, IR stretching frequency and ESI-MS strongly supports the formation of cyanomethanimine. The plausible mechanism for the formation of the cyanide adducts which is proposed in **Figure III.14**.



**Figure III.16**  $^1\text{H}$  NMR titration of **1** in  $\text{CDCl}_3$  solution in presence of 1.25 equivalent of  $\text{CN}^-$  ion.  $\text{H}_a$  and  $\text{H}_b$  represents  $-\text{OH}$  proton and aldimine proton respectively. Generation of cyanomethanimine proton is shown by (\*).

At room temperature in solution state the complexes are very weak emitters when complex **1** was excited at 426 nm and complex **2** was excited at 507 nm. Quantum yield of **1-CN** was found to be 0.658. To gain an insight into the relaxation dynamics of **1-CN**, excited state lifetime was measured in acetonitrile solution at room temperature at 471 nm. It displays bi-exponential decay having lifetime  $\tau_1 = 2.6$  ns and  $\tau_2 = 7$  ns.



quenching of emission intensity of **1**-CN in presence of molecular oxygen in acetonitrile solution suggests the triplet nature of the emissive state. It is presumably assumed that the origin of the bi-exponential decay with short lifetime is attributed to the existence of two closely lying triplet excited states. A very small Stokes shift with respect to the lowest energy absorption band is probably due to the <sup>3</sup>IL (intraligand,  $\pi^* \rightarrow \pi$ ) character of the emissive state. The high luminescence intensity along with strong radiative decay constant ( $k_r = 5.92 \times 10^7 \text{ s}^{-1}$ ) is associated with the confinement of the <sup>3</sup>IL transition between two fragments of ligand moiety which arises after the addition of cyanide into the imine (CH=N) bond seizing the conjugation with 2-hydroxynaphthyl moiety. This result is in good agreement with the non-radiative decay rate ( $k_{nr} = 3 \times 10^7 \text{ s}^{-1}$ ) of excited **1**-CN.

### III.4. CONCLUSION

This chapter focuses on the reactivity of a rhenium complex towards  $d^{10}$  cations and various anions. The NN coordinated species show tremendous reactivity in the presence of specific cation and anion. Complex **1** reacts with  $\text{Zn}(\text{OAc})_2$  and we have isolated and characterized the highly reactive  $\alpha$ -amino ether containing rhenium(I) complex. We have also studied the transformation by UV-Vis spectroscopic method. The complex **1** selectively detect the cyanide ion. The cyanide ion terminates the ICT process of the metalloreceptor which enhance the luminescence property of the system. The reasonably high detection limit ( $5.0 \times 10^{-8} \text{ M}$ ) for  $\text{CN}^-$  ion proves the sensitivity for the cyanide detection. The studies presented herein provide valuable insights into the synthetic strategy in the field of generation metalloreceptor of rhenium(I). In addition, these results are proved to be helpful in the identification of the behaviour of metalloreceptor incorporating multifunctional ligands.

### III.5. REFERENCES

- (1) (a) V. W-W. Yam, Y-L. Pui, K. M-C. Wong, K-K. Cheung *Chem. Commun.* **2000**, 1751–1752.
- (2) (a) C. J. Cooper, M. Jones, S. K. Brayshaw, B. Sonnex, M. L. Russell, M. Mahon, D. Allan *Dalton Trans.* **2011**, 40, 3677  
(b) R. J. Hooley, T. Iwasawa, J. Jr. Rebek *J. Am. Chem. Soc.* **2007**, 129, 15330  
(c) T. Kawamichi, T. Haneda, M. Kawano, M. Fujita *Nature* **2009**, 461, 633  
(d) P. Abhayawardhana; A. Patricia, T. Perera, F. R. Fronczek, Luigi G. Marzilli, *Inorg. Chem.* **2012**, 51, 7271-7283  
(e) T. Perera, F. R. Fronczek, P. A. Marzilli, L. G. Marzilli, *Inorg. Chem.* **2010**, 49, 7035–7045  
(f) T. Perera, F. R. Fronczek, P. A. Marzilli, L. G. Marzilli, *Inorg. Chem.* **2010**, 49, 2123–2131.
- (3) (a) S. A. Rommel, D. Sorsche, M. Fleischmann, S. Rau *Chem. Eur. J.* **2017**, 23, 18101 – 18119  
(b) H.-J. Mo, Y. Shen, B.-H. Ye *Inorg. Chem.* **2012**, 51, 7174 – 7184  
(c) S.-S. Sun, A. J. Lees, *Chem. Commun.* **2000**, 1687 – 1688  
(d) S. Saha, A. Ghosh, P. Mahato, S. Mishra, S. K. Mishra, E. Suresh, S. Das, A. Das, *Org. Lett.* **2010**, 12, 3406 – 3409  
(e) N. Kumari, S. Jha, S. Bhattacharya, *J. Org. Chem.* **2011**, 76, 8215– 8222  
(f) K. -S. Lee, H. -J. Kim, G. -H. Kim, I. Shin, J.-I. Hong, *Org. Lett.* **2008**, 10, 49 – 51  
(g) N. Gimeno, X. Li, J. R. Durrant, R. Vilar, *Chem. Eur. J.* **2008**, 14, 3006 – 3012  
(h) S.-S. Sun, A. J. Lees, P. Y. Zavalij, *Inorg. Chem.* **2003**, 42, 3445 – 3453  
(i) A. S. kumar, R. Manivannan, K. P. Elango, *J. Organomet. Chem.* **2014**, 750, 98 –106
- (4) (a) H. H. Nguyen, T. Tran, P. L. M. Wong, *A Hydrometallurgy* **1997**, 46, 55–69  
(b) M. A. Chaaban, *J. Mater. Process. Technol.* **2001**, 119, 336–343

- (c) G. J. Hathaway, N. H. Proctor, *Chemical Hazards of the Workplace*, 5th ed.; Wiley: Hoboken, NJ, **2004**, pp 2190–2191
- (d) Patnaik, P. A. *Comprehensive Guide to the Hazardous Properties of Chemical Substance*; van Nostrand Reinhold: New York, **1992**; pp 1229–1244
- (e) B. Vennesland, E. E. Comm, C. J. Knownles, J. Westly, F. Wissing, *Cyanide in Biology*; Academic Press: London, **1981**
- (f) Koenig, R. *Science* **2000**, *287*, 1737–1738
- (g) R. J. Takano, *Exp. Med.* **1916**, *24*, 207–211.
- (5) (a) S. Karmakar, S. Mardanya, P. Pal, S. Baitalik *Inorg. Chem.* **2015**, *54*, 11813–11825
- (b) J. Taylor, N. Roney, M. E. Fransen, S. Swarts, *Toxicological Profile for Cyanide*; DIANE Publishing: Atlanta, GA, **2006**
- (c) C. Young, L. Tidwell, C. Anderson, *Cyanide: Social, Industrial, and Economic Aspects, Minerals, Metals, and Materials Society*, Warrendale, **2001**.
- (d) K. W. Kulig, *Cyanide Toxicity*, U.S. Department of Health and Human Services: Atlanta, **1991**
- (e) S. I. Baskin, T. G. Brewer, *Medical Aspects of Chemical and Biological Warfare*; Eds. (F. Sidell, E. T. Takafuji, D. R. Franz) TMM Publication: Washington, **1997**; Chapter 10, pp 271–286.
- (6) (a) R. Badugu, J. R. Lakowicz, C. D. Geddes *J. Am. Chem. Soc.* 2005, **127**, 3635–3641
- (b) Y. Shiraishi, M. Nakamura, K. Yamamoto, T. Hirai, *Chem. Commun.* **2014**, *50*, 11583–11586.
- (7) (a) K. S. Bejoymohandas, AjayKumar, S. Sreenadh, E. Varathan, S. Varughese, V. Subramanian, M. L. P. Reddy, *Inorg. Chem.* **2016**, *55*, 3448–346
- (b) S. Khatua, D. Samanta, J.W. Bats, M. Schmittel, *Inorg. Chem.* **2012**, *51*, 7075–7086
- (c) H. J. Kim, K. C. Ko, J. H. Lee, J. Y. Lee, J. S. Kim *Chem. Commun.* **2011**, *47*, 2886–2888
- (d) X. Lv, *Chem. Commun.* **2011**, *47*, 12843–12845

- (e) X. Cheng, Y. Zhou, J. Qin, Z. Li, *ACS Appl. Mater. Interfaces* **2012**, *4*, 2133–2138
- (8) (a) S.-S. Sun, A. J. Lees *Chem. Commun.* **2000**, 1687–1688  
(b) H. Miyaji, J. L. Sessler, *Angew. Chem., Int. Ed.* **2001**, *40*, 154–157  
(c) Y.-H. Kim, J.-I. Hong, *Chem. Commun.* **2002**, 512–513  
(d) Y.-K. Yang, J. Tae, *Org. Lett.* **2006**, *8*, 5721–5723  
(e) M. Tomasulo, S. Sortino, A. J. P. White, F. M. Raymo *J. Org. Chem.* **2006**, *71*, 744–753  
(f) N. Gimeno, X. Li, J. R. Durrant, R. Vilar, *Chem. Eur. J.* **2008**, *14*, 3006–3012.
- (9) (a) A. Bencini, V. Lippolis, *Environ. Sci. Pollut. Res.* **2016**, *23*, 24451  
(b) J.H. Lee, A.R. Jeong, I.-S. Shin, H.-J. Kim, J.-I. Hong, *Org. Lett.* **2010**, *12*, 764–767  
(c) I. Bhowmick, D.J. Boston, R.F. Higgins, C.M. Klug, M.P. Shores, T. Gupta *Sens. Actuators B* **2016**, *235*, 325–329 (d) M.E. Jun, B. Roy, K. H. Ahn *Chem. Commun.* **2011**, *47*, 7583–7601.
- (10) (a) T. K. Mole, W. E. Arter, I. Marques, V. Felix, P. D. Beer, *J. Organomet. Chem.* **2015**, *792*, 206–210  
(b) L. Ion, S. Nieto, J. Perez, L. Riera, V. Riera, J. Daz, R. Lopez, K. M. Anderson, J. W. Steed, *Inorg. Chem.* **2011**, *50*, 8524–8531  
(c) T. -P. Lin, C.-Y. Chen, Y.-S. Wen, S.-S. Sun, *Inorg. Chem.* **2007**, *46*, 9201–9212  
(d) B. R. Mullaney, A. L. Thompson, P. D. Beer, *Angew. Chem.* **2014**, *53*, 11458–11462  
(e) C.-O. Ng, S. -C. Cheng, W. -K. Chu, K. -M. Tang, S.-M. Yiu, C.-C. Ko, *Inorg. Chem.* **2016**, *55*, 7969–7979
- (11) (a) B. Chen, Y. Ding, X. Li, W. Zhu, J. P. Hill, K. Ariga, Y. Xie, *Chem. Commun.* **2013**, *49*, 10136–10138
- (12) Analytical Methods Committee; Recommendations for the definition, estimation and use of the detection limit *Analyst* **1987**, *112*, 199–204.

A decorative scroll with a black outline and a white fill. The scroll is oriented horizontally and has a slightly curved top and bottom edge. The text "CHAPTER IV" is centered within the scroll in a bold, black, serif font. The scroll has a small, decorative flourish at the top right corner and a small, decorative flourish at the bottom left corner.

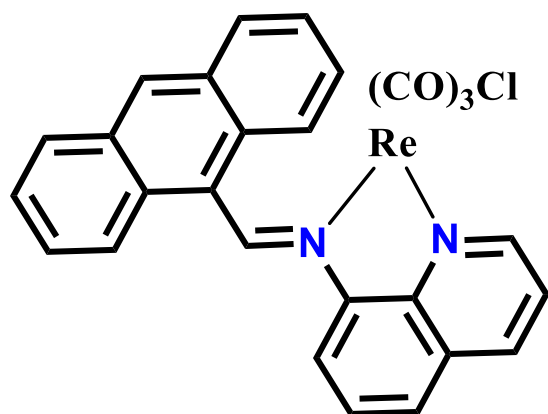
**CHAPTER IV**



# Synthesis, Characterization and DFT studies of Complexes Bearing $[\text{Re}(\text{CO})_3]^+$ Core and Reactivity Towards Cyanide ion

## ABSTRACT

Mononuclear rhenium(I) complexes having *fac*- $[\text{Re}(\text{CO})_3]^+$  core of general formula *fac*- $[\text{Re}(\text{CO})_3(\text{L})\text{Cl}]$  have been synthesized in excellent yield by reacting  $[\text{Re}(\text{CO})_5\text{Cl}]$  with  $\text{L}_1$  and  $\text{L}_2$  in a ratio of 1:1 in toluene under inert atmosphere. Here  $\text{L}_1$  and  $\text{L}_2$  are N-((quinolin-2-yl)methylene)-9H-fluoren-2-amine and N-((anthracen-10-yl)methylene)quinolin-8-amine



respectively. Spectroscopic measurements such as NMR, ESI-MS and IR spectroscopy were used to ensure the formations of desired complexes. Molecular structures of *fac*- $[\text{Re}(\text{CO})_3(\text{L}_1)\text{Cl}]$ , (4) and *fac*- $[\text{Re}(\text{CO})_3(\text{L}_2)\text{Cl}]$ , (5) were confirmed by single-crystal X-ray diffraction. The

ligands are emissive whereas the metal complexes are weak emitter. A remarkable change in absorption as well as emission behaviour was observed in complex 5 upon addition of cyanide ion. Interruption in intra-ligand charge transfer in complex 5 is the probable reason for the obvious change in spectral response of the same.  $^1\text{H}$  NMR titration was performed as the evidence of the previously stated fact. The ground and excited-state geometries, absorption properties of rhenium (I) complexes were examined by DFT and TDDFT methods. The natural transition orbital (NTO) and analysis reveal the nature of excitations.





## IV.1. INTRODUCTION

Rhenium tricarbonylchloro complexes with NN coordinating Schiff base ligands having  $d^6$  electronic configuration is one of the widely studied area in coordination chemistry due to its interesting photophysical properties<sup>1-2</sup> such as room-temperature luminescence from low-lying tunable metal to ligand charge transfer (MLCT) excited states<sup>3-9</sup>, solar-energy conversion<sup>10-12</sup>, OLED and sensor development<sup>13-18</sup>, and biological labeling<sup>19-20</sup>. These imine-based rhenium complexes having  $[\text{Re}(\text{CO})_3]^+$  core show interesting optical behaviour in presence of toxic anions. It is possible to create a highly potential receptor molecule by varying ligand architecture with the photoactive rhenium(I) metal center. A few group of researchers have shown the sensing properties of rhenium (I) complex by hydrogen bonding ( $\text{NH}\cdots\text{X}$ ) followed by deprotonation<sup>21-25</sup>. Anion sensing mechanism by deprotonation of O-H bond has also been reported<sup>26</sup>. But, anion recognition through the addition of an anion into the imine bond is rare. Cyanide ion is a very toxic anion which comes into environment through its use in pharmaceutical industries, insecticides, fertilizers, plastic manufacturing processes, extraction of metals, electroplating industries etc<sup>27-30</sup>. It is necessary to replace the conventional methods of testing for cyanide such as titration, distillation, chromatography or potentiometry as they are expensive, laborious and time consuming. Therefore, there is still a need to develop more robust and less laborious testing methodologies for cyanide. In this context, the complexes of rhenium (I) are suitable. It has proven that  $\text{Re}(\text{CO})_3^+$  core potentially influence the imine based complex to detect cyanide ion selectively among other anions<sup>31</sup>. So, the main focus of this paper is the successful synthesis of two rhenium complexes with NN coordinating two different Schiff base ligands. We have also described the details of synthetic procedures of these mononuclear complexes and the characterization is done by various spectroscopic techniques and single crystal X-Ray diffraction study. The reactivity of these complexes towards various anions has also been studied. To describe the ground and excited state behavior of the rhenium (I)-diimine complexes, the contribution of the fundamental computational chemistry such as DFT/TDDFT<sup>32</sup> and NTO analysis is indispensable. To get better insight into the geometry, electronic structure and

optical properties, TDDFT calculations of several excited states have been performed.

## IV.2. EXPERIMENTAL SECTION

### *A. Materials*

Re(CO)<sub>5</sub>Cl, 2-Aminofluorene, 9-Anthraldehyde, 8-Aminoquinoline, Quinoline-2-carboxaldehyde, tetrabutylammonium salts of all the anions under study were purchased from Sigma Aldrich. All solvents and chemicals are analytically pure. All the reactions with Re(CO)<sub>5</sub>Cl were carried out under argon atmosphere.

*Caution! Cyanide salts are highly toxic and should be handled with care and in very small amounts.*

### *B. Preparation of Compounds*

#### *LIGAND*

**(9H-Fluoren-2-yl)-quinolin-2-ylmethylene-amine (L<sub>1</sub>):** 2-Aminofluorene (500 mg, 2.75 mmol) was dissolved in 20 ml ethanol followed by addition of 2-quinolinecarboxaldehyde (433.15 mg, 2.75 mmol). The resultant mixture was stirred for 2 hour. A yellow precipitate was obtained and it was collected under suction filtration and washed with ethanol. Yield: 70 %, <sup>1</sup>H NMR (CDCl<sub>3</sub>, 300 MHz): δ 8.86 (s, 1H); 8.35 (d, 1H, J = ); 8.17 (dd, 1H, J= 9), 8.67 (d, 1H, J = 9), 8.43 (d, 1H, J = 9), 8.30 (d, 1H, J= 8), 8.17 (t, 1H, J = 12), 7.94 (t, 1H, J = 8), 7.6-7.3 (Ar, 5H), 3.91(9H of fluorine, 2H). <sup>13</sup>C NMR {(CDCl<sub>3</sub>, 500 MHz, δ (ppm)}: 193.05, 150-110; ESI-MS (CH<sub>2</sub>Cl<sub>2</sub>): m/z 321.159[M+H]<sup>+</sup>. IR (cm<sup>-1</sup>): ν(imine C=N): 1614.

**3-Ethylidene-2-methylene-2,3-dihydro-naphthalen-1-ylmethylene)-quinolin-8-yl-amine (L<sub>2</sub>):** 9-Anthraldehyde (500 mg, 2.25 mmol) was dissolved in 20 ml ethanol followed by addition of 8-Aminoquinoline (396.46 mg, 2.25 mmol). The resultant mixture was refluxed for 2 h with the addition of 1 drop of acetic acid. A yellow precipitate was obtained and it was collected under suction filtration and washed with ethanol. Yield: 80%, <sup>1</sup>H NMR (CDCl<sub>3</sub>, 500 MHz): δ 8.88(s, 1H); 8.39 (d, 1H, J=10);

8.23 (q, 2H, J=10), 7.85-7.74 (m, 4H), 7.60 (q, 3H, J=10), 7.38 (t, 1H, J=5).  $^{13}\text{C}$  NMR  $\{(\text{CDCl}_3, 500 \text{ MHz}, \delta \text{ (ppm)})\}$ : 160-111; ESI-MS ( $\text{CH}_3\text{CN}$ ):  $m/z$  333.190  $[\text{M}+\text{H}]^+$ ; IR ( $\text{cm}^{-1}$ ):  $\nu$  (imine  $\text{C}=\text{N}$ ): 1610.

### *COMPLEX*

*fac*- $[\text{Re}(\text{L}_1)(\text{CO})_3\text{Cl}]$ , **4**.  $\text{Re}(\text{CO})_5\text{Cl}$  (50mg, 0.147mmol),  $\text{L}_1$  (47.09 mg, 0.147 mmol) were taken in 30 ml toluene and then the resulting mixture was refluxed for 10 h. After cooling to room temperature, the solvent was removed under reduced pressure. A red coloured solid was obtained. The product on recrystallization from dichloromethane-hexane afforded red coloured crystals. Yield: 60%,  $^1\text{H}$  NMR ( $\text{DMSO-d}_6, 500 \text{ MHz}$ ):  $\delta$  9.7 (s, 1H); 9.03 (d, 1H, J=10); 8.71(d, 1H, J=10), 8.4 (d, 1H, J=10), 8.33 (d, 1H, J=10), 8.19 (q, 2H, J=10), 7.99(t, 2H, J=10), 4.09 (s, 2H).  $^{13}\text{C}$  NMR  $\{(\text{DMSO-d}_6, 500 \text{ MHz}, \delta \text{ (ppm)})\}$ : 196, 206 (CO), 171-118; ESI-MS ( $\text{CH}_2\text{Cl}_2$ ):  $m/z$  642.15  $[\text{M}+\text{H}]^+$ . IR ( $\text{cm}^{-1}$ ):  $\nu$  (CO): 1881, 1920 and 2019.

*fac*- $[\text{Re}(\text{L}_2)(\text{CO})_3\text{Cl}]$ , **5**.  $\text{Re}(\text{CO})_5\text{Cl}$  (50mg, 0.147mmol),  $\text{L}_2$  (48.86 mg, 0.147 mmol) were taken in 30 ml toluene and then the resulting mixture was refluxed for 10 h. After cooling to room temperature, the solvent was removed under reduced pressure. A red coloured solid was obtained. The product on recrystallization from dichloromethane-hexane afforded red coloured crystals. Yield: 68%,  $^1\text{H}$  NMR ( $\text{CDCl}_3, 500 \text{ MHz}$ ):  $\delta$  10.28 (s, 1H); 9.36(d, 1H, J=5), 8.70(s, 1H), 8.60(s, 1H), 8.26-7.45(m, 3H);  $^{13}\text{C}$  NMR  $\{(\text{CDCl}_3, 500 \text{ MHz}, \delta \text{ (ppm)})\}$ : 196, 198, 207 (CO), 173-120; ESI-MS ( $\text{CH}_2\text{Cl}_2$ ):  $m/z$  661.10  $[\text{M}+\text{Na}]^+$ . IR ( $\text{cm}^{-1}$ ):  $\nu$  (CO): 1879, 1919 and 2013.

### *C. X-Ray Structure Determination*

The single crystal suitable for X-ray crystallographic analysis of complexes *fac*- $[\text{Re}(\text{L}_1)(\text{CO})_3\text{Cl}]$  and *fac*- $[\text{Re}(\text{L}_2)(\text{CO})_3\text{Cl}]$ , was obtained through direct evaporation of solvent at room temperature. Details of the X-ray work are given in tabular form in **Table IV.1** and **Table IV.2** (See also Chapter I).

#### D. Physical Measurements

All physical measurements that included elemental analyses, IR, absorption spectra,  $^1\text{H}$  NMR and spectra, ESI mass spectra, emission spectra measurement were performed as described in **Chapter I**.

**Table IV.1** Atomic coordinates and isotropic thermal parameters complexes 4 and 5

Data collection		
	Complex 4	Complex 5
Total refl. Collected	39392	15517
Unique refl.( $R_{\text{int}}$ )	5133	5387
Used refl.	4538	3880
h k l range	-9<h<9 -11<k<11 -24<l<24	-12<h<12 -13<k<13 -16<l<16

Structure solution and refinement		
	Complex 4	Complex 5
Solution	Patterson	Patterson
Refinement	Full-matrix least-squares on $F^2$	Full-matrix least-squares on $F^2$
GOF on $F^2$	1.117	1.032
$R1,^a[I > 2\sigma(I)]$	0.1052	0.0680
$wR2^b[I > 2\sigma(I)]$	0.2766	0.1797
$R1[\text{alldata}]$	0.1147	0.0935
$wR2[\text{alldata}]$	0.2766	0.1797

**Table IV.2.** Crystal data and structure refinement parameters for complexes **4** and **5**

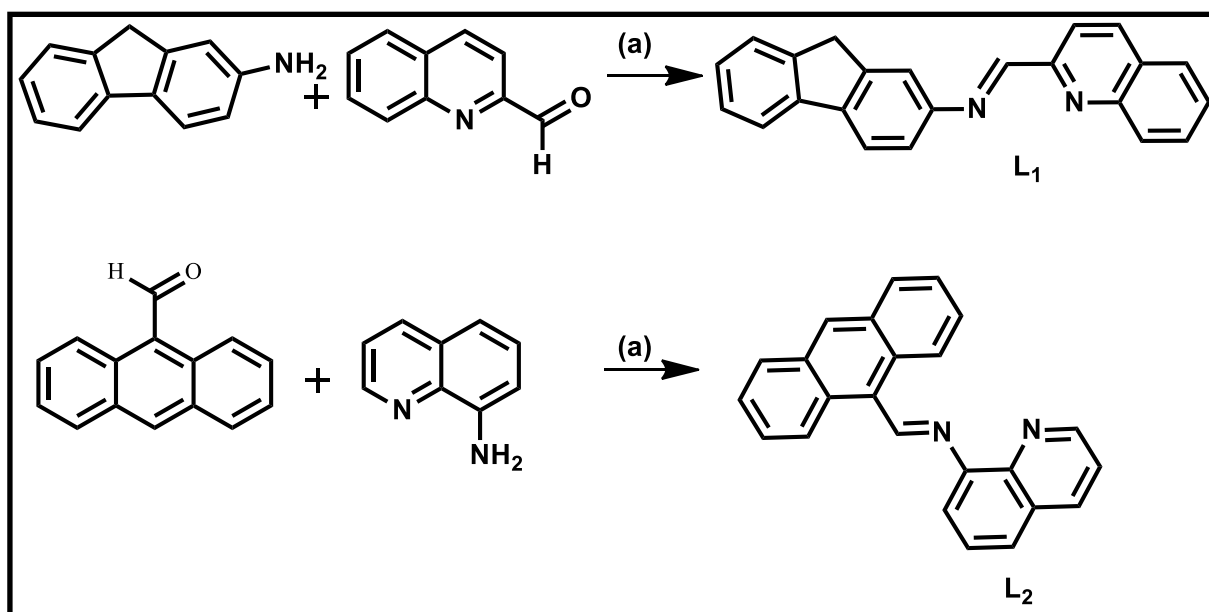
	<b>4</b>	<b>5</b>
Formula	C <sub>26</sub> H <sub>16</sub> ClN <sub>2</sub> O <sub>3</sub> Re	C <sub>28</sub> H <sub>18</sub> Cl <sub>3</sub> N <sub>2</sub> O <sub>3</sub> Re
M <sub>r</sub>	626.06	722.99
Crystal system	Triclinic	Triclinic
Space group	<i>P</i> -1	<i>P</i> -1
<i>a</i> / Å	6.9438(7)	10.0610(17)
<i>b</i> / Å	9.0741(8)	10.9620(19)
<i>c</i> / Å	18.6879(17)	13.023(2)
<i>α</i> /°	99.723(3)	86.860(13)
<i>β</i> /°	98.947(3)	77.069(13)
<i>γ</i> /°	100.024(3)	69.510(12)
<i>V</i> / Å <sup>3</sup>	1121.94(18)	1310.9(4)
<i>Z</i>	2	2
<i>D</i> <sub>calcd</sub> / g cm <sup>-3</sup>	1.853	1.832
<i>μ</i> / mm <sup>-1</sup>	5.566	4.974
<i>θ</i> /°	2.253-27.482	1.521-26.855
<i>T</i> /K	273	296

$${}^a R1 = \Sigma ||F_o| - |F_c|| / \Sigma |F_o|. {}^b wR2 = [\Sigma[w(F_o^2 - F_c^2)^2] / \Sigma[w(F_o^2)^2]]^{1/2}$$

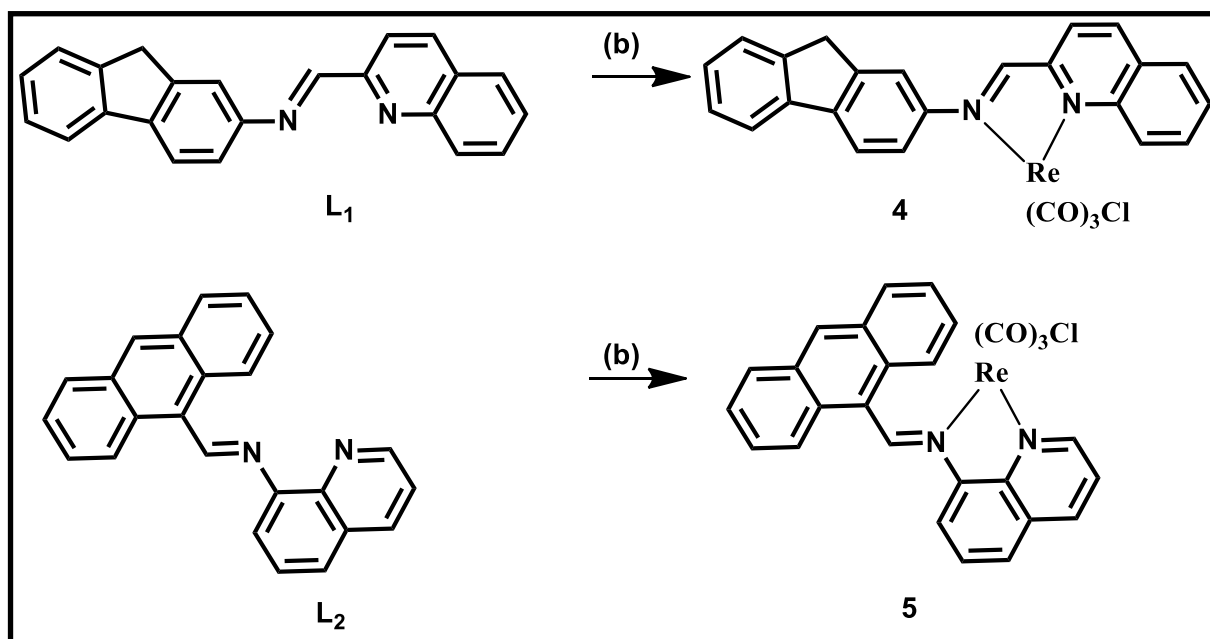
## IV.1. RESULT AND DISCUSSION

### A. Synthesis

*Ligand (L<sub>1</sub> & L<sub>2</sub>):* The Schiff base ligands L<sub>1</sub> and L<sub>2</sub> were synthesized by the condensation reaction of 2-Amino fluorene with 2-Quinoline aldehyde and 9-Anthraldehyde with 8-Amino quinolone respectively (**Figure IV.1**). These two ligands were used as neutral bidentate NN donor ligands towards rhenium (I) metal centre (**Figure IV.2**). These complexes consist of two different fluorophore segments i.e. fluorine and anthracene, by the presence of which complexes **4** and **5** are able to show interesting photo-physical properties. It is to be noted that the choice of such ligands helps us to achieve our goal in the context of synthesis of mononuclear rhenium (I) complexes with interesting optical properties.



**Figure IV.1** Schematic representation for the synthesis of the ligand where a = stirred for 2 h in methanol.



**Figure IV.2** Schematic representation for the synthesis of the Complexes where *b* = reflux in toluene for 10 h.

### ***B. Characterization***

**IR Spectra:** The ligands L<sub>1</sub>, L<sub>2</sub> and the corresponding complexes [Re(CO)<sub>3</sub>(L<sub>1</sub>)Cl], (**4**) and [Re(CO)<sub>3</sub>(L<sub>2</sub>)Cl], (**5**) were characterized satisfactorily by IR, ESI-MS and <sup>1</sup>H NMR spectroscopy. The IR spectra of the complexes exhibited the characteristic metal carbonyl stretching frequency in the range of 1880-2023 cm<sup>-1</sup>, which is due to the presence of fac-[Re(CO)<sub>3</sub>]<sup>+</sup> core having C<sub>3v</sub> symmetry. The IR data of all these compounds are given in the experimental section.

**NMR Spectra:** The <sup>1</sup>H NMR spectra of the complexes and ligands was recorded in CDCl<sub>3</sub> and DMSO-d<sub>6</sub>. The complexes were diamagnetic and displayed well resolved NMR spectra in CDCl<sub>3</sub> and DMSO-d<sub>6</sub> solution and the spectral data are given in the experimental section. The assignment of NMR peaks is based on the intensity and spin-spin splitting pattern. A singlet due to azomethine hydrogen atom observed at ~ 10 ppm in both the complexes. The active methylene hydrogens (-CH<sub>2</sub>) of complex **4** is observed at 4.091 and in ligand L<sub>1</sub> it is observed at 3.91 ppm which depicts the downfield shift of methylene proton upon complexation. The <sup>1</sup>H NMR spectral

features for other aromatic protons of the ligands and complexes matched well with the composition and structure.

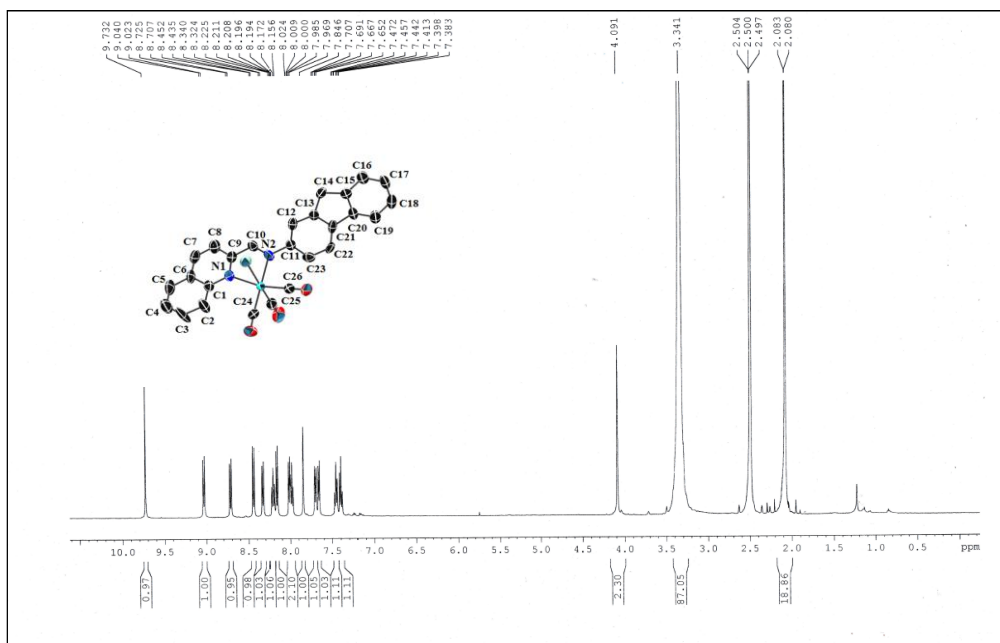


Figure IV.3 Mass spectrum of Complex 4

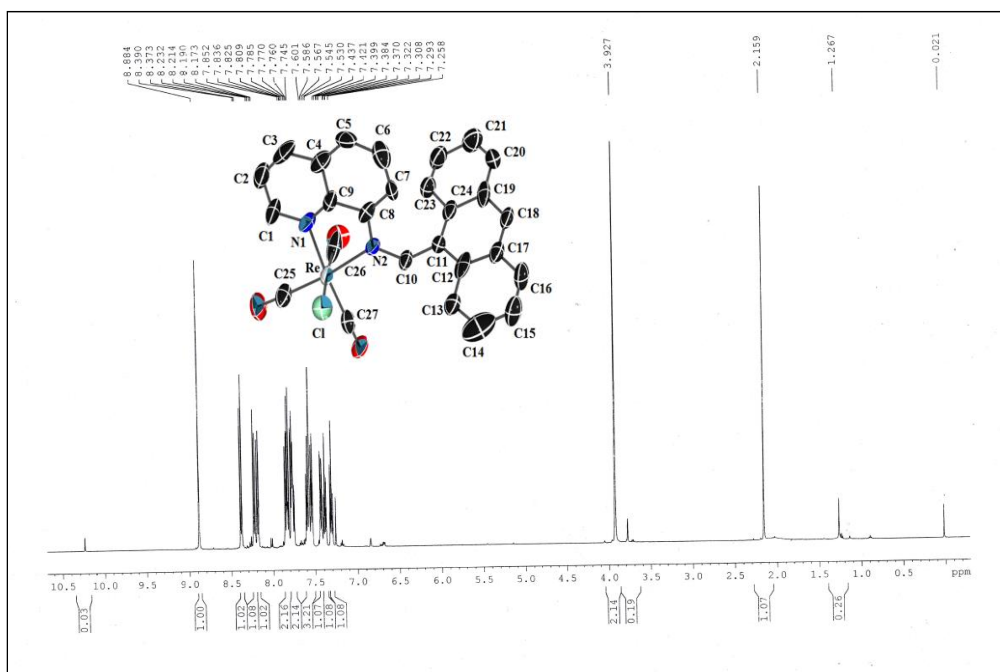
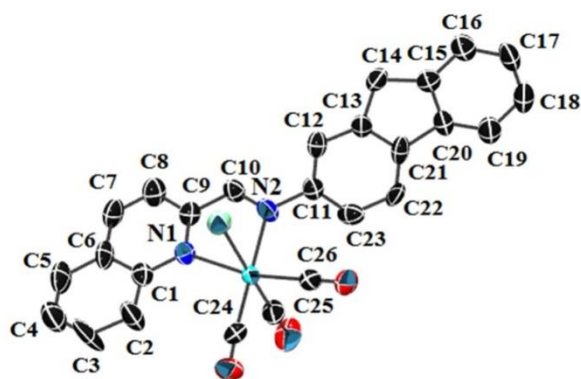


Figure IV.4 Mass spectrum of Complex 4



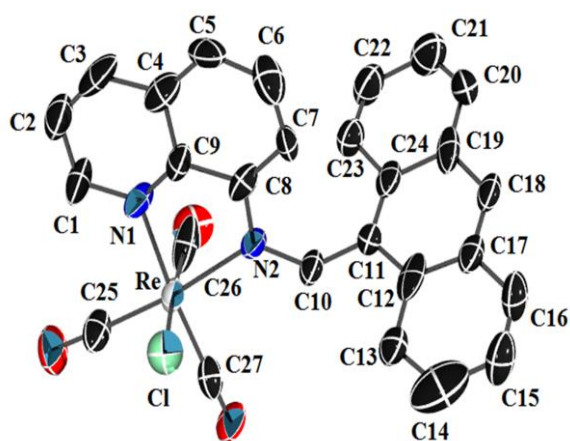
**Mass Spectra:** Electrospray ionization mass spectrometry (ESI-MS) of all the compounds was done. L<sub>1</sub> and L<sub>2</sub> displayed the highest m/z peak at 321.159[M+H]<sup>+</sup> and 333.190 [M+H]<sup>+</sup> respectively whereas complexes **4** and **5** displayed the highest m/z peak at 642.15 [M+H]<sup>+</sup> and 661.10 [M+Na]<sup>+</sup> respectively.

**Crystal Structure:** The molecular structures of the complexes *fac*-[Re(CO)<sub>3</sub>(L<sub>1</sub>)Cl], **4**



**Figure IV.5** Perspective view of complex **4** [Re(HL)(CO)<sub>3</sub>Cl] and hydrogens are omitted For clarity.

the geometry around the rhenium (I) metal centre is distorted octahedral. It can be



**Figure IV.6** Perspective view of complex **5** [Re(L)(CO)<sub>3</sub>] and hydrogens are omitted For clarity.

and *fac*-[Re(CO)<sub>3</sub>(L<sub>2</sub>)Cl], **5** were determined by single-crystal X-ray diffractometer. Both the complexes crystallize in the *P*-1 space group. The selected bond distances and bond angles for **4** and **5** are listed in **Table IV.3** and the molecular views are shown in **Figure IV.5** and **Figure IV.6**. In these two complexes, ligands behave as NN coordinating neutral ligand. Here,

the geometry around the rhenium (I) metal centre is distorted octahedral. It can be characterized by C26-Re-N2 bond angle (167.5) in **4** and C27-Re-N1 bond angle (174.7) in **5**. The Re-Cl bond is relatively longer (~ 0.3 Å) than other Re-N and Re-C bonds. N1-Re-N2 bond angles are 74.3° and 75.5° for **4** and **5** respectively, which give rise to cyclic five member ring in both complexes. The carbonyl ligands

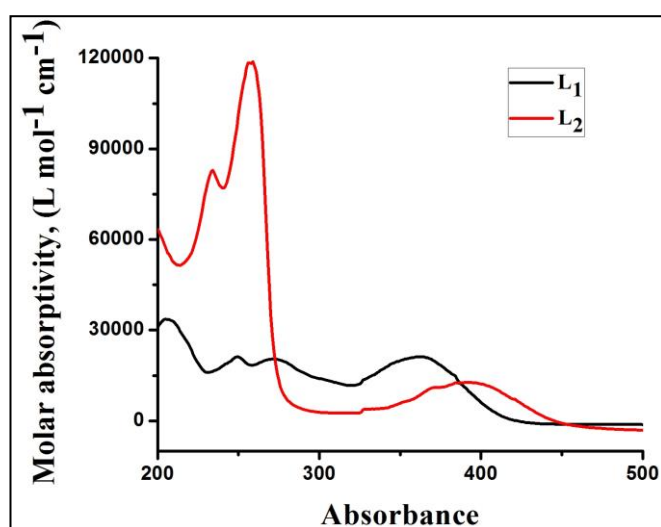
are arranged in a facial mode and the remaining equatorial sites are occupied by pyridyl nitrogen and nitrogen coming from other part of the ligand moiety. The remaining axial site is occupied by a chlorine atom.

**Table IV.3** Selected Bond Distances (Å) and Angles (°) for complexes **4** and **5**

<b>4</b>		<b>5</b>	
<b>Bond Length (Å)</b>			
C24-Re	1.890(18)	Re1-C25	1.934(12)
C25-Re	1.897(18)	Re1-C27	1.952(13)
C26-Re	1.93(2)	Re1-C26	1.960(19)
N1-Re	2.253(14)	Re1-N1	2.167(9)
N2-Re	2.180(16)	Re1-N2	2.194(8)
Re1-Cl1	2.466(5)	Re1-Cl1	2.459(4)
<b>Bond Angles(°)</b>			
C24-Re-C25	85.5(9)	C25-Re1-C27	86.8(5)
C24-Re-C26	85.8(8)	C25-Re1-C26	91.5(7)
C25-Re-C26	90.8(9)	C27-Re1-C26	89.2(6)
C24-Re-N2	179.0(7)	C25-Re1-N1	98.4(4)
C25-Re-N2	93.5(8)	C27-Re1-N1	174.7(3)
C26-Re-N2	94.3(7)	C26-Re1-N1	91.9(6)
C24-Re-N1	105.6(7)	C25-Re1-N2	173.9(4)
C25-Re-N1	95.1(7)	C27-Re1-N2	99.3(4)
C26-Re-N1	167.5(6)	C26-Re1-N2	89.4(6)
N2-Re-N1	74.3(6)	N1-Re1-N2	75.5(3)
C24-Re-Cl	96.8(6)	C25-Re1-Cl1	95.1(4)
C25-Re-Cl	177.4(7)	C27-Re1-Cl1	93.9(4)
C26-Re-Cl	90.5(7)	C26-Re1-Cl1	172.8(5)
N2-Re-Cl	84.2(5)	N1-Re1-Cl1	84.4(3)
N1-Re-Cl	83.2(4)	N2-Re1-Cl1	83.7(3)

### C. Photophysical studies of ligand

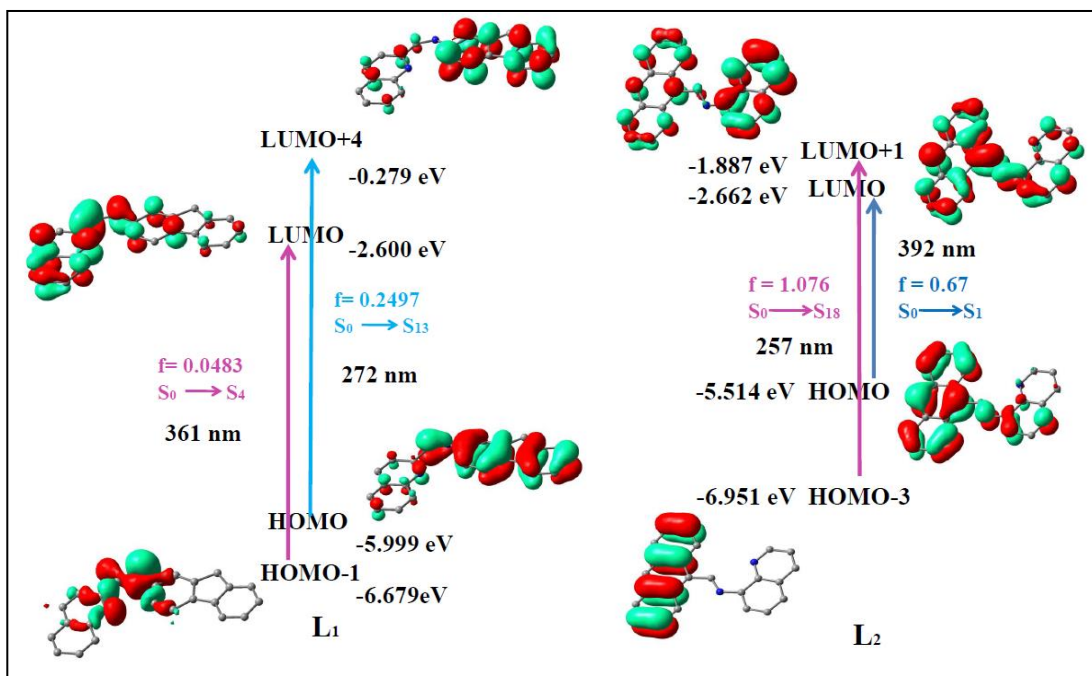
The absorption spectra of the ligands  $L_1$  and  $L_2$  were recorded in acetonitrile at room temperature (given in **Figure IV.7**).  $L_1$  and  $L_2$  show absorption bands of lowest energy at 361 and 390 nm respectively which are attributed to the  $n \rightarrow \pi^*$  transition. The higher energy absorptions were observed in UV region at 272 nm and 257 nm for  $L_1$  and  $L_2$  respectively. The higher energy absorption of these ligands arises in the UV region at 272 nm and 257 nm respectively. These bands can be reasonably assigned as an admixture of  $\pi \rightarrow \pi^*$  transitions and weaker  $n \rightarrow \pi^*$  transition which are submerged under a stronger  $\pi \rightarrow \pi^*$  transition.



**Figure IV.7** Absorption spectra of  $L_1$  and  $L_2$  in acetonitrile keeping the concentration ( $c = 2 \times 10^{-5} \text{ M}$ ).

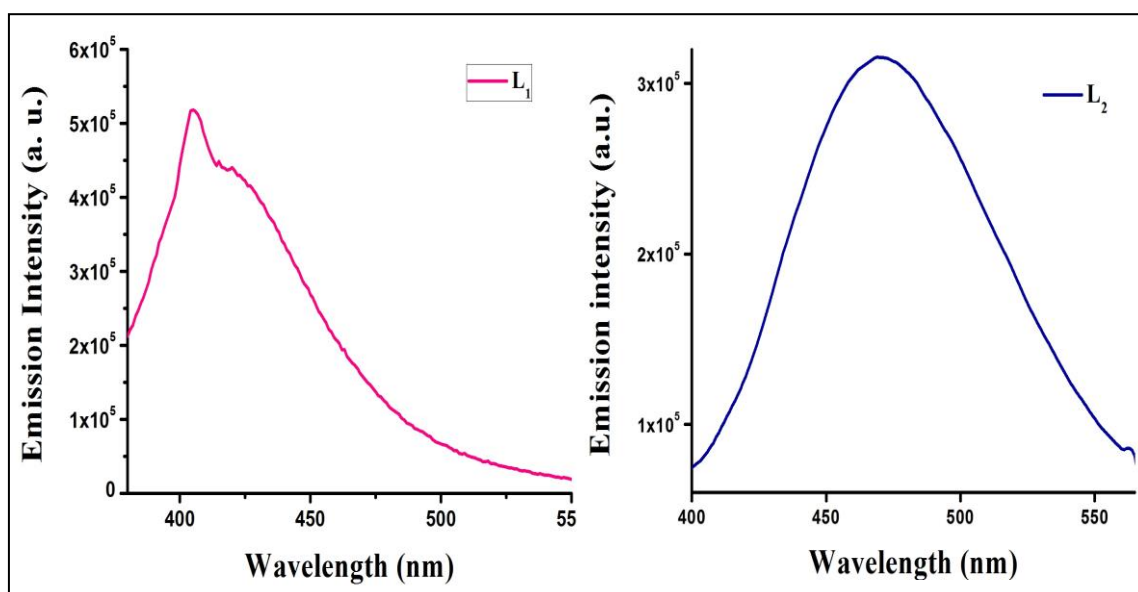
To get better agreement with the experimental photophysical values, TDDFT calculations were performed for the ligands  $L_1$  and  $L_2$  on the basis of the optimized geometry both in the singlet ground state ( $S_0$ ) and excited state ( $S_1$ ) in acetonitrile solvent. The absorption energies associated with their oscillator strengths, the main configurations and their assignments calculated using the TDDFT method and the  $S_0$  geometry for  $L_1$  and  $L_2$  is discussed here (**Figure IV.8**). The energy difference between HOMO and LUMO of  $L_1$  and  $L_2$  is 3.3 eV and 2.8 eV respectively. The calculated absorption bands are in good agreement with the experimental result. These absorption bands can be assigned to intramolecular charge transfer (ICT) band

with some rearrangement of electron density from fluorene moiety to quinoline moiety in **L**<sub>1</sub> and from anthracene moiety to quinoline moiety in **L**<sub>2</sub>.



**Figure IV.8** Frontier molecular orbitals involved in the UV–Vis absorption spectrum of ligands **L**<sub>1</sub> and **L**<sub>2</sub> (for clarity we considered the molecular orbital with the higher value of CI (<0.5) for the appropriate transition).

The emission property of the ligands is measured in acetonitrile solution. Ligands **L**<sub>1</sub> and **L**<sub>2</sub> show emission band at 405 nm and 470 nm when excited at 360 nm and 390 nm respectively. A relatively larger Stokes shift is observed in case of **L**<sub>2</sub> (80 nm) than **L**<sub>1</sub> (45 nm). The emission intensity of **L**<sub>2</sub> is also greater than **L**<sub>1</sub>. The ligands **L**<sub>1</sub> and **L**<sub>2</sub> were strong emitters with quantum yields 0.03 and 0.11 respectively. The luminescence parameters for all the ligands are listed in **Table IV.4**. The high emission intensity of the ligands is mainly attributed to the changes in its singlet excited state geometrical parameters, which activates fluorophore moieties (fluorine and anthracene) in ligands. The emission spectra of ligands are shown in **Figure IV.9**.



*Figure IV.9* Experimental emission spectra of the ligands  $L_1$  and  $L_2$  ( $c = 2 \times 10^{-5} M$ ) in acetonitrile at room temperature.

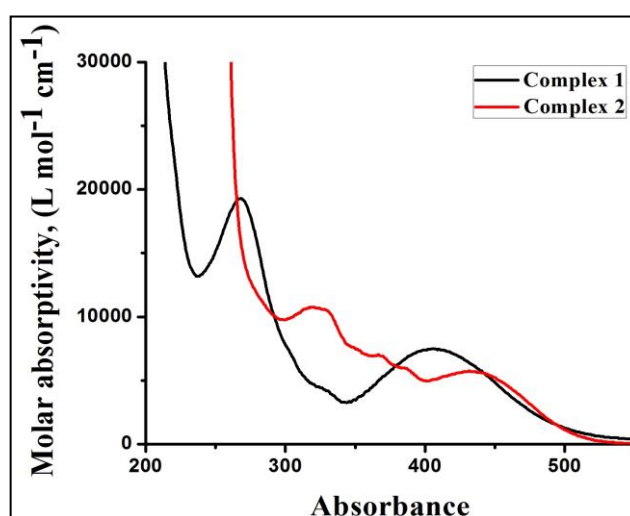
Time-resolved luminescence spectra are proved to be an important tool to understand the decay process and the emissive nature of the compounds. Thus time-resolved luminescence spectra were recorded for  $L_1$ ,  $L_2$ . The emission lifetime ( $\tau$ ), radiative ( $k_r$ ) and nonradiative ( $k_{nr}$ ) decay rate constants were collected in **Table IV.4**. All these ligands display a bi-exponential decay nature which suggests that there are two excited states close to each other. Two closely lying singlet excited states are mainly responsible for the bi-exponential decay in ligands. The lifetime of  $L_1$  ( $\tau_1 = 0.17$  ns and  $\tau_2 = 1.5$  ns) is relatively higher than that of  $L_2$  ( $\tau_1 = 0.48$  ns and  $\tau_2 = 0.15$  ns). The reason behind the high intensity of fluorescence is attributed to the change in excited state geometry.

**Table IV.4** Photophysical parameters of the mononuclear complexes in acetonitrile solution at room temperature

Compound	$\lambda_{\text{excitation}}$ (nm)	$\lambda_{\text{emission}}$ (nm)	Quantum Yield ( $\Phi$ )	$K_{\text{nr}} \times 10^8 \text{ s}^{-1}$	$K_{\text{r}} \times 10^7 \text{ s}^{-1}$	$\tau_1 \text{ ns}$	$\tau_2 \text{ ns}$
L <sub>1</sub>	360	405	0.03	6.2	2.5	0.17	1.54
L <sub>2</sub>	390	470	0.11	18	24	0.48	0.15
5-CN	437	505	0.19	1.3	3.05	1.83	6.29

#### D. Photophysical study of complex

The absorption spectra of the mononuclear complexes (4 and 5) are recorded in acetonitrile at room temperature (given in **Figure IV.10**). As compared to the ligands, the corresponding complexes show bathochromic shift in the longer wavelength region. This fact illustrates that the incorporation of rhenium(I) actually responsible for the bathochromic shift. The low lying absorption bands of these complexes  $\sim 400 \text{ nm}$  are assigned as metal to ligand charge transfer (MLCT) band [ $\text{Re}(\text{d}\pi) \rightarrow \text{ligand } \pi^*$  orbital]. The higher energy absorption band with high molar absorption value  $\sim 250 \text{ nm}$  can be assigned as the intraligand charge transfer band (ILCT) and weaker contribution of MLCT band. **Table IV.5** confirms the usual assignments of all the absorption bands for complexes 4 and 5.

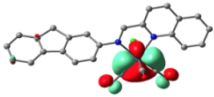
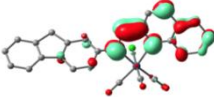
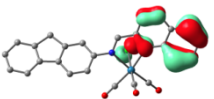
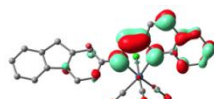
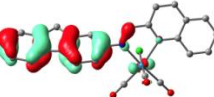
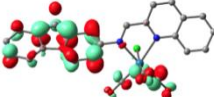
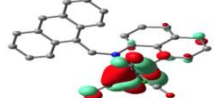
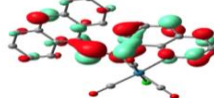
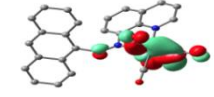
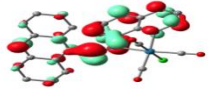
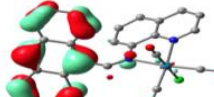
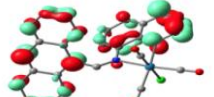
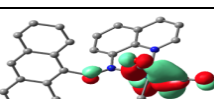
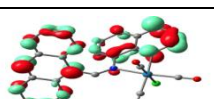
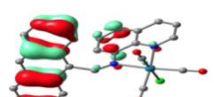
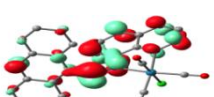
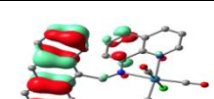
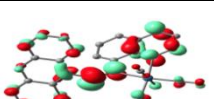


**Figure IV.10** Absorption spectra of the complexes 4 and 5 in acetonitrile keeping the concentration ( $c = 2 \times 10^{-5} \text{ M}$ ).

**Table IV.5** Main calculated optical transition for complexes **4** and **5** with vertical excitation energies and oscillator strength in acetonitrile.

Compound	Electronic transition	Composition	Excitation energy (eV)	Oscillator Strength (f)	CI	Assign	$\lambda_{\text{exp}}$ in nm ( $\epsilon$ in $\text{M}^{-1}\text{cm}^{-1}$ )
1	$S_0 \rightarrow S_4$	H-3 $\rightarrow$ L	2.8284 (438 nm)	0.0515	0.6800	$^1\text{MLCT}$	405 (26722)
		H-5 $\rightarrow$ L	3.2150 (385 nm)	0.0248	0.6866		
	$S_0 \rightarrow S_{10}$	H $\rightarrow$ L+1	3.8822 (319 nm)	0.2263	0.5165	$^1\text{ILCT}$	327 (14725)
	$S_0 \rightarrow S_{25}$	H $\rightarrow$ L+5	4.6646 (265 nm)	0.1538	0.4619	$^1\text{MLCT}/^1\text{LLCT}$	267 (75764)
2	$S_0 \rightarrow S_2$ $S_0 \rightarrow S_3$	H-1 $\rightarrow$ L	2.8336 (437 nm)	0.0134	0.6594	$^1\text{MLCT}$ $^1\text{MLCT}$	437(5631)
		H-2 $\rightarrow$ L	2.9175 (424 nm)	0.0377	0.6358		
	$S_0 \rightarrow S_4$	H $\rightarrow$ L+1	2.9774 (416 nm)	0.1000	0.6607	$^1\text{ILCT}$	385 (5429)
	$S_0 \rightarrow S_7$	H-2 $\rightarrow$ L+1	3.4143 (363nm)	0.0132	0.6083	$^1\text{MLCT}$	369 (6268)
	$S_0 \rightarrow S_{10}$	H-5 $\rightarrow$ L	3.6114 (343 nm)	0.1543	0.5641	$^1\text{ILCT}$	328 (9724)
	$S_0 \rightarrow S_{39}$	H-5 $\rightarrow$ L+2	4.8800 (254 nm)	0.8658	0.4158	$^1\text{ILCT}$	254 (43477)

**Table IV.6** Natural transition orbitals (NTOs) for the complexes illustrating the nature of singlet excited states. For each complex, the respective number of the state, transition energy (eV), and the oscillator strength (in parentheses) are listed.

Complex	Transition	Hole	Electron	Assignment
4	S <sub>4</sub> W=0.92 2.82eV(0.05)			MLCT
	S <sub>10</sub> W=0.94 3.21eV(0.02)			ILCT
	S <sub>25</sub> W=0.42 4.66eV(0.15)			LLCT
5	S <sub>2</sub> W=0.86 2.83eV(0.03)			MLCT
	S <sub>3</sub> W=0.79 2.91eV(0.03)			MLCT
	S <sub>4</sub> W=0.87 2.97eV(0.1)			ILCT
	S <sub>7</sub> W=0.72 3.414eV(0.01)			MLCT
	S <sub>10</sub> W=0.62 3.61eV(0.15)			ILCT
	S <sub>39</sub> W=0.33 4.88eV(0.86)			ILCT/LLCT



In order to analyze the nature of absorption, we performed an NTO analysis based on the calculated transition density matrices. This method offers the most compact representation of the transition density between the ground and excited states in terms of an expansion into single-particle transitions (hole and electron states for each given excitation). Here we refer to the unoccupied and occupied NTOs as “electron” and “hole” transition orbitals, respectively. Note that NTOs are not the same as virtual and occupied MO pairs from the ground state calculations. **Table IV.6** illustrate the natural transition orbitals (NTOs) for mononuclear complexes (**4** and **5**) respectively.

Based on the TDDFT NTO analysis, it is clear that the absorption bands at longer wavelength region of these two complexes are purely metal to ligand charge transfer band. In complex **4** the metal charge density completely shifts over quinoline moiety and in complex **5**, metal charge density is delocalized throughout the anthracene and quinoline moiety in their excited states  $S_4$  and  $S_2$  respectively which in turn makes the metal center devoid of electron density.

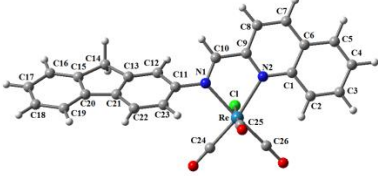
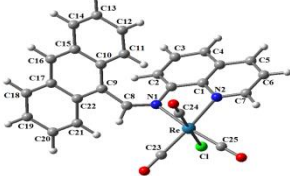
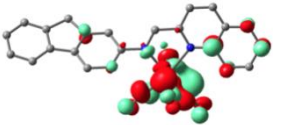
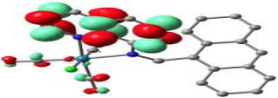
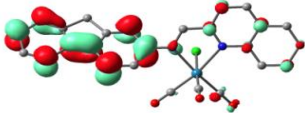
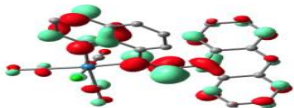
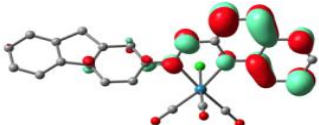
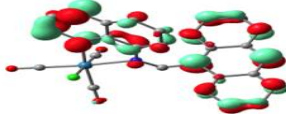
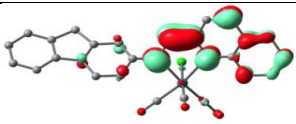
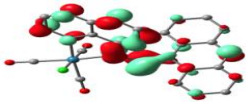
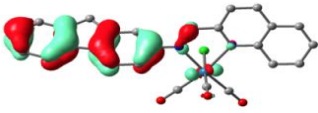
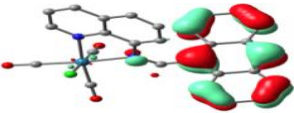
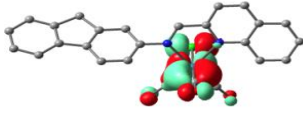
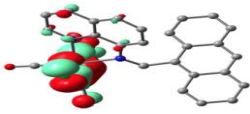
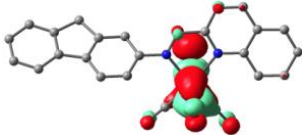
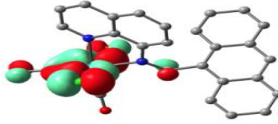
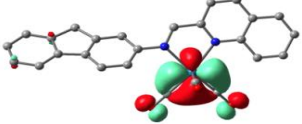
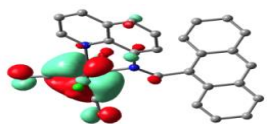
The higher energy absorptions of complex **4** comprises of intraligand charge transfer band and less contributing ligand to ligand charge transfer band where electron density moves from fluorine moiety to carbonyl ligands. In case of complex **5**, higher energy absorption bands are observed due to ILCT transition with weaker MLCT character as the four excited states ( $S_4$ ,  $S_7$ ,  $S_{10}$ ,  $S_{39}$ ) depicts that the charge density moves in between two ligand fragments and CO ligands.

The emission spectral behaviour of two mononuclear complexes was recorded in acetonitrile solution at room temperature the complexes displayed poor luminescence property due to the excited state quenching in presence of  $[\text{Re}(\text{CO})_3]^+$  core, which practically makes them non-emitters.

### 3.6. Geometry optimization and electronic structure

Molecular structures of the complexes **4** and **5** were optimized by DFT at their electronic ground state ( $S_0$ ) using LANL2DZ basis set. The optimized structures of the complexes are given in **Table IV.7**.

**Table IV.7** Optimized geometries, HOMO and LUMO contour plots of the metal complexes at the B3LYP/6-31G\* level

	Complex 4	Complex 5
Optimized geometries at the B3LYP/631G* level		
LUMO+3		
LUMO+2		
LUMO+1		
LUMO		
HOMO		
HOMO-1		
HOMO-2		
HOMO-3		

The optimized ground state structures of complexes **4** and **5** at their singlet ( $S_0$ ) state, possesses distorted octahedral geometry around rhenium (I) metal center. The *fac*-[Re(CO) $_3$ ] $^+$  core is consisted with each complexes having the angles of  $\sim 90^\circ$  between the CO ligands. Theoretical structural parameters are in excellent agreement with the experimental data for the complexes for which X-ray data are available. In these complexes all the Re-C bond length occurs near 1.91 Å and Re-N bond length occurs near 2.25 Å. The Re-Cl bond length of all the complexes is slightly longer than the Re-C and Re-N bond lengths. All these values deviate from the experimental parameters faintly, which is dependent on the errors originated from the environmental factors such as crystal packing and the impact of the medium.

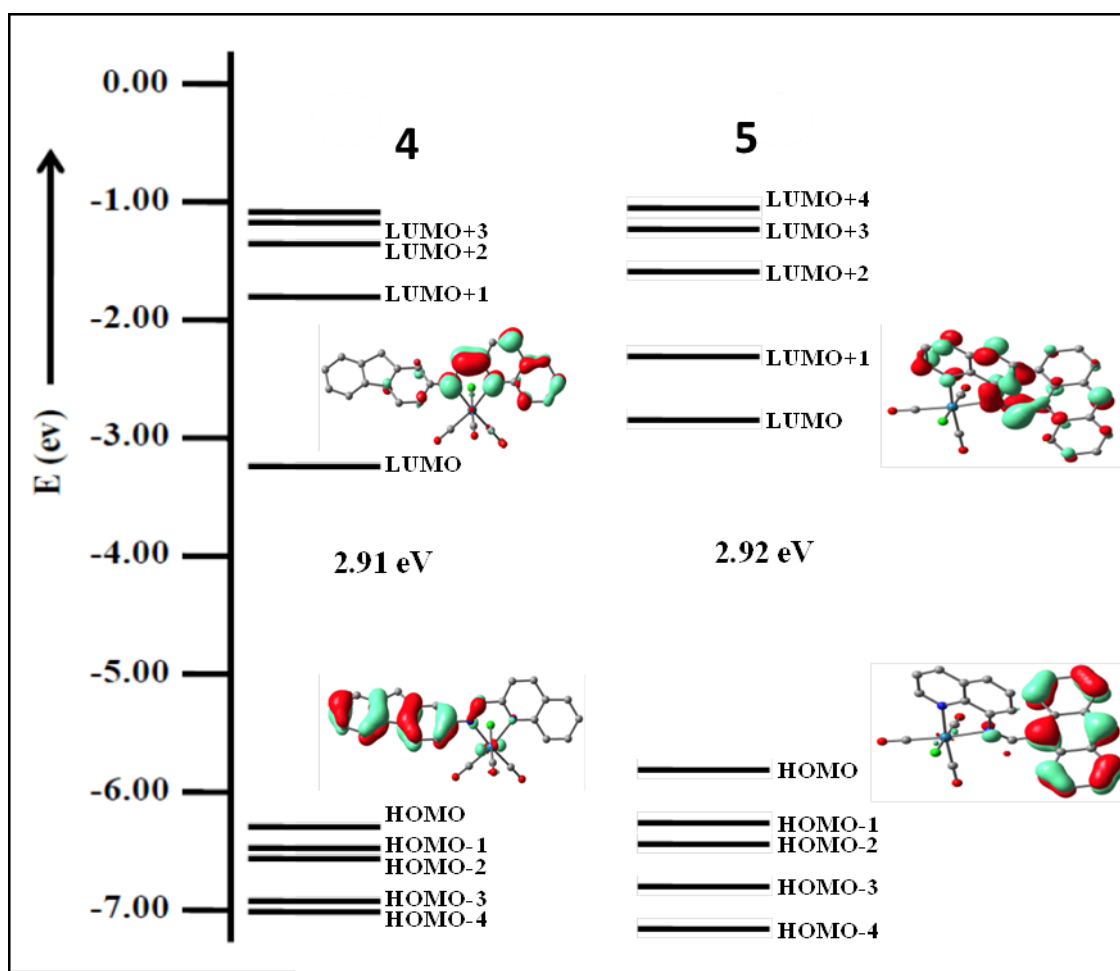


Figure IV.11 Partial molecular orbital diagram of the complexes **4** and **5**.

The partial frontier molecular orbital compositions in their singlet ground state ( $S_0$ ) are listed in. The partial molecular orbital diagram of frontier molecular orbital, which are mainly involved in the electronic transitions for mononuclear complexes **4** and **5** are shown in **Figure IV.11**.

*Table IV.8 Energies (eV) and composition (%) of frontier molecular orbitals of the complex **4** and **5**.*

<b>Complex 4</b>		<b>% Contribution</b>						<b>Main Bond Type</b>
<b>MO</b>	<b>CO</b>	<b>Cl</b>	<b>C=N</b>	<b>Re</b>	<b>AF</b>	<b>Quin</b>		
126	L+4	53	0	-1	27	5	16	$\pi^*(CO)+\pi^*(Quin)+d(Re)$
125	L+3	42	0	0	27	21	12	$\pi^*(CO)+\pi^*(AF)+\pi^*(Quin)+d(Re)$
124	L+2	3	0	0	1	14	80	$\pi^*(AF)+\pi^*(Quin)$
123	L+1	1	0	10	0	78	11	$\pi^*(C=N)+\pi^*(AF)$
122	LUMO	3	1	32	2	53	8	$\pi^*(C=N)+\pi^*(AF)$
121	HOMO	2	1	5	4	4	84	$\pi^*(Quin)$
120	H-1	22	23	0	46	3	7	$\pi^*(CO)+\pi^*(AF)+p(Cl)+d(Re)$
119	H-2	20	25	5	45	6	0	$\pi^*(CO)+p(Cl)+d(Re)$
118	H-3	27	1	0	63	2	9	$\pi^*(CO)+d(Re)$
117	H-4	1	0	0	3	1	94	$\pi^*(Quin)$

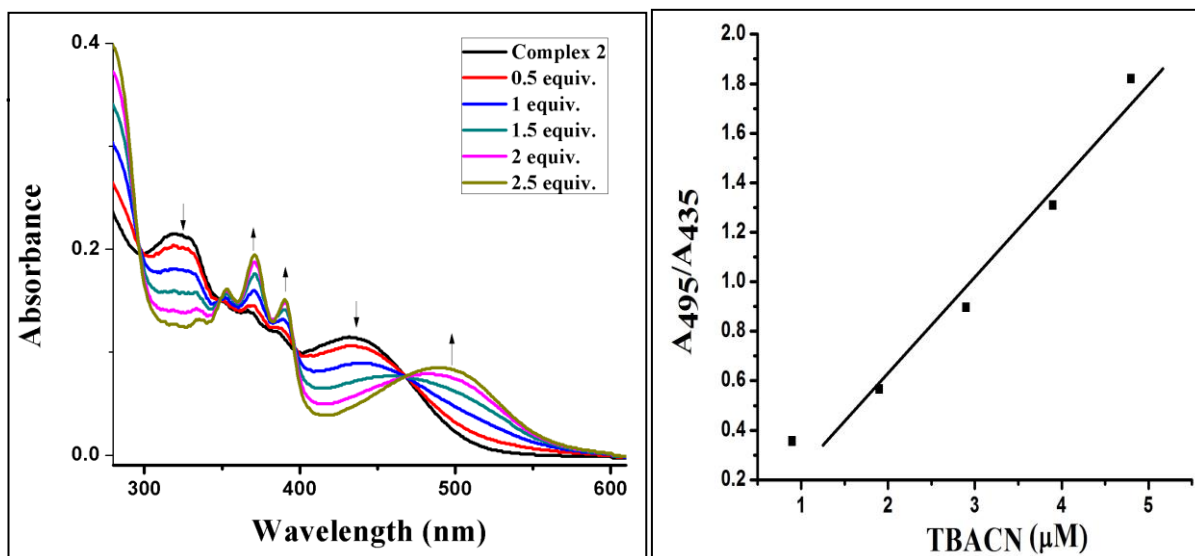
<b>Complex 5</b>		<b>% Contribution</b>						<b>Main Bond Type</b>
<b>MO</b>	<b>CO</b>	<b>Cl</b>	<b>C=N</b>	<b>Re</b>	<b>Quin</b>	<b>Anth</b>		
129	L+4	49	0	4	31	8	9	$\pi^*(CO)+d(Re)$
128	L+3	7	0	1	5	82	6	$\pi^*(Quin)$
127	L+2	8	1	34	3	29	25	$\pi^*(C=N)+\pi^*(Quin)+\pi^*(Anth)$
126	L+1	2	0	3	1	44	49	$\pi^*(Quin)+\pi^*(Anth)$
125	LUMO	1	0	32	0	42	24	$\pi^*(C=N)+\pi^*(Quin)+\pi^*(Anth)$
124	HOMO	1	0	4	2	3	90	$\pi^*(Anth)$
123	H-1	22	20	0	46	11	1	$\pi^*(CO)+p(Cl)+d(Re)$
122	H-2	21	23	5	44	1	7	$\pi^*(CO)+p(Cl)+d(Re)$
121	H-3	27	4	3	60	4	2	$\pi^*(CO)+d(Re)$
120	H-4	6	5	5	13	44	28	$\pi^*(Quin)+\pi^*(Anth)+d(Re)$

In the ground state ( $S_0$ ), the energy difference between HOMO (H) and LUMO (L) of all three mononuclear complexes are very similar to each other, which is 2.91 eV and 2.92 eV for complexes **4** and **5** respectively. Clearly, the energy gap between HOMO and LUMO is comparable to each other. Each mononuclear rhenium(I) complex possesses ligand consist of two moiety joined through imine bond. HOMO of the complexes shows high electron densities around fluorene [FL (84%)] and anthracene [Anth (90%)] moiety for **4** and **5** respectively but, in case of LUMO, high electron density is observed in other part of the ligands i.e. quionline moiety (in the range of 42- 55%). In these two complexes H-1 lies in the range of 0.21-0.63 eV below the respective HOMO levels and H-2 resides below H-1 by  $\sim 0.10$  eV. This calculation indicates that H-1 and H-2 levels of these complexes are almost degenerate. Metal orbital contribution towards molecular orbitals occurs in lower energy levels. Predominant participation of rhenium d orbitals occurs from H-2 energy level where  $\sim 45\%$  or more contribution arises due to the metal centre. Partial involvement of  $\pi^*$  orbital of CO contributes  $\sim 25\%$  whereas the p orbital of Cl contributes  $\sim 22\%$  in each complex. The HOMO-3 and HOMO-4 are apart from each other by 0.35 eV in **4**, 0.12 eV in **5** and 0.06 eV. LUMO (L) and L+1 of all mononuclear complexes originates from the ligand  $\pi^*$  orbital localized on the C=N bond, quinoline moiety and aromatic systems attached to the C=N bond contribution.

### *E. Anion sensing properties*

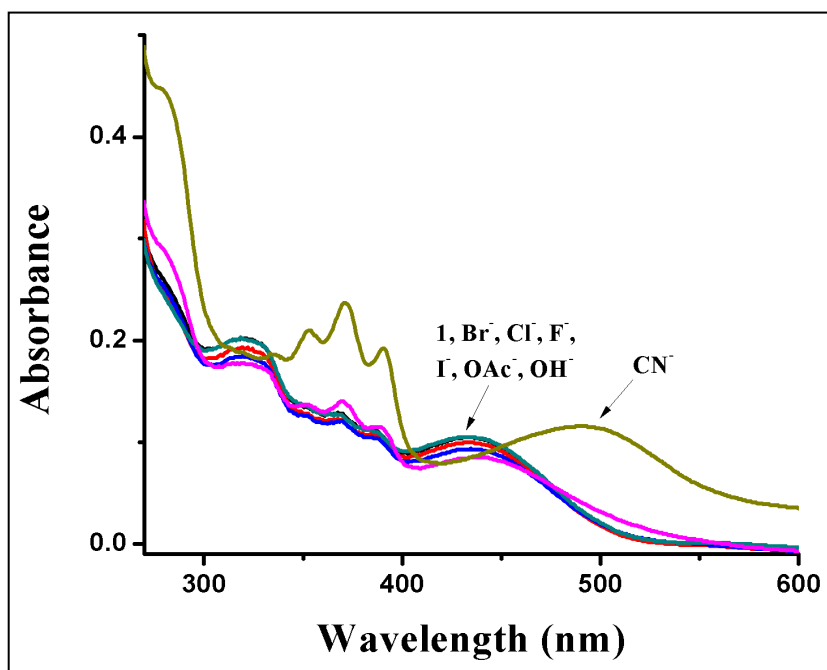
The anion binding properties of the complexes **4**, **5** and ligands **L**<sub>1</sub>, **L**<sub>2</sub> have been studied by spectrophotometric and fluorometric titration method in acetonitrile solution of these compounds (20  $\mu$ M) at room temperature. Tetrabutylammonium salts of OH<sup>-</sup>, F<sup>-</sup>, Cl<sup>-</sup>, OAc<sup>-</sup>, Br<sup>-</sup>, CN<sup>-</sup>, I<sup>-</sup> were used in this study. Among all the compounds, only complex **2** responded positively towards cyanide ion. All the other anions (OH<sup>-</sup>, F<sup>-</sup>, Cl<sup>-</sup>, OAc<sup>-</sup>, Br<sup>-</sup>, I<sup>-</sup>) remained silent upon addition of 10 equivalents (**Figure IV.13**) of each anion. The absorption titration curve of **5** with cyanide ion passes through several isobestic points in UV-Vis region. These isobestic points indicate the formation of new species in the solution medium. In the electronic absorption spectrum, the <sup>1</sup>MLCT [ $d\pi(\text{Re}) \rightarrow L_2$ ] absorption band at 435 nm exhibits a

red shift to 495 nm with a sharp isobestic point at 467 nm (**Figure IV.12**) when cyanide ion concentration slowly increases. It is clearly visible that the peak at 435 nm gradually decreases with the simultaneous increment of the peak at 495 nm.



**Figure IV.12** Absorption titration of 5 ( $c = 2 \times 10^{-5} M$ ) with  $CN^-$  up to 2.5 equivalent ( $c = 2 \times 10^{-3} M$ ) in acetonitrile (left); the ratiometric plot of absorbance ratio at 495 and 435 nm vs concentration of cyanide ion(right)

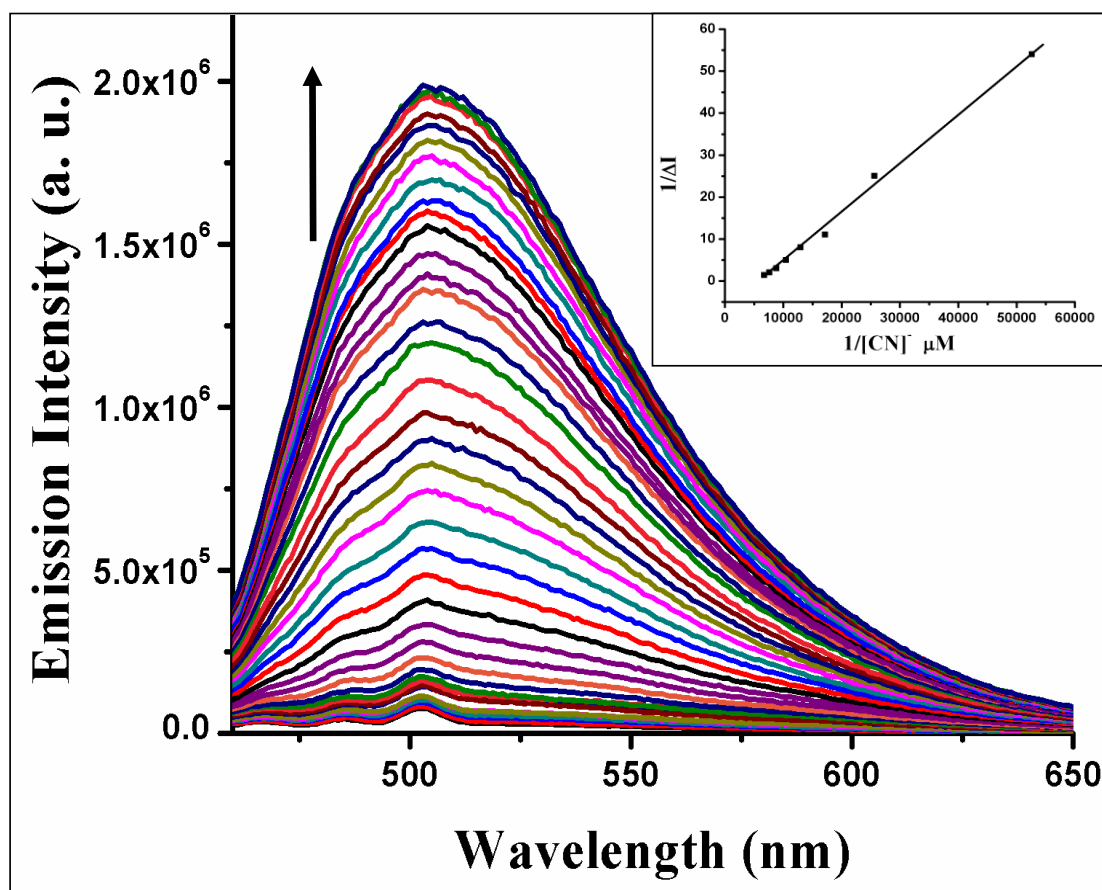
It is assumed that cyanide ion interacts with the complex by attacking the imine bond and forming a 5-CN adduct (shown in **Figure IV.16**). The binding of cyanide ion is expected to enrich the electron density of the nitrogen atom of imine bond attached to the anthracene unit and thus render the <sup>1</sup>MLCT transition to occur at lower energy. A plot of the absorbance ratio at 495 and 435 nm ( $A_{495}/A_{435}$ ) vs concentration of cyanide clearly indicates that  $A_{435}/A_{495}$  increases linearly with  $R^2=0.95307$  (**Figure IV.12**).



*Figure IV.13 Selective change in absorption in presence of various anions.*

We have investigated the luminescence properties of the non-emissive complexes **4** and **5** in presence of various anions ( $\text{OH}^-$ ,  $\text{F}^-$ ,  $\text{Cl}^-$ ,  $\text{OAc}^-$ ,  $\text{Br}^-$ ,  $\text{CN}^-$ ,  $\text{I}^-$ ) in acetonitrile at room temperature. Both the complexes were excited with their corresponding lowest energy absorption band and the spectral change was monitored by varying those anions. An appreciable change was observed for **5** in presence of cyanide ion. The non-emissive complex **5** displayed a strong emission at 505 nm (Excited at 437 nm) when 15 equivalents of cyanide ion was added to the complex solution (**Figure IV.14**). This observation suggests that the upcoming cyanide ions somehow can prevent the conjugation between anthracene and quinoline unit which is likely to be observed in the ground state picture of ligand unit in **5**. Therefore, the interruption of conjugation has occurred by the addition of cyanide ion into the imine bond attached with anthracenemioiety. As a result, the ICT (intramolecular charge transfer transition) process stopped and the fluorophore moiety becomes free to emit. We

have calculated the detection limit on the basis of  $3\sigma/k$ , where  $\sigma$  is the standard deviation of blank measurement. The calculated detection limit is found to be  $7.0 \times 10^{-7}$  M. In order to further investigate the binding constant of complex 5 with incoming cyanide ion, a plot of  $1/\Delta I$  (where,  $\Delta I = I - I_0$ ,  $I$  = intensity after cyanide addition,  $I_0$  = intensity before cyanide addition) vs  $1/[\text{CN}^-]$  is carried out. As a result, the fluorescence binding constant is found to be  $4.4 \times 10^4 \text{M}^{-1}$ .

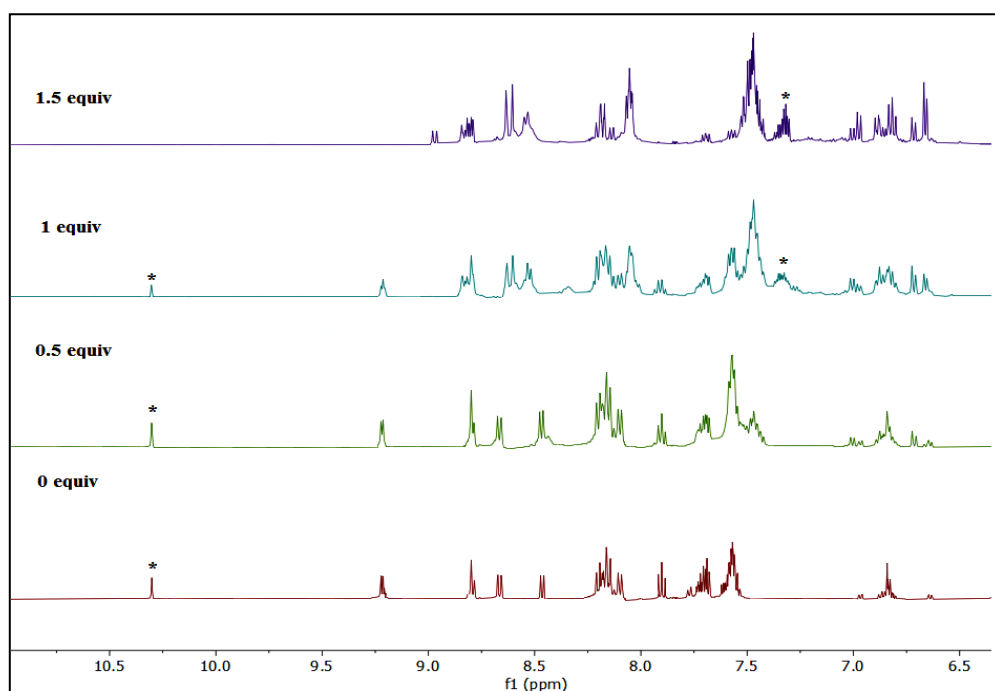


**Figure IV.14** Spectrofluorometric titration of 5 ( $c = 2 \times 10^{-5}$  M) with 10 equivalents of TBACN in acetonitrile solution (left). The plot of  $1/\Delta I$  vs.  $1/[\text{CN}^-]$ , where  $\Delta I = I - I_0$  ( $I$  = intensity after cyanide addition,  $I_0$  = intensity before cyanide addition) (right).

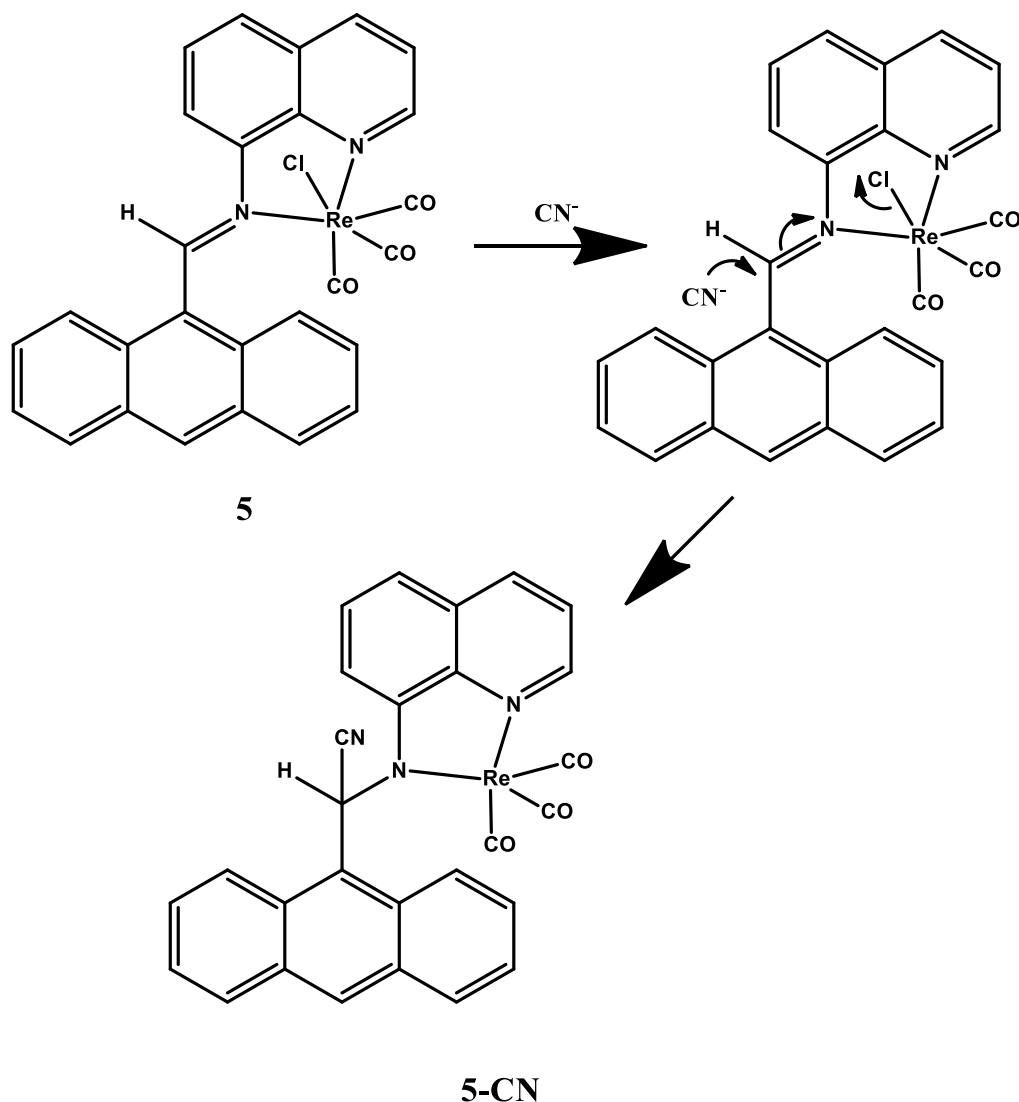
For the better insight of the reaction occurring in presence of  $\text{CN}^-$  ion,  $^1\text{H}$  NMR titration was carried out in  $\text{CD}_3\text{CN}$  solution of 5 and the change in spectra was recorded after gradual increment of cyanide ion upto 1.5 equivalents. The  $^1\text{H}$  NMR peak of aldimine proton at 10.3 ppm disappeared slowly upto the addition of 1.5 equivalents of cyanide ion. A new peak appeared at 7.3 ppm simultaneously which



is assigned as the cyanomethanamine proton. The aromatic protons were shifted towards slightly upfield region. This observation supports the fact that the imine bond of **5** was affected by cyanide ion which induces different electronic atmosphere around the aromatic region and caused the aromatic protons as well as the cyanomethanamine proton to shift towards upfield region. The relevant  $^1\text{H}$  NMR titration is shown in **Figure IV.15**.



**Figure IV.15** The  $^1\text{H}$  NMR titration of complex **5** in  $\text{CD}_3\text{CN}$  solution in presence of 1.5 equivalents of  $\text{CN}^-$  ion. Generation of cyanomethanamine proton is shown by (\*).



*Figure IV.16 Probable mechanism for the formation of 5-CN adduct.*

Furthermore the time resolved luminescence spectra also give evidence to understand the decay process and the emissive nature of the 5-CN adduct. Life time data are recorded for 5-CN adduct at room temperature in acetonitrile solution when excited at 437 nm. The emission lifetime ( $\tau$ ), radiative ( $k_r$ ) and non-radiative ( $k_{nr}$ ) decay rate constant of 5-CN adduct were collected in **Table IV.4**. It shows a bi-exponential decay. Upon addition of  $\text{CN}^-$  ion into the solution of **5** enhances the emission intensity as well as the excited state lifetime due to the formation of 5-CN adduct. This photoluminescence property mainly originates from the triplet state

charge transfer transitions, which is confirmed by the treatment of triplet oxygen as no quenching of emission intensity occurs. The short Stokes shift of **5**-CN with respect to the longer wavelength absorption of **5** reveals the ligand-centred  $^3IL$  nature of the  $T_1$  state of **5**-CN.

#### **IV.4. CONCLUSION**

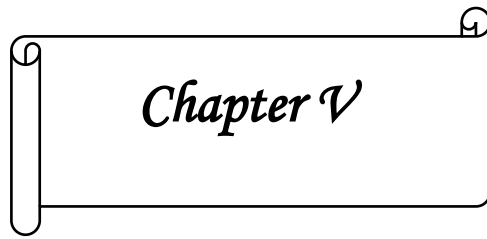
In summary, we have synthesized two Schiff base based ligands (**L**<sub>1</sub> and **L**<sub>2</sub>) and two monomeric rhenium (I) complexes of these two ligands. The aim of the present work is to explore their optical properties and reactivity with various anions. The complexes are characterized by different spectroscopic techniques and X-ray crystal structure determination. This work includes investigation of the ground and excited-state geometries of both the ligands and complexes as well as the study of absorption and luminescence properties of two rhenium(I) complexes by DFT and TDDFT methods. Furthermore, the complex **5** has shown a very interesting photophysical property by selective binding with cyanide ion in acetonitrile solution. The spectral change of complex **5** in presence of high amount of cyanide is prominent in UV-Vis spectroscopy as well as in fluorescence spectroscopy. Proton NMR spectra confirms that the change in spectral response is due to the attachment of cyanide ion into the imine bond of complex **5**. So, the studies presented herein provide valuable information about the synthetic strategy of metal complexes as well the ligands.

### III.5. REFERENCES

- (1) (a) N. Akabar, V. Chaturvedi, G. E. Shillito, B. J. Schwehr, K. C. Gordon, G. S. Huff, J. J. Sutton, B. W. Skelton, A. N. Sobolev, S. Stagni, D. J. Nelson and M. Massi, DOI: 10.1039/C9DT02198A, *Dalton Trans.* (2019) Advance Article  
(b) D. Sinha, S. P. Parua, K. K. Rajak, *Journal of Organometallic Chemistry*, **2019**, 889, 62-69  
(c) L. D. Ramos, R. N. Sampaio, F. F. de Assis, K. T. de Oliveira, P. Homem-de-Mello, A. O. T. Patrocinio and K. P. M. Frin, *Dalton Trans.* **2016**, 45, 11688-11698
- (2) (a) G. Balakrishnana, T. Rajendrana, K. S. Murugana, M. Ganesana, V. K. Sivasubramaniana, S. Rajagopal, *Journal of Luminescence* **2019**, 205, 51-60  
(b) P. Gómez-Iglesias, F. Guyon, A. Khatyr, G. Ulrich, M. Knorr, J. M. Martín-Alvarez, D. Miguela, F. Villafañe, *Dalton Trans.* **2015**, 44, 17516-17528
- (3) C. -O. Ng, S. -C. Cheng, W. -K. Chu, K. -M. Tang, S. -M. Yiu, C. -C. Ko, *Inorg Chem.* **2016**, 55, 167969-7979
- (4) M. M. Lee, J. -L. Lin, C. -W. Chang, C. -Y. Hung, C. -W. Chen, C. -P. Hsu, S. -S. Sun, *Eur. J. Inorg. Chem.* **2017**, 5224-5237
- (5) P. A. Scattergood and P. I. P. Elliott, *Dalton Trans.* **2017**, 46, 16343-16356
- (6) (a) P. V. Simpson, M. Falasca and M. Massi, *Chem. Commun.* **2018**, 54, 12429-12438  
(b) Y. Kim, F. W. M. Vanhelfmont, C. L. Stern, J. T. Hupp, *Inorganica Chimica Acta* **2001**, 318, 53-60
- (7) A. Wilting, T. Stolper, R. A. Mata, I. Siewert, *Inorg. Chem.* **2017**, 56, 4176-4185
- (8) (a) A. Świtlicka, K. Choroba, A. Szlapa-Kula, B. Machura and K. Erfurt, *Polyhedron* **2019**, 171, 551  
(b) T. B. J. Hall, D. Preston, P. Traber, L. Wu, K. E. A. Reynolds, R. Horvath, X. Z. Sun, N. T. Lucas, J. D. Crowley, M. W. George, S. Kupfer, K. C. Gordon, G. E. Shillito, *J. Am. Chem. Soc.* **2018**, 140, 4534-4542
- (9) L. A. Faustino, A. E. H. Machado, A. O. T. Patrocinio, *Inorg. Chem.* **2018**, 57, 2933-2941

- (10) (a) L. Veronese, E. Q. Procopio, T. Moehl, M. Panigati, K. Nonomura and A. Hagfeldt, *Phys. Chem. Chem. Phys.* **2019**, *21*, 7534-7543  
(b) M. Busby, P. Matousek, M. Towrie, A. Vlček, *J. Phys. Chem.* **2005**, *A109* 3000
- (11) S. Sato, A. Sekine, Y. Ohashi, O. Ishitani, A. M. B. Rodriguez, A. Vlcek, T. Unno, K. Koike, *Inorg. Chem.* **2007**, *46*, 3531
- (12) A. Otavio, T. Patrocinio, M. K. Brennaman, T. J. Meyer and N. Y. M. Iha, *J. Phys. Chem. A.* **2010**, *114*, 12129.
- (13) N. J. Lundin, P. J. Walsh, S. L. Howell, A. G. Blackman and K. C. Gordon, *Chem.-Eur. J.* **2008**, *14*, 11573
- (14) S. T. Lam, N. Zhu, V. W. W. Yam, *Inorg. Chem.* **2009**, *48*, 9664
- (15) X. Li, D. Zhang, G. Lu, G. Xiao, H. Chi, Y. Dong, Z. Zhang and Z. Hu, *J. Photochem. Photobiol.* **2012**, *A241*, 1
- (16) W. K. Chu, C. C. Ko, K. C. Chan, S. M. Yiu, F. L. Wong, C. S. Lee and V. A. L. Roy, *Chem. Mater.* **2014**, *26*, 2544
- (17) G. W. Zhao, Y. X. Hu, H. J. Chi, Y. Dong, G. Y. Xiao, X. Li and D. Y. Zhang, *Opt. Mater.* **2015**, *47*, 173
- (18) X. Li, D. Zhang, W. Li, B. Chu, L. Han, J. Zhu, Z. Su, D. Bi, D. Wang, D. Yang and Y. Chen, *Appl. Phys. Lett.* **2008**, *92*, 083302
- (19) (a) L. Veronese, N. Zaffaroni, M. Folinic, E. Licandro, S. Cauteruccio, M. Panigati, *Journal of Organometallic Chemistry* **2019**, *887*, 32-39
- (20) C. Otero, A. Carreno, R. Polanco, F. M. Llancahuen, R. Arratia-Perez, M. Gacitua and J. A. Fuentes, <https://doi.org/10.3389/fchem.2019.00454>
- (21) K.-C. Chang, S.-S. Sun, A. J. Lees, *Inorganica Chimica Acta* **2012**, *389*, 16-28
- (22) A. Ramdass, V. Sathish, M. Velayudham, K. - L. Lu, S. Rajagopal, *Inorganic Chemistry communications* **2013**, *35*, 186-191
- (23) T. - P. Lin, C. - Y. Chen, Y. - S. Wen, S. - S. Sun, *Inorg. Chem.* **2007**, *46*, 9201-9212
- (24) S.-S. Sun, A. J. Lees, P.Y. Zavalij, *Inorg. Chem.* **2003**, *42*, 3445-3453
- (25) K. - C. Chang, S. - S. Sun, M. O. Odago, A. J. Lees, *Coordination Chemistry Reviews* **2015**, *284*, 111-123

- (26) A.Ramdass, V. Sathish, M. Velayudham, P. Thanasekaranand S. Rajagopal, *ChemistrySelect* **2018**, 3, 2277 – 2285
- (27) Yibing Shen B. Patrick Sullivan, *J. Chem. Educ.* **1997**, 74, 6685
- (28) H. H. Nguyen, T. Tran, P. L. M. Wong, *Hydrometallurgy* **1997**, 46, 55–69
- (29) M. A. Chaaban, *J. Mater. Process. Technol.* **2001**, 119, 336–343
- (30) Koenig, Environmental disasters - wildlife deaths are a grim wake-up call in Eastern Europe, *R. Science* **2000**, 287, 1737–1738
- (31) T. Das, K. K. Rajak, *Dalton Trans.* **2019**, 48, 6879-6891
- (32) M.A.L. Marques and E.K.U. Gross, Time dependent density functional theory, *Annu. Rev. Phys. Chem.* **2004**, 55, 427–455

A decorative scroll with a black outline, featuring a rolled-up edge on the left and a small loop on the right. The text "Chapter V" is centered within the scroll in a black, italicized serif font.

*Chapter V*

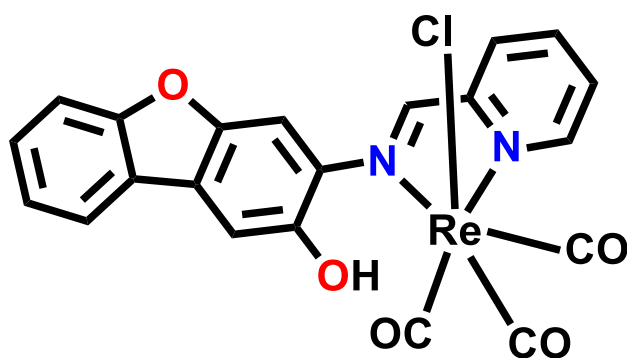




# *Metal assisted rearrangement in rhenium (I) complex transforming into red emitting species*

## **ABSTRACT**

The reaction of  $\text{Re}(\text{CO})_5\text{Cl}$  with L [(E)-3-((pyridin-2-ylmethylene)amino)dibenzo[b,d]furan-2-ol)] led to the formation of  $[\text{Re}(\text{CO})_3(\text{L})\text{Cl}]$  (complex **6**), showing a strong hydrogen bond  $[\text{L-OH}\cdots\text{Cl}(\text{Re})]$  and metal to ligand charge transfer transition at 409 nm. A remarkable in situ structural modification of **6**



is witnessed when methanolic solution of **6** was allowed to react with  $\text{Zn}(\text{OAc})_2$ . Methanol insertion as well as conversion of imine to oxazole was detected in the reaction forming three unique rhenium (I) complexes, *fac*- $[\text{Re}(\text{CO})_3(\text{L-oxazole})(\text{OAc})]$ , **6a** and *fac*-

$[\text{Re}(\text{CO})_3(\text{L-methoxy})]$ , **6b**. The reactant and products are structurally characterized by x-ray diffraction where those crystals are grown from hexane diffusion into dichloromethane solution of the complexes. Excited state proton transfer reaction occurs by the rearranged products when excited at 409 nm showing red emission at 646 nm. Density Functional Theory supports the experimental findings. The rate constant of the reaction was found to be  $5.4 \times 10^{-3} \text{ min}^{-1}$  by UV-Vis spectroscopy. It is worthy to mention that the unusual rearrangement is facilitated by the flexibility of ligand system of **6** having imine bond and free -OH group.



## V.6. INTRODUCTION

Decades of research have been invested upon rhenium (I) tricarbonyl diimine complexes owing to their potential applications in catalysis, optoelectronics, nuclear medicines, sensors, biology, organic light emitting diodes and solar energy conversion<sup>1-3</sup>. Imine based complexes with *fac*-[Re(CO)<sub>3</sub>]<sup>+</sup> core hold numerous - functionalities<sup>4</sup> which can be unfolded by applying proper chemical environment around the complex molecules. Introduction of other metal ions into the reaction medium of complex solution in presence of suitable solvent can raise the scope of exploring critical insights of structure, bonding and reactivity. Metal assisted rearrangement of rhenium (I) complexes influencing strong emission with large Stokes shift is rare and still need extensive research. In this regard, zinc acetate shows unique behaviour with facial rhenium (I) complexes which creates interesting photophysical properties. Enhancement of emission intensity is often observed when a molecular probe is exposed to Zn<sup>2+</sup> ion which can be responsible due to photoinduced electron/energy transfer (PET)<sup>5</sup>, intramolecular charge transfer (ICT)<sup>6</sup>, excimer/exciple formation<sup>7</sup>, excited-state intra-intermolecular proton transfer (ESIPT)<sup>8</sup> etc. Still many chemists intend to recognize the true reason of enhancement of emission. A wide variety of receptor has been established to show increased emission intensity through chelation enhanced fluorescence (CHEF)<sup>9</sup> mechanism with Zn<sup>2+</sup> but the same through zero incorporation of zinc into rhenium (I) complex is uncommon. In this work, we have reported rhenium (I) complex with dibenzofuran based imine linked ligand in which zinc acetate can actually increase the functionality of C=N bond of rhenium (I) bound ligand moiety followed by solvent activation. In situ generation of these rearranged rhenium (I) complexes assist in enhancement of emissions which transform a non-emissive material into emissive one. We have also structurally characterized these complexes with various spectroscopic techniques and single crystal X-Ray diffraction study. To get better insight into the geometry, electronic structure and optical properties, DFT and TDDFT calculations have been performed.

## V.2. EXPERIMENTAL SECTION

### A. Materials

Re(CO)<sub>5</sub>Cl, 3-Amino-2-methoxydibenzofuran, Pyridine-2-carboxaldehyde were purchased from Sigma Aldrich. All solvents and chemicals are analytically pure. All the reactions with Re(CO)<sub>5</sub>Cl were carried out under argon atmosphere.

### B. Preparation of Compounds

#### *Synthesis of ligand*

3-[(Quinolin-2-ylmethylene)-amino]-dibenzofuran-2-ol (HL): The ligand HL was prepared by two step reaction. At first, to a solution of the 3-Amino-2-methoxydibenzofuran (5g, 23.4 mmol) dissolved in methylene chloride (200 ml) at 0°C, 7 ml of BBr<sub>3</sub> (200 mL, 6 M in CH<sub>2</sub>Cl<sub>2</sub>) was added via addition funnel drop wise and stirred. Then the mixture was allowed to come to room temperature over 6 hour and then quenched with water followed by potassium carbonate (63g). The resulting solid was recovered by vacuum filtration and dried to afford the 3-Amino-2-hydroxydibenzofuran as a white solid.

The product obtained from above procedure (500 mg, 2.56 mmol) was dissolved in 20 ml ethanol followed by addition of 2-pyridinecarboxaldehyde (395 mg, 2.56 mmol). The solution was then stirred for 6 hours. A brown colour precipitate was obtained. It was collected under suction filtration and washed with ethanol. Yield: 80%, <sup>1</sup>H NMR (CDCl<sub>3</sub>, 300 MHz): δ 8.9 (s, 1H); 8.27-8.24 (m, 3H); 8.67 (t, 2H, J=9), 7.86(m, 6H), 7.73-7.46(m, 5H), 7.28(t, 1H, J=6). Anal. Calcd for C<sub>22</sub>H<sub>16</sub>N<sub>4</sub>O: C, 78.09; H, 4.67; N, 8.28. Found: C, 78.23; H, 4.20; N, 8.36. IR (cm<sup>-1</sup>): ν(O-H): 3043; ν(imine C=N): 1622, 1603

#### *Complex Synthesis*

*fac*-[Re(L)(CO)<sub>3</sub>Cl]<sub>6</sub>: Re(CO)<sub>5</sub>Cl (50mg, 0.647mmol), HL (47.09 mg, 0.647 mmol) were taken in 30 ml toluene and then the resulting mixture was refluxed for 10 h. After cooling to room temperature, the solvent was removed under reduced pressure. A red coloured solid was obtained. The product on recrystallization from dichloromethane–hexane afforded red coloured crystals. <sup>1</sup>H NMR (DMSO-d<sub>6</sub>, 300

MHz):  $\delta$ 160.42 (s, 1H); 9.45 (d, 1H, J=10); 9.64 (d, 1H, J=6), 8.42 (d, 2H, J=6), 8.64 (d, 1H, J=6), 7.87 (q, 1H, J=10), 7.65 (m, 6H, J=10), 7.39-7.57 (t, 2H). Anal.calcd for  $C_{26}H_{66}N_2O_3ClRe$ : C, 49.88, H, 2.58, N, 4.47. Found: C, 49.97, H, 2.62, N, 4.55; ESI-MS ( $CH_2Cl_2$ ):  $m/z = 597 [M]^+$ . IR ( $cm^{-6}$ ):  $\nu$  (CO): 1886, 1920 and 2069.

*fac*-[Re(CO)<sub>3</sub>(L-oxazole)(OAc)], **6a** and *fac*-[Re(CO)<sub>3</sub>(L-methoxy)],**6b**: 60 mg (0.066 mmol) of complex **6** and 3.35 mg (0.066 mmol) of zinc acetate was mixed together in methanol and heated to reflux for 30 mins. The resulting red solution was evaporated and the crude product was washed with hexane. The solid obtained was recrystallized in dichloromethane-hexane layer. ( $CH_2Cl_2$ ):  $m/z = 597 [M]^+$ .

### C. X-Ray Structure Determination

The single crystal suitable for X-ray crystallographic analysis of complexes *fac*-[Re(HL)(CO)<sub>3</sub>Cl] and *fac*-[Re(CO)<sub>3</sub>(L-oxazole)(OAc)]  $\cdots$  *fac*-[Re(CO)<sub>3</sub>(L-methoxy)], were grown by slow diffusion of dichloromethane into hexane at room temperature. Details of the X-ray work are given in tabular form in **Table V.1** and **Table V.2** (See also Chapter I).

### D. Physical Measurements

All physical measurements that included elemental analyses, IR, absorption spectra, <sup>1</sup>H NMR and spectra, ESI mass spectra, emission spectra measurement were performed as described in **Chapter I**.

**Table V.1** Atomic coordinates and isotropic thermal parameters complexes 6 and (6a.6b)

<b>Data collection</b>		
<b>Complex</b>	<b>6</b>	<b>(6a.6b)</b>
Total refl. Collected	69599	148058
Unique refl.( $R_{int}$ )	8795	9689
Used refl.	7768	7532
h k l range	-10<h<10 -15<k<15 -27<l<27	-16<h<16 -30<k<30 -24<l<24
<b>Structure solution and refinement</b>		
<b>Complex</b>	<b>6</b>	<b>(6a.6b)</b>
Solution	Patterson	Patterson
Refinement	Full-matrix least-squares on $F^2$	Full-matrix least-squares on $F^2$
<i>GOF on <math>F^2</math></i>	1.189	1.058
$R1,^a[I>2\sigma(I)]$	0.0529	0.0365
$wR2^b[I>2\sigma(I)]$	0.1441	0.1344
$R1[alldata]$	0.0637	0.0472
$wR2[alldata]$	0.1647	0.1061

**Table V.2** Crystal data and structure refinement parameters for complexes **6** and **6a.6b**

	<b>6</b>	<b>6a.6b</b>
Formula	C <sub>21</sub> H <sub>12</sub> ClN <sub>2</sub> O <sub>5</sub> Re	C <sub>45</sub> H <sub>28</sub> N <sub>4</sub> O <sub>13</sub> Re <sub>2</sub>
<i>M<sub>r</sub></i>	626.06	1205.13
Crystal system	Triclinic	Monoclinic
Space group	<i>P</i> -1	<i>P</i> 21/ <i>n</i>
<i>a</i> / Å	8.0451(9)	9.3532(10)
<i>b</i> / Å	11.8807(13)	23.867(3)
<i>c</i> / Å	21.460(2)	18.8200(19)
<i>α</i> /°	75.965(3)	90
<i>β</i> /°	80.805(3)	96.903(3)
<i>γ</i> /°	88.969(3)	90
<i>V</i> / Å <sup>3</sup>	1963.9(4)	4170.8(8)
<i>Z</i>	4	4
<i>D</i> <sub>calcd</sub> /g cm <sup>-3</sup>	2.009	1.919
<i>μ</i> /mm <sup>-1</sup>	6.361	5.873
<i>θ</i> /°	1.767-27.280	2.025-27.129
<i>T</i> /K	273(2)	273(2)
Reflns collected	8795	9189
R1, <sup>a</sup> wR2 <sup>b</sup> [ <i>I</i> > 2σ( <i>I</i> )]	0.0529, 0.1441	0.0315, 0.1344
GOF on <i>F</i> <sup>2</sup>	1.189	1.058

$${}^a R1 = \sum ||F_o| - |F_c|| / \sum |F_o|, {}^b wR2 = [\sum [w(F_o^2 - F_c^2)^2] / \sum [w(F_o^2)^2]]^{1/2}$$

### V.3. RESULT AND DISCUSSION

Complex **6**, *fac*-[Re(CO)<sub>3</sub>(HL)Cl] was synthesized by refluxing rhenium (I)pentacarbonylchloride with HL, [(E)-3-((pyridin-2-ylmethylene)amino)dibenzo[b,d]furan-2-ol] in toluene at 600°C for 6h and was structurally analysed by single crystal X-ray diffraction. The mixed donor (NNO) dibenzofuran based Schiff base ligand, HL was designed in such a way that -OH group could be free after coordinating with rhenium (I) centre and show unique functionality in presence of other metal ions. In this regard, we have studied the interaction between complex **6** and acetate salt of zinc. At room temperature such interaction was very slow but at slightly elevated temperature, Zn(OAc)<sub>2</sub> showed significant time dependent change in both UV-Vis spectra and emission spectra in methanol. The important fact is that in presence of Zn(OAc)<sub>2</sub>, complex **6** becomes emissive with large stokes shift which was non emissive previously. In search of the reason behind such beautiful change, we have found that in methanol medium the complex **6** get rearranged in presence of Zn(OAc)<sub>2</sub>, generating three different structurally modified facial rhenium (I) complexes.

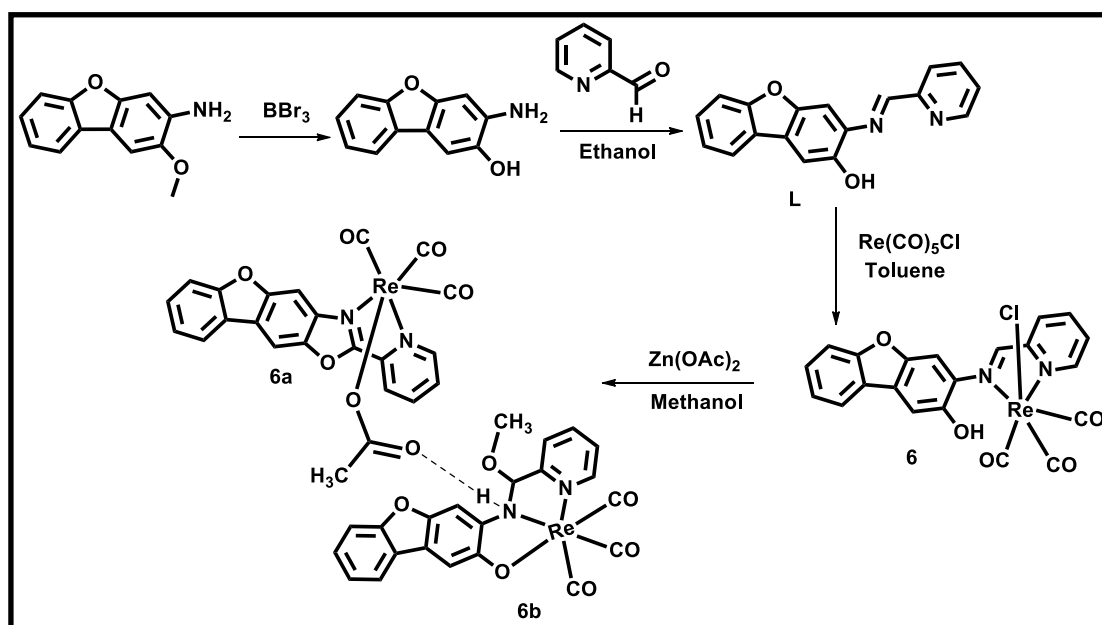


Figure V.1 Schematic diagram for synthesis of rhenium (I) complexes **6**, **6a** and **6b**.

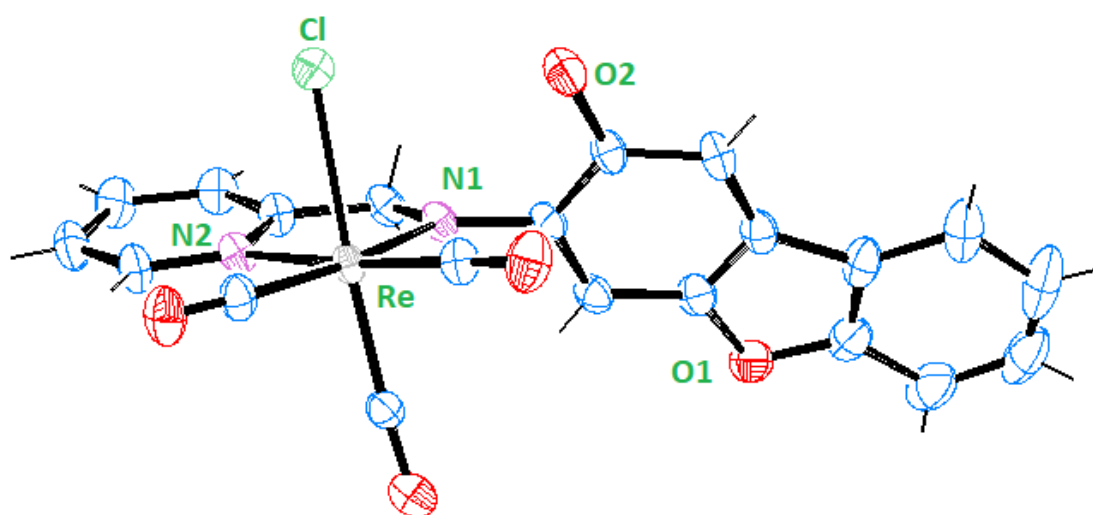


X-ray crystal study revealed the structural difference of these complexes and presence of intermolecular hydrogen bonding. Synthetic route of these complexes is given in **Figure V.1**.

### *Structural characterization of Complex 6*

The molecular structures of *fac*-[Re(HL)(CO)<sub>3</sub>Cl], 6, *fac*-[Re(CO)<sub>3</sub>(L-oxazole)(OAc)], 6a, *fac*-[Re(CO)<sub>3</sub>(L-methoxy)], 6b were determined by using single crystal X-ray diffractometer. The molecular structures of 6, 6a and 6b are shown in **Figure V.6** and **V.5** respectively.

When complex **6** was allowed to diffuse from dichloromethane into hexane layer, it crystallizes in triclinic crystal system with space group P-6. The geometry around the rhenium (I) metal centre is distorted octahedral having C-Re-N bond angles  $\sim 676^\circ$ , which is much lesser than  $680^\circ$ . The carbonyl ligands are arranged in a facial mode and the remaining equatorial sites are occupied by pyridyl nitrogen and imine nitrogen. The free -OH group of **6** is tilted away from the rhenium (I) centre in order to make hydrogen bond (H68  $\cdots$  Cl6=2.534 Å) with axial Chlorine atom (**Figure V.2**).

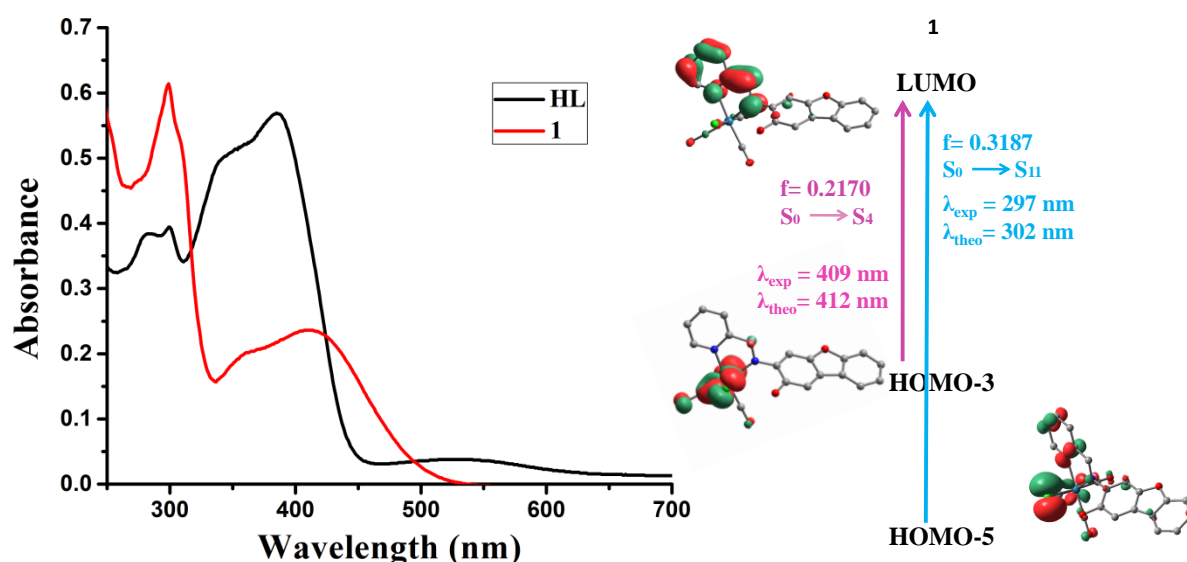


**Figure V.2** ORTEP plot of **6** showing essential atom numbering and H atoms are omitted for clarity

The formation of complex **6** was clearly indicated by the chemical shifts at 60.42 (s, 6H) ppm which accounts for the free -OH proton and at 9.45 (s, 6H) ppm for imine proton. Aromatic protons were in the range of 9-7.3 ppm. Besides, complexes having fac-[Re(CO)<sub>3</sub>]<sup>+</sup> core show characteristic facial CO stretch in the range of 1885 -2015 cm<sup>-1</sup>. All the relevant data are given in experimental section in ESI.

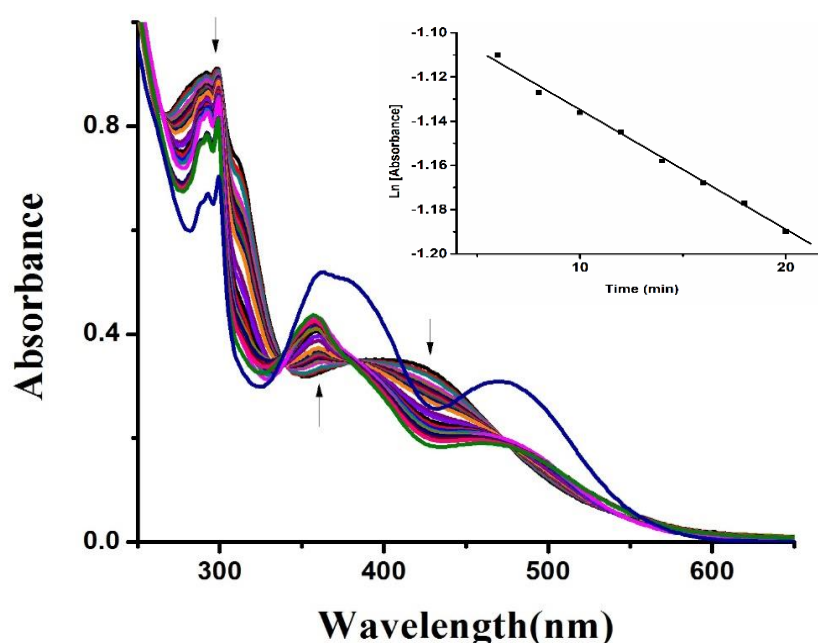
### E. Electronic Spectroscopy

The electronic spectra of the complex **6** and ligand (**Figure V.2.**) were estimated through UV-Vis spectrophotometer in methanol at room temperature keeping concentration at 20 μM. The major peak of L arises at 383 nm which is due to the intraligand charge transfer transition. The absorption peaks were observed at 296 nm ( $\epsilon = 45,700 \text{ M}^{-1} \text{ cm}^{-1}$ ) and 409 nm ( $\epsilon = 67,650 \text{ M}^{-1} \text{ cm}^{-1}$ ) which can be assigned as  $\pi \rightarrow \pi^*$  transition and metal to ligand charge transfer [Re (d $\pi$ ) $\rightarrow$ L] transition respectively. The TDDFT data shows good agreement with experimental data. The frontier molecular orbital involved in main transitions are given in **Figure V.3.**



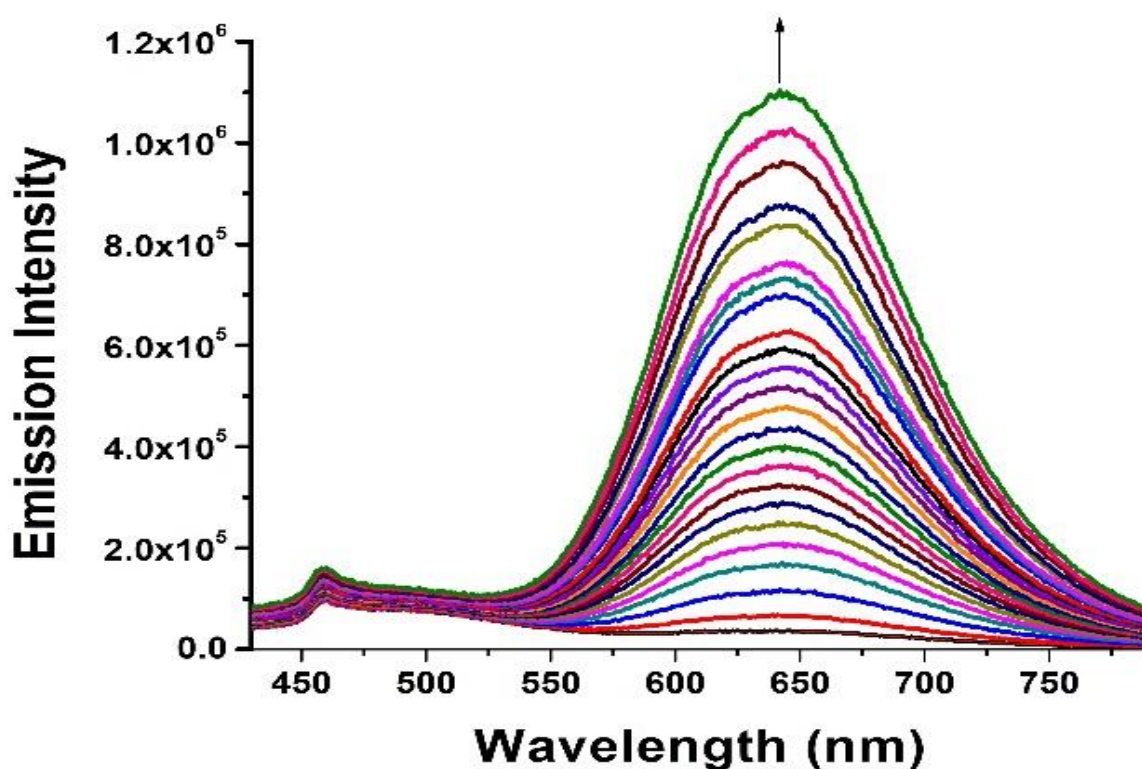
**Figure V.3** Absorption spectra of **L** and **6** in methanol keeping the concentration ( $c = 2 \times 10^{-5} \text{ M}$ ) at room temperature (left). Frontier molecular orbital involved in the UV-Vis absorption spectrum of **6** (for clarity we considered the molecular orbital with the higher value of CI ( $< 0.5$ ) for the appropriate transition).

It is well established that an anionic rhenium (I) compound can be transformed into bimetallic Re-Zn-Zn-Re complex which shows the ability of Zn to interact in a way with rhenium centre if proper condition is applied. In search of such unique phenomenon we have examined the reactivity of complex **6** towards  $\text{Zn}(\text{OAc})_2$ . Complex **6** in methanolic solution at slightly elevated temperature react with  $\text{Zn}(\text{OAc})_2$  turning yellow solution into red. Hence, a time dependent UV-Vis titration was performed after immediate addition of zinc acetate into the solution of **6** in methanol applying heat. Figure3 represents the UV-Vis titration graph showing prominent change in spectra of **6** as with time the spectral curve passes through several isobestic points at 475, 378, 335 nm suggesting the formation of new species in reaction medium. It is clearly visible that the peak at 409 nm decreased gradually and started to form new peaks at 355 nm and 470 nm. At  $T_\infty$ , the initial absorbance peaks completely disappeared and settled at 360 and 470 nm. A plot of  $\text{Ln} [\text{absorbance}]$  vs time gives straight line ( $R^2=0.99$ ) with negative slope. The calculated rate constant was found to be  $5.4 \times 10^{-3} \text{ min}^{-1}$  [Figure V.4.]



**Figure V.4.** Time evolution of the UV-Vis spectra of **6** with  $\text{Zn}(\text{OAc})_2$  in methanol at room temperature. Blue curve shows absorption spectra at infinite time. Inset: Plot of  $\text{Ln} [\text{absorbance}]$  vs time (monitored at 409 nm).

We have also investigated the luminescence property of complex **6** and in presence of  $\text{Zn}(\text{OAc})_2$  separately in methanol at room temperature. **6** is very weakly emissive at the excitation of 409 nm but it shows ligand centred emission during high energy excitation. The emission occurs at 646 nm with 36 fold increment of emission intensity when methanolic solution of **6** and  $\text{Zn}(\text{OAc})_2$  was excited at 409 nm. A gradual rise in intensity (**Figure V.5.**) was observed with passing time having a large stokes shift of 232 nm ( $43,603 \text{ cm}^{-1}$ ). This abnormal high stokes shift is a consequence of fast relaxation from the initial state to the emissive state. This may occur due to the excited state proton transfer reactions between the newly generated complexes. A part of these molecules may act as donor by absorbing light and another part may act as acceptor which emits light delivering large red shift.



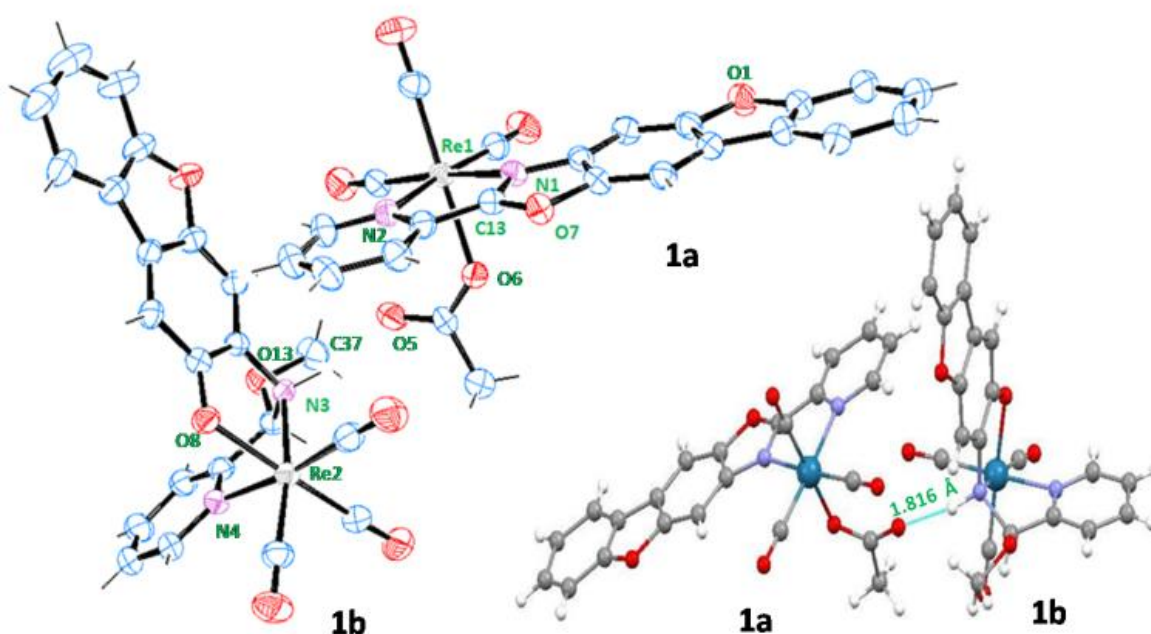
**Figure V.5** Time evolution spectrofluorometric titration of **6** with  $\text{Zn}(\text{OAc})_2$  in methanol at room temperature where  $\lambda_{\text{excitation}} = 409 \text{ nm}$  and  $\lambda_{\text{emission}} = 646 \text{ nm}$ .

These spectroscopic studies prompted us to search deeply into the reaction mechanism. In the reaction between complex **6** and Zn(OAc)<sub>2</sub>, zinc incorporated complex formation was expected but practically zinc excluded three rearranged products were observed. The first evidence for zinc free three different rhenium (I) complexes became apparent by analysing three distinct molecular ion peaks in ESI-MS spectrometry. The major peaks obtained at  $m/z = 617.09 [M+H]^+$ ,  $596.07 [M+H]^+$ , where these peaks are responsible for complexes **6a**, **6b** and respectively.

The exact structures of these complexes were confirmed through X-ray diffraction study. **6a** and **6b** were obtained as co-crystal (**6a.6b**) in dichloromethane: hexane layer. It crystallizes in monoclinic crystal system with space group P26/n. It reveals that two separate complexes **6a** and **6b** are attached with each other through hydrogen bonding (N3-H...O5=6.866 Å) associated with acetate oxygen of **6a** and amine hydrogen of **6b** (shown in **Figure V.6**). Analysis of structure of **6a** depicts the formation of oxazole ring by cyclization of free -OH group and imine bond of complex **6**. All the equatorial Re-N and Re-CO bonds including aromatic moieties of **6a** reside in the same plane whereas the axial positions are occupied by CO and acetate group. The oxazole ring is confirmed by the bond lengths of associated atoms where N1-C13 = 1.298 Å and C13-O7 = 1.349 Å. Here, rhenium (I) centre is coordinated with oxazole nitrogen and pyridine nitrogen forming an NN complex having facially bound CO group. In addition, incorporation of acetate group into rhenium (I) centre by breaking the Re-Cl bond is also noticed where Re-O6 bond length (2.654 Å) is shorter than Re-Cl bond (2.485 Å) of complex **6**.

In **6b**, a folded structure arises as a result of methanol insertion into the imine bond of **6**, where  $sp^2$  carbon (C36) transformed into  $sp^3$ . A distorted octahedral geometry

around rhenium (I) centre is observed where planarity of the aromatic centres is not possible due to tetrahedral arrangement of C36. N4-C34 and N4-C36 distances at 1.45 Å and 1.502 Å are suggestive of amine nature rather than amide character of N4. Here, the Re-Cl bond is replaced by Re-O bond, where the free –OH bond has coordinated with rhenium (I) centre. Selected bond lengths and bond angles of **6**, **6a** and **6b** are given in **Table V.3**.



**Figure V.6** ORTEP plot of co-crystal, [(6a.6b)] showing essential atom numbering and H atoms are omitted for clarity (left). H-bonding between 6a and 6b is 6.866 Å is shown in the left side figure.

The exact role of zinc acetate is unknown till now but the probable role of Zinc acetate lies on the removal of chloride from Re-Cl bond. The strong hydrogen bond of H18•••Cl1 in **6** prevents coordination between Re and phenoxy oxygen which gets destroyed in presence of Zinc acetate and facilitate the rearrangement reaction.

The rearrangement of the complexes is possible only when the ligand is structurally suitable to coordinate with rhenium (I) and satisfy the +1 oxidation state of central metal. Another important fact is that methanol as a small molecule eases the reaction by attacking the imine bond with negligible steric hindrance with adjacent atoms.

**Table V.3** Bond length and bond angle of complexes **6**, **6a** and **6b**.

<b>1</b>		<b>1a</b>		<b>1b</b>	
<b>Bond Length (Å)</b>					
Re01-C20	1.907(9)	Re01-N1	2.192(5)	N4-C34	1.459(7)
Re01-C21	1.921(8)	Re01-N2	2.217(5)	N4-C36	1.502(7)
Re01-C19	1.932(8)	Re01-C21	1.903(7)	Re02-C45	1.909(7)
Re01-N1	2.179(6)	Re01-C19	1.903(7)	Re02-C44	1.916(7)
Re01-N2	2.187(6)	Re01-C20	1.908(7)	Re02-C43	1.917(7)
Re01-Cl1	2.485(2)	Re01-O6	2.151(4)	Re02-O8	2.108(4)
<b>Bond Angles(°)</b>					
C20-Re01-C21	84.6(4)	C21-Re01-C19	85.2(3)	C45-Re02-C44	85.9(3)
C20-Re01-C19	91.0(4)	C21-Re01-C20	88.2(3)	C45-Re02-C43	90.3(3)
C21-Re01-C19	91.0(3)	C19-Re01-C20	86.5(3)	C44-Re02-C43	87.9(3)
C20-Re01-N1	99.0(3)	C21-Re01-O6	97.8(2)	C45-Re02-O8	98.4(2)
C21-Re01-N1	174.5(3)	C19-Re01-O6	176.8(2)	C44-Re02-O8	174.6(2)
C19-Re01-N1	93.1(3)	C20-Re01-O6	94.6(2)	C43-Re02-O8	95.3(2)
C20-Re01-N2	92.8(3)	C21-Re01-N1	173.2(2)	C45-Re02-N3	96.1(2)
C21-Re01-N2	100.9(3)	C19-Re01-N1	98.1(2)	C44-Re02-N3	96.1(2)
C19-Re01-N2	167.8(3)	C20-Re01-N1	97.9(2)	C43-Re02-N3	172.6(2)
N1-Re01-N2	74.8(2)	O6-Re01-N1	78.78(17)	O9-Re02-N3	80.27(18)
C20-Re01-Cl1	176.5(2)	C21-Re01-N2	98.7(2)	C45-Re02-N4	171.1(2)
C21-Re01-Cl1	93.2(3)	C19-Re01-N2	96.9(2)	C44-Re02-N4	96.6(2)
C19-Re01-Cl1	91.9(3)	C20-Re01-N2	172.5(2)	C43-Re02-N4	98.3(2)
N1-Re01-Cl1	82.97(19)	O6-Re01-N2	81.61(17)	O8-Re02-N4	78.70(15)
N2-Re01-Cl1	84.86(18)	N1-Re01-N2	75.10(18)	N3-Re02-N4	75.12(17)

The role of hydrogen bonded two unique complexes is crucial in excited state. As, in (**6a.6b**) hydrogen bond acts as a connector between **6a** and **6b** in the ground state, proton transfer is feasible in the excited state from **6b** to **6a** resulting in emission of red light. In situ modification of complexes with excited state reactions is mainly responsible for the

continuous increment of emission intensity and transformation of non-emissive complex **6** to an emissive species.

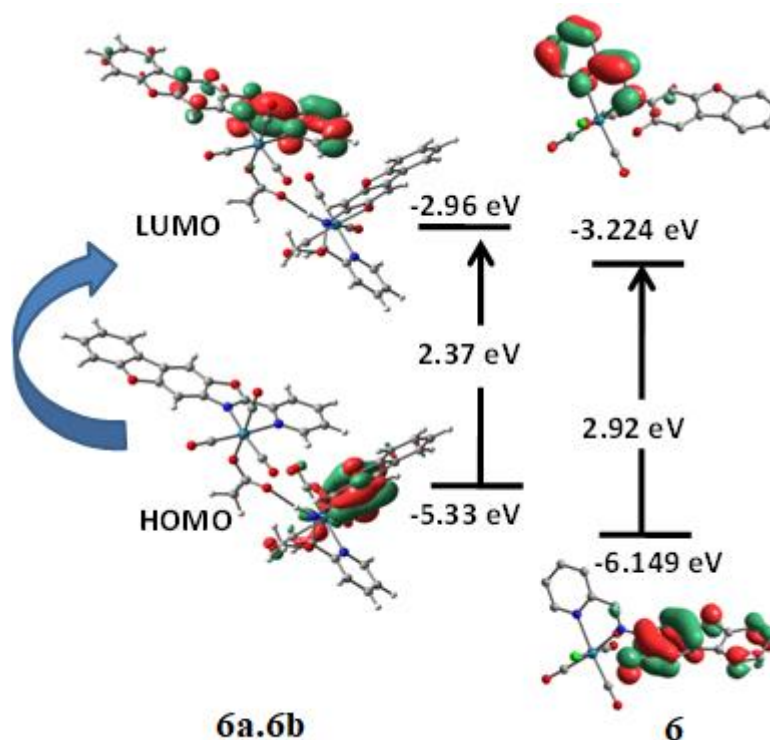
Geometrical optimisation of complexes **6** and (**6a.6b**) are accomplished in presence of solvent by DFT at their electronic ground state ( $S_0$ ) using LANL2DZ basis set. The optimized parameters (bond length and bond angle) of the complexes are given in ESI. The optimized ground state structures of complexes **6** and (**6a.6b**) at their singlet ( $S_0$ ) state, possesses distorted octahedral geometry around rhenium (I) metal centre. The fac-[Re(CO)<sub>3</sub>]<sup>+</sup> core is consisted with each complexes having the angles of  $\sim 90^\circ$  between the CO ligands.

Theoretical structural parameters are in well agreement with the experimental data for the complexes for which X-ray data are available. In these complexes all the Re-C bond length occurs near 6.96 Å and Re-N bond length occurs near 2.26 Å. The Re-Cl bond length of all the complexes is slightly longer than the Re-C and Re-N bond lengths. All these values deviate slightly from the experimental parameters, which is dependent on the errors originated from the environmental factors such as crystal packing and the impact of the medium.

The HOMO-LUMO energy gap in the ground state geometry of **6** is 2.92 eV and the same for (**6a.6b**) is 2.37 eV which is much lower than the former complex (**Figure V.7**). The reduction of energy gap is due to the occurrence of H-bonding between **6a** and **6b**. From the frontier molecular orbital diagram of (6a.6b), it is observed that the amino dibenzofuran centre of **6b** is electron rich in HOMO whereas in LUMO, oxazole- pyridine moiety of **6a** is electron dense. It suggests the possibility of the movement of electron density from one molecule to another through hydrogen bond, which supports the experimental facts. Hence, **6b** acts as



donor and 6a acts as acceptor molecule resulting in strong emission intensity with large stokes shift.



**Figure V.7** Partial molecular orbital diagram with HOMO and LUMO showing electron density over **6** and (**6a.6b**) molecules.

### III.5. CONCLUSION

In conclusion, we have presented our observation on molecular rearrangement of *fac*-[Re(CO)<sub>3</sub>LCl] complex in the presence of zinc acetate in methanol solvent. X-ray crystal structure clearly proves the fate of rearrangement reaction and existence of intermolecular interaction through H-bonding. DFT studies were employed to model the variable impacts of the electronic movement between molecules which shows the donor-acceptor relation in excited state resulting in large stokes shift in emission spectra. There are still many scopes to explore the potential application of the rearranged products which is in progress.

### III.5. REFERENCES

- (1) T. A. Gillam, C. Caporale, R. Books, C. A. Bader, A. Sorvina, M. V. Werrett, P. J. Wright, J. L. Morrison, M. Massi, D. A. Brooks, S. Zacchini, S. M. Hickey, S. Stagni, S. E. Plush, *Inorg. Chem.* **2021**, *60*, 60673–60685.
- (2) N. J. Lundin, A. G. Blackman K. C., Gordan, D. L. Officer, *Angew. Chem. Int. Ed* **2006**, *45*, 2582 –2584.
- (3) A. S. Polo, M. K. Itokazu, N. Y. M. Iha, *Coord. Chem. Rev.* **2004**, *248*, 6343–6366.
- (4) Liu,Z. ;Peng,C. ; Wang, Y. ;Pei, M. and Zhang\*,G. ; *Organic & Biomolecular Chemistry*, **2016**, *64* ,4260-4266.
- (5) P. Ashokkumar, V. T.Ramakrishnan and P. J. Ramamurthy, *Phys. Chem. A* **2016**, *665*, 64292–64299.
- (6) S. Sasaki, G. P. C. Drummen and G. IchiKonishiac, *J. Mater. Chem.*, **2016**, *4*, 2736-2743.
- (7) D.W. Cho, D. W. Cho, *New J. Chem.*, **2014**, *38*, 2233-2236
- (8) J. Wang, X. Liu and Y. Pang *J. Mater. Chem.* **2014**, *2*, 6634-6638
- (9) L.Tang, X. Dai, K. Zhong, X. Wen, D. Wu, *Journal of Fluorescence* **2014**, *24*, 6487–6493

# *List of Publications*



- 1) **Tapashi Das**, Kajal Krishna Rajak, "Experimental and theoretical investigation of a metalloreceptor bearing a  $[Re(CO)_3]^+$  core incorporating a multifunctional ligand: selective reactivity towards  $Zn^{2+}$  and  $CN^-$  ions" *Dalton Transaction* **48 (20)**, 6879-6891
- 2) **Tapashi Das**, Kajal Krishna Rajak, "Synthesis, characterization and DFT studies of complexes bearing  $[Re(CO)_3]^+$  core and reactivity towards cyanide ion" *Journal of Organometallic Chemistry* **908**, 121098
- 3) Sohini Basu Roy, Amit Maity, **Tapashi Das**, Kajal Krishna Rajak, "Tuning the selectivity of aggregation induced enhanced emission active terephthalohydrazide template via modulating the terminal sensory side chain" *Journal of Luminescence* **206**, 649-659
- 4) Supriya Debnath, **Tapashi Das**, Sankar Prasad Parua, Kajal Krishna Rajak, "Synthesis and characterization of blue-violet emitting iridium(III) complex coordinated via chlorinated ancillary ligand" *Journal of Coordination Chemistry*, 1-15.
- 5) Mitali Majumder, **Tapashi Das**, Nayim Sepoy, Kajal Krishna Rajak, "A study of DNA/BSA interaction and catalytic potential of oxidovanadium (V, IV) complexes incorporating dibenzofuran based ONO ligand" *Journal of Organometallic Chemistry* **961**, 122244